TECHNISCHE UNIVERSITÄT MÜNCHEN
Institut für Luft- und Raumfahrt

Conceptual Design Methods for Sizing and Performance of Hybrid-Electric Transport Aircraft

Clément Pornet

Vollständiger Abdruck der von der Fakultät für Maschinenwesen der Technischen Universität München zur Erlangung des akademischen Grades eines

Doktor-Ingenieurs (Dr.-Ing.)

genehmigten Dissertation.

Vorsitzender:	Prof. Dr.-Ing. Volker Gümmer
Prüfer der Dissertation:	1. Prof. Dr.-Ing. Mirko Hornung
	2. Prof. Dr.-Ing. Manfred Hajek

Die Dissertation wurde am 23.11.2017 bei der Technischen Universität München eingereicht und durch die Fakultät für Maschinenwesen am 25.04.2018 angenommen.

Preamble

In the following, I would like to thank the ones who inspired me along my career as an aeronautical engineer and towards this academic achievement.

First I wish to thank Dr. Wolfgang Heinze from the Institute of Aircraft Design of the Technical University of Braunschweig. Wolfgang launched my career with his recommendations that led me first to the Airbus Future Projects Office in Hamburg and then to the Bauhaus Luftfahrt in Munich. Wolfgang was the very first person who encouraged me to consider a doctoral degree. My most grateful thanks Wolfgang for having believed in me in the very early stage of my career.

I would like to follow by thanking Michael Schiebel from the department of Aircraft Design within the Airbus Future Projects Office in Hamburg. I would not forget the long walks with Michael passing the A380 Delivery Centre, sharing his passion for aviation which inspired me to become today an aircraft designer.

Joining the ATR company in Toulouse, I had the chance to meet Dr. Yann Chauvat and Gauthier Spoerry. Certainly the most passionate engineers and privat pilots I ever met in my career. Inspiring me technically notably by inviting me to participate to aircraft design workshops organized by the french association Inter-Action, they also made me discover the passion of flying by motivating me to engage as a glider pilot. I am very grateful to have cross the path of Yann and Gauthier and to still share with them a great friendship. I would also like to thanks Marie-Laure Groud, former flight test engineer at Airbus who took the head of the Flight Physics department at ATR for her inspiring leadership, her dedication to foster the professional development of her team and the great support she gave me along my career.

With the advise of Dr. Wolfgang Heinz in my mind to be involved in a doctoral degree, I joined the Bauhaus Luftfahrt in Munich. My very first thank goes to Dr. Askin Isikveren who welcomed me in his department for advanced aircraft concepts. Askin's passion for aviation gives him an incredible force to lead the aerospace community to a next level. I will always have a great respect for Askin, his vision and his highly technical expertise in aircraft design. His leadership transformed my career by fostering my expertise in aircraft design and performance and by propelling me to my current position as an aircraft designer. I would like to thank you Askin for your support along all these years, I would not have achieved this level of technicality in this work without your leadership.
I would like then to thank the "pionniers" of the advanced aircraft concepts department, Dr.

Corin Gologan, Hans-Joerg Steiner, Dr. Arne Seitz and Dr. Oliver Schmitz. Highly skilled and motivated, they created the technical foundations of the group that I used to build-on and to achieve this work. A special thanks goes to Corin, leader of my team, who guided me in my first year at Bauhaus Luftfahrt to define the nature of this thesis and who always encouraged me to pursue with this work.
In my last years at Bauhaus Luftfahrt, I had the blissful personal and professional experience to meet Sascha Kaiser, Dr. Michael Schmidt, Patrick Vratny and Ulrich Kling. Forming the core team of the advanced aircraft concepts department, we were all involved in a doctoral degree. Thanks to our great team spirit, we managed to keep motivated in face of the professional challenges. The level of details achieved in this work is a reflection of our many technical discussions and the share of our expertises. I will never forget all the great times we spent in Munich. Thank you all!

Finally I would like to thank Prof. Dr. Mirko Hornung from the Institute of Aircraft Design of the Technical University of Munich and executive director research and technology of Bauhaus Luftfahrt for the supervision of this thesis.

My last words go to my parents Jean-Paul and Françoise and to my sister Lorine for their unconditional love and support that elevated me to where I stand today.

Paris, 11th April 2018

Abstract

The European Flightpath 2050 and corresponding Strategic Research and Innovation Agenda as well as the NASA Environmentally Responsible Aviation N+ series have elaborated ambitious emissions and external noise reduction targets according to chronological waypoints. However, the evolutionary improvements of conventional technologies might not be sufficient to fulfil the declared objectives. Disruptive technologies need consequently to be envisioned to reach the set of future goals. In order to deliver ultra-low or even zero in-flight emissions levels, there exists an increasing amount of international research and development focusing on the electrification of aircraft propulsion and power systems. While aiming for the ultimate goal of universally electric transport aircraft, a hybrid-electric approach will be first necessary to match the requirements of aircraft propulsion systems and the development pace of electrical components technology. The introduction of hybrid-electric technology expands dramatically the design space and the full-potential of these technologies will be drawn through synergistic morphological and systems integration. Perturbing the conventional design paradigms, the design of hybrid-electric aircraft poses a genuine challenge to traditional sizing and performance methods.

Conceptual design methods for sizing, performance analysis and identification of flight techniques for hybrid-electric transport aircraft are proposed in this thesis. Considering the available legacy industry programs, the methods are developed with the capability of being integrated in traditional sizing and performance environment. The models of the standalone engineering components which constitute hybrid-electric propulsion systems are first described. By establishing the interfaces between the engineering component modules, the layout of the hybrid-electric propulsion architecture and the system integration at aircraft level are then comprehensively detailed. The conventional methods are extended to map the intrinsic characteristics of hybrid-electric propulsion system within the aircraft design and performance environment. The tracking of the electric energy consumed and the calculation of the maximum thrust available are in the focus of the methods development. New degrees-of-freedom such as the degrees-of-hybridization and new constraints associated with the sizing of hybrid-electric propulsion system are introduced. The specificities related to the sizing of hybrid-electric propulsion system are explained by describing the sizing criterion of the components. The overall aircraft sizing process and the evaluation of the aircraft integrated performance are finally highlighted.

The vehicular efficiency function is an essential metric in conceptual design phase as it evaluates the overall efficiency of the aircraft to perform its dedicated transport task. Used notably for identification of optimum flight techniques it enables to match the altitude-speed operations of the aircraft with its aerodynamic, weight and propulsion characteristics. New figures-of-merit which take into account the novel characteristics of hybrid-electric propulsion system are established in this thesis for the flight techniques optimization of hybrid-electric transport aircraft.

The proposed conceptual design methods are applied to evaluate integrated performance of hybrid-electric narrow-body transport aircraft. The assessment focuses on fuel-battery hybrid-electric propulsion system technology targeting a 2035 year entry-into-service. The investigations of a retrofitted narrow-body transport aircraft with a parallel hybrid-electric propulsion system and of narrow-body clean-sheet designs with parallel and partial parallel hybrid-electric propulsion system enable the derivation of design heuristics and sizing axioms. The sizing sensitivities of hybrid-electric narrow-body aircraft are investigated against the design range, the degree-of-hybridization for power and the battery technology level. Increasing design range results in a degradation of the integrated performance in terms of fuel consumption, aircraft weight and vehicular efficiency due to the raising electric energy demand which translates basically into increasing battery system mass installation. Lower battery gravimetric specific energy results in the installation of a larger battery mass for a given amount of energy which results in penalizing weight sizing cascading effects. Growing degree-of-hybridization for power up to a moderate level results in an increasing block fuel reduction, however, at the expense of a degradation in vehicular efficiency. The fuel saving benefit obtained by increasing degree-of-hybridization for power is explained by the increasing use of electrical energy and by the improvement in overall propulsion system efficiency. The degradation in vehicular efficiency is caused by the sizing of the electric propulsion system for higher power and by the increase in electric energy demand requirement which result in higher battery system mass installation. In the context of the hybrid-electric transport aircraft integrated performance investigation, the market application of these concepts is found to be subject to the regional segment with design ranges in the order of 900 nautical miles (nm) to 1300 nm and for low-to-moderate degree-of-hybridization for power considering battery technology above 1000 Wh/kg. In terms of the influence on flight techniques optimization, increasing the degree-of-hybridization for power has a tendency to lower the optimum speed. However, by mirroring cruise flight technique strategy of conventional aircraft such as the long-range cruise speed, this effect should not drastically change the contemporary altitude-speed flight profiles.

Contents

List of Figures

List of Tables

Nomenclature

List of Latin Symbols

a	m/s	Speed of sound
Alt	m	Altitude
c	\$/kWh	Specific Cost of Energy
C	\$	Cost
C_0	\$	Fixed Cost
C_D	-	Coefficient of Drag
CI	-	Cost Index
C_L	-	Coefficient of Lift
$COSAR$	m/\$	COst Specific Air Range
$C_{rel,EM}$	-	Relative Torque of the Electric Motor
$D_{Fan,PD}$	m	Fan Diameter of the Propulsive Device
$D_{Fan,TF}$	m	Fan Diameter of the Turbofan
$FPR_{des,PD}$	-	Design Fan Pressure Ratio of the Propulsive Device
$FPR_{des,TF}$	-	Design Fan Pressure Ratio of the Turbofan
$e_{Bat,Syst}$	W h/kg	Battery Gravimetric Specific Energy at System Level
e_{Bat}	W h/kg	Battery Gravimetric Specific Energy at Cell-Level
ERC	-	Economical Range Cruise
$ESAR$	m/(W h)	Energy Specific Air Range
FF	kg/s	Fuel Flow
FF_{FC}	kg/s	Fuel Flow of the Fuel Cell System
FHV	J/kg	Fuel Heating Value
FL	100 ft	Flight Level
H_E	-	Degree-of-Hybridization for Energy
H_P	-	Degree-of-Hybridization for Power
H_{Puse}	-	Degree-of-Hybridization for Useful Power
ΔISA	-	International Standard Atmosphere Deviation
$LCRC$	-	Long COSAR Range Cruise
L/D	-	Lift-to-Drag ratio
$LERC$	-	Long ESAR Range Cruise
LFL	m	Landing Field Length

LRC	-	Long Range Cruise
m	kg	Mass
M	-	Mach Number
$m_{Bat,energy}$	kg	Battery Mass sized with respect to the Energy criterion
$m_{Bat,power}$	kg	Battery Mass sized with respect to the Power criterion
$MCRC$	-	Maximum COSAR Range Cruise
MD	-	Dive Mach Number
$MERC$	-	Maximum ESAR Range Cruise
MLW	kg	Maximum Landing Weight
MMO	-	Maximum Operating Mach Number
MRC	-	Maximum Range Cruise
$MTOW$	kg	Maximum Take-Off Weight
$N_{rel,PD}$	-	Relative Corrected Speed of the Propulsive Device
$N_{rel,CE}$	-	Relative Corrected Speed of the Combustion Engine
$N_{rel,EM}$	-	Relative Speed of the Electric Motor
OEW	kg	Operating Empty Weight
P	W	Power
$p_{Bat,Syst}$	W/kg	Battery Gravimetric Specific Power at System Level
P_{CE}	W	Shaft Power of the Combustion Engine
$P_{CE,Offtake}$	W	Power Off-Take at the Combustion Engine
P_{Elec}	W	Electrical Power required at the Energy and Power Device
$P_{Elec,Offtake}$	W	Electrical Power Off-Take
$P_{Supply,Elec}$	W	Electrical Power Supply
P_{EM}	W	Power of the Electric Motor
$P_{Supply,Fuel}$	W	Fuel Power Supply
P_G	W	Power delivered by the Generator
PL_{CE}	-	Power Lever of the Combustion Engine
PL_{EEPD}	-	Power Lever of the Electrical Energy and Power Device
PL_{EM}	-	Power Lever of the Electric Motor
$P_{Bat,max}$	W	Maximum Power of the Battery System
$P_{CE,max}$	W	Maximum Power of the Combustion Engine
$P_{Shaft,Conv,max}$	W	Maximum Shaft Power delivered by the Conventional System
$P_{EEPD,max}$	W	Maximum Power of the Electrical Energy and Power Device
$P_{Shaft,Elec,max}$	W	Maximum Shaft Power delivered by the Electrical System
$P_{EM,max}$	W	Maximum Power of the Electric Motor
$P_{FC,max}$	W	Maximum Power of the Fuel Cell System
$P_{G,max}$	W	Maximum Power of the Generator
P_{PMAD}	W	Power required at the PMAD
P_{Shaft}	W	Shaft Power required
$P_{Shaft,Conv}$	W	Shaft Power required at the Conventional System
$P_{Shaft,Elec}$	W	Shaft Power required at the Electrical System
P_{SLS}	W	Sea-Level Static Power
$P/MTOW$	W/kg	Power-to-MTOW

R	m	Range
S_{ref}	m^2	Wing Reference Area
SAR	m/kg	Specific Air Range
SOC	-	Battery State-Of-Charge
T	N	Thrust
T_{des}	N	Total Design Thrust
$T_{des,EF}$	N	Design Thrust of the Electrical Fan
$T_{des,PD}$	N	Design Thrust of the Propulsive Device
$T_{des,TF}$	N	Design Thrust of the Turbofan
$TOFL$	m	Take-Off Field Length
TOW	kg	Take-Off Weight
$TSFC$	kg/(N s)	Thrust Specific Fuel Consumption
$TSPC$	W/N	Thrust Specific Power Consumption
$T/MTOW$	-	Thrust-to-MTOW
V	m/s	Speed
VD	m/s	Dive Speed
VFE	m/s	Flaps Extended Speed
VLE	m/s	Landing Gear Extended Speed
VLO	m/s	Landing Gear Operating Speed
VMO	m/s	Maximum Operating Speed
W	N	Weight
$MTOW/S_{ref}$	kg/m^2	Wing-Loading

List of Greek Symbols

η	-	Efficiency
η_{Bat}	-	Efficiency of the Battery System
η_{CE}	-	Efficiency of the Combustion Engine
η_{EEPD}	-	Efficiency of the Electrical Energy and Power Device
η_{EM}	-	Efficiency of the Electric Motor
η_{FC}	-	Efficiency of the Fuel Cell System
η_G	-	Efficiency of the Generator
η_{PD}	-	Efficiency of the Propulsive Device
η_{PMAD}	-	Efficiency of the Power Management and Distribution System
ρ	kg/m^3	Density

List of Subscripts and Superscripts

Battery	Battery	**des**	Design
Cell	Cell	**Elec**	Electrical
Conv	Conventional	**Energy**	Energy

Fuel	Fuel	**Shaft**	Shaft
i	Index	**Supply**	Supply
max	Maximum	**Syst**	System
Offtake	Off-Take	**Time**	Time
ref	Reference	**Total**	Total
rel	Relative	**use**	Useful

List of Acronyms

AEO	All Engine Operative
ATLRS	Aircraft Top-Level Requirements
BCU	Battery Controller Unit
BLI	Boundary Layer Ingestion
BWB	Blended Wing Body
CE	Combustion Engine
DF	Ducted Fan
EEPD	Electric and Energy Power Device
EF	Electric Fan
EM	Electric Motor
FC	Fuel Cells
G	Generator
GTF	Geared Turbofan
HTS	High-Temperature Superconductive
MCL	Maximum Climb rating
MCO	Maximum Continuous rating
MCR	Maximum Cruise rating
MTO	Maximum Take-Off rating
nm	nautical miles
OEI	One Engine Inoperative
PAX	Passengers
PD	Propulsive Device
PMAD	Power Management And Distribution
SLS	Sea-Level Static
SSPC	Solid State Power Controller
TF	Turbofan
TO	Take-Off
TOC	Top-Of-Climb
YEIS	Year Entry-Into-Service

List of Organisations

NASA	National Aeronautics and Space Administration

List of Research Programs

SRIA	Strategic Research and Innovation Agenda

List of Software

PACELab APD	PACELab Aircraft Preliminary Design
APP	Aircraft Performance Program
FLOPS	FLight Optimization System
GasTurb	GasTurb performance software
NPSS	Numerical Propulsion System Simulation
Piano	Aircraft Analysis Tool Piano
PROOSIS	PRopulsion Object Oriented SImulation Software

Chapter 1

Introduction

The aviation community is considering with great attention the application of electrical technology and power electronics to transport aircraft propulsion as it is viewed as a promising technological pathway to achieve the international environmental targets set for aviation. Growing environmental concern was translated into the declaration of goals for aviation by Europe and by the United States of America. The Flightpath 2050 program and corresponding Strategic Research and Innovation Agenda (SRIA) [1] as well as the NASA Environmentally Responsible Aviation N+ series [2] aim at reduction in terms of emissions and external noise. Within the SRIA document, 75% reduction in emissions is targeted for the year 2050. Of this total 75% reduction target, 68% result from the combined improvement of advanced propulsion systems and airframe while the remaining 7% come from improvement in air traffic management. The fulfilment of the future goals will rely consequently in majority on the technological development of propulsion system.
The consideration of electrical technology and power electronics is motivated by the growing evidence that evolutionary improvement of the technologies might not be sufficient to fulfil these targets. As evaluated within the project SELECT [3] contracted by Northrop Grumman for NASA, the N+3 fuel burn goals could not be achieved assuming evolutionary improvements. Scenarios presenting the possible integrated benefits of combined evolutionary improved technologies [4] indicated that emission reduction in term of CO_2 will fall short by around 8% of the target for the year 2035 and that the deficit becomes even more substantial with respect to the 2050 target. This trend can be best understood by the high maturity reached by contemporary technologies and in particular by the conventional propulsion system technology implemented in transport aircraft. Prospects for technological improvements have consequently reached an asymptote leaving not enough potentials for achieving the targets. The introduction of innovative technologies and more specifically disruptive propulsion system technologies turns out to be essential in view of meeting the future goals for aviation.

1.1 The Need for Hybrid-Electric Technology Towards an All-Electric Economy

The application of electrical technology to transport aircraft could revolutionize aircraft propulsion and power systems. The progress of electrical component technologies, the development perspective of key enabling technologies and the electrical system configuration for synergistic integration at aircraft level make the field of electrically driven propulsion and power system very promising in providing the technological rupture required for the fulfilment of the future goals.
The feasibility of electric propulsion system application to transport aircraft will depend upon the improvement in energy and power capability of storage device, the development of components key performance characteristics such as gravimetric specific power and efficiency, the scalability potential of electrical components [5, 6] as well as the maturation of key technology such as high-temperature superconductive (HTS) technology [7, 8]. While striving for the development of universally-electric transport aircraft [7–10], offering a vision for zero-in-flight emissions, significant progress in electrical component technology needs to be achieved to reach the technological requirement enabling universally-electric commercial flight. In order to match the propulsion system requirement of transport aircraft and the development pace of the electrical technology, hybrid-electric approach to propulsion and power will pave the way towards universally-electric propulsion system. Referring to the emergence of an all-electric economy, Sehra and Shin [11] stated that "hybrid propulsion system will be required to meet the challenges of transition and timely introduction of fledgling new power systems".
The feasibility of applying hybrid-electric technology to the propulsion system of transport aircraft has to be examined and the potential advantages assessed at aircraft level. The benefits of hybrid-electric aircraft need to be evaluated for future market segments in terms of emission reduction potentials, vehicular efficiency change and operating economics.

1.2 Definition of the Research Objectives

The integration of an electrical drive to the propulsion system of an aircraft disrupts the traditional sizing and performance methods. The design variables and objective functions for the sizing and optimization of the aircraft need to be redefined due notably to the electrical energy source participating to the propulsion of the aircraft. The tracking of the electrical energy requires the development of methods to map this additional energy source within the integrated performance calculation. The characteristics of the electrical components need to be considered for the sizing of the propulsion system. According to intrinsic physical behaviours of the electrical components new constraints need to be taken into account within the sizing process. Aiming at evaluating the prospects of hybrid-electric aircraft in the conceptual design phase, new methods need to be developed to enable the design, sizing and performance assessment of hybrid-electric transport aircraft. Pre-design methods for the sizing and performance of hybrid-electric aircraft found in the literature [12, 13] are based mainly on

first-order equations for the modelling of the aircraft and the propulsion system. As a result, detailed secondary effects cannot be taken into account in the evaluation of integrated hybrid-electric propulsion systems. Besides overcoming the limitations of contemporary methods, the newly developed methods need to offer higher fidelity modelling than pre-design methods. Concerned by the use in industry of legacy or commercial sizing and performance programs, a constraint in the methods development is set on their capability to be integrated into a traditional sizing and performance programs. The development of a completely new sizing and performance environment is not the focus of this thesis. Hence, the first objective can be formulated by the development of new conceptual design methods which can be implemented in contemporary program to enable the sizing and the performance assessment of hybrid-electric aircraft and to enhance the fidelity of the modelling compared to pre-design methods. The identification of optimum flight techniques is essential in conceptual design phase to match the speed-altitude operations to the aircraft characteristics. The classical metrics for flight technique optimization are deficient when introducing an additional source of energy for the propulsion system. Consequently, the second research objective of the thesis is the development of methods for the determination of flight technique optimality of hybrid-electric aircraft. Finally, the investigation of the integrated prospects of hybrid-electric aircraft in terms of market segment range application, potential reduction in emissions and change in vehicular efficiency is the third research objective defined in this thesis.

1.3 Scope and Structure of the Thesis

With respect to the research objectives formulated previously, the scope and the structure of the thesis are outlined. The thesis focuses on the development of conceptual design methods for sizing, performance and flight technique optimality of hybrid-electric aircraft in order to assess hybrid-electric propulsion systems at aircraft level and to examine the integration implications. Visualized in Figure 1.1, the perimeter of the thesis is drawn around the sizing and performance module of the aircraft and it includes the establishment of the interfaces with the expert modules to capture the sensitivities of hybrid-electric propulsion technology at aircraft level. As indicated the modelling of the component characteristics and the architectural layout of the conventional and the electrical system are provided by external engineering modules.
In Chapter 2, the state-of-the-art in electric components technology and the development perspectives are reviewed. Potential key technological enablers for the application of electric drive to propulsion and power system of transport aircraft are then discussed. The topological options for the layout of hybrid-electric propulsion system are finally identified. The review is then extended to aircraft level offering a compendium of advanced transport aircraft concepts employing electric drive to the propulsion system. The classical methods for aircraft sizing and performance are reviewed in Chapter 3 and their limitations for the integrated assessment of hybrid-electric propulsion technology are identified. The proposed methods for the sizing and performance assessment of hybrid-electric aircraft are then detailed. The methods developed for the identification of optimum flight technique of hybrid-electric aircraft are de-

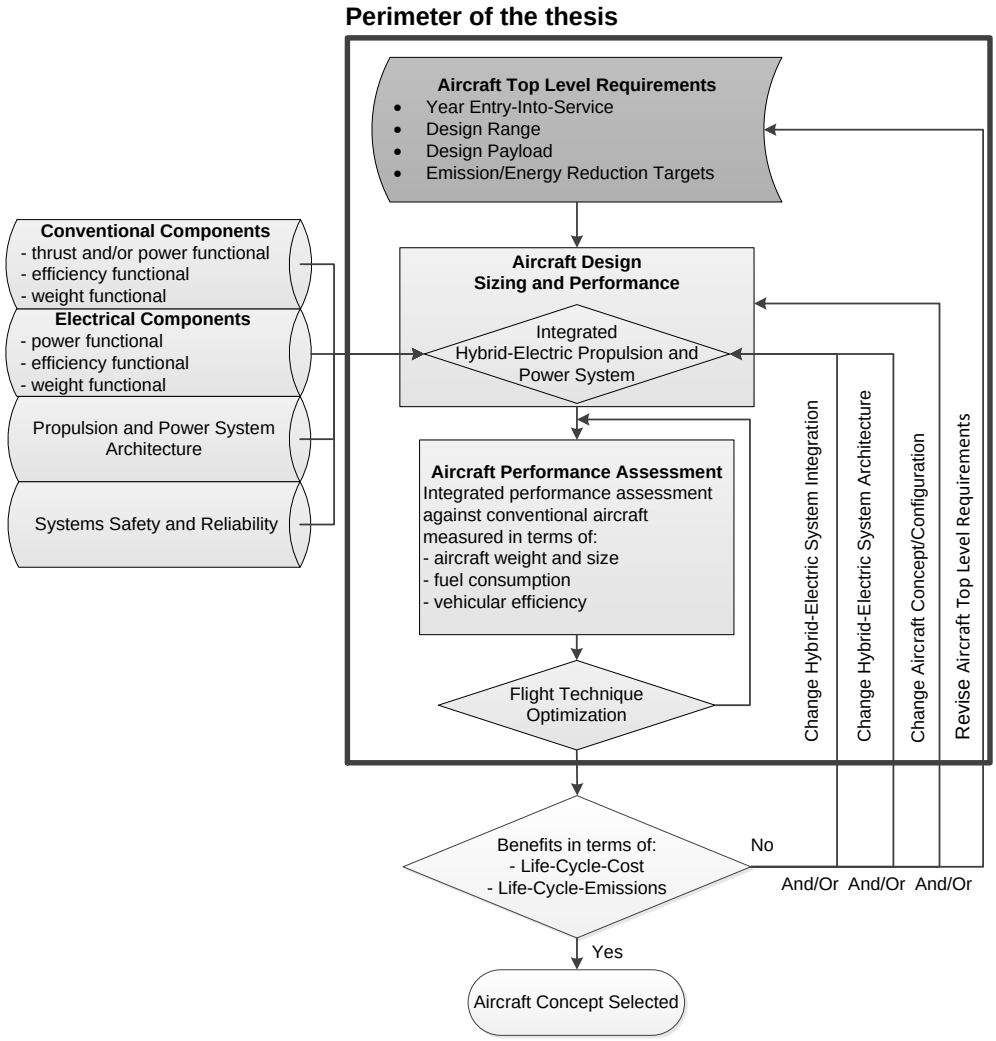

Figure 1.1: Scope of the thesis

scribed in Chapter 4. Finally the integrated prospects of fuel-battery hybrid-electric aircraft are analysed in Chapter 5, highlighting the integration implications of fuel-battery hybrid-electric propulsion system at aircraft level in terms of aircraft size, potential reduction in emissions, change in vehicular efficiency as well as identifying suitable market segment range for their application.

Chapter 2

Hybrid-Electric Technology State-of-the-Art and Beyond

State-of-the-art and mid- to long-term development in hybrid-electric technology for propulsion system of transport category aircraft are reviewed in this chapter. The objective is to describe the different topologies considered for hybrid-electric propulsion system and to provide the technological level assumed for the components constituting the propulsion system. This knowledge lays out the basis for the development of the methods in Chapter 3 and for the integrated performance analysis of the advanced aircraft concepts featuring hybrid-electric propulsion systems investigated in Chapter 5. The topological options for the layout of hybrid-electric propulsion systems are described in Section 2.1. By representing the combinatorial variety of component chains, the components constituting hybrid-electric propulsion systems are introduced and the architectural layouts are conceptualized. The relevant characteristics of the electrical components are reviewed in Section 2.2 discussing the technological state-of-the-art level and the development perspectives. The potential key enabling technologies for the deployment of electric power drives to transport aircraft are identified in Section 2.3. Finally, the application of hybrid-electric technology to aircraft propulsion is reviewed in Section 2.4.

2.1 Hybrid-Electric Propulsion System Topology

The narrative presented in this section reflects the argumentation published in [14, 15]. Figure 2.1 illustrates a comprehensive representation of the most relevant combinatorial variety of propulsion systems featuring an electric drive application by distinguishing between the components (or component chains) generating the shaft power and the devices consuming it. Electric approaches to aircraft propulsion system are known as hybrid-electric and universally-electric [10]. Hybrid-electric means intrinsically that electric power is used in combination to at least one additional power source. Universally-electric implies that the propulsion and power systems rely solely on electrical energy. Focusing on the propulsion system, the consumer of the power is the propulsive device. For transport aircraft, the required thrust is

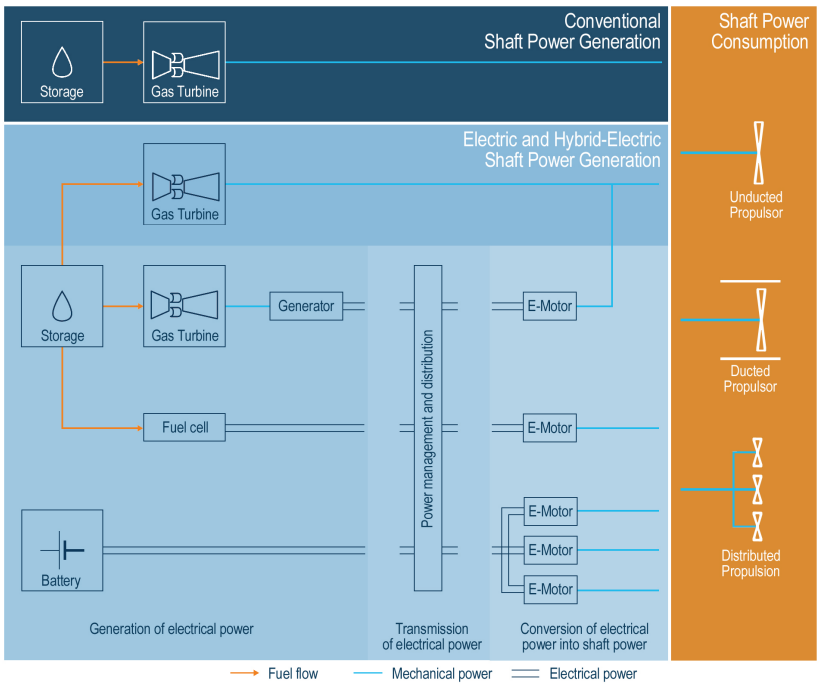

Figure 2.1: Conventional, hybrid and universally-electric propulsion system topology [14]. Adapted from [16]

.

provided by unducted or ducted-propulsors. For a conventional fuel-based propulsion system, a reciprocating engine or a gas-turbine are typically considered. The shaft power is created by converting chemical energy resulting from the combustion of the fuel into mechanical power through an aero-thermodynamic process.
In an electrical propulsion system, shaft power is produced through a process that can be subdivided into the generation, the distribution and the conversion of electrical energy into mechanical power as represented in Figure 2.1. For the electrical energy generation, the following devices or their possible combinations are most commonly considered to provide the electrical power:

- an electrochemical battery which converts stored chemical energy into electric energy as detailed in Section 2.2.3.1,
- a fuel cell generating electrical power through chemical reaction facilitated by a fuel (such as liquid hydrogen) and oxygen as developed in Section 2.2.3.2,
- a generator, driven by a conventional fuel powered combustion engine, which converts mechanical power into electric power. This arrangement is commonly known under the terminology of turboelectric (see Section 2.1.1).

Even if not explicitly shown in Figure 2.1, supercapacitors or flywheels could be also considered to provide electrical power [17].

The role of distributing the electrical power is realized by the power management and distribution (PMAD) which conveys and monitors the electrical energy from the energy sources to the consumers (see Section 2.2.2). The PMAD is typically composed of controllers, converters, rectifiers, inverters, cables, electrical buses and circuit breakers. Optimum layout of the PMAD system results from the analysis of level of working voltage, system efficiency, mass, bill-of-material, reliability and maintenance under constraints of abnormal mode of operation. Another important aspect related to the electrical system layout is the integration of the thermal control and regulation system to provide for every operating condition an appropriate thermal environment to the electrical and power electronics components. It is essential to consider thermal management in the early design phase of the integrated electric drive as it has strong implications to the design of the propulsion and power systems [18, 19]. Finally, the useful electrical power needs to be converted into shaft power in order to drive the propulsive device. In electrical system architectures, this role is adopted by an electric motor (see Section 2.2.1). It can drive by itself the propulsor device directly or through a gear-box. As illustrated in Figure 2.1 it can also be mounted to the shaft of a combustion engine to support its operations. Due to the nature of the electric energy which can be easily partitioned, the field of distributed propulsion aiming at improving structural-aero-propulsive integration, is often considered with hybrid-electric and universally-electric approaches (see Section 2.3.2).

2.1.1 Serial Hybrid System

In a serial hybrid, only the electric motor is combined to the shaft of the propulsive device [20]. The different power chains are combined together to an electric power node. The main power chains considered in a serial propulsion system for transport aircraft are represented in the region entitled “Generation of electrical power” in Figure 2.1. The most common serial arrangement is known as full turboelectric [6, 21–23]. In a pure turboelectric system, the electric power is produced by a generator driven by a combustion engine commonly a gas-turbine. The main advantage claimed is the improvement of the propulsion system efficiency. As the generation of power and the consumption of power are decoupled in a turboelectric system, the gas-turbine operation is now independent of the operational constraints of the propulsor [21, 24]. Enhancement in propulsion system efficiency results from the separate optimization of the gas-turbine core efficiency and the propulsor efficiency. However the transmission efficiency is penalized due to the accounting of the efficiency of the additional electric components composing the propulsion system architecture.
Because of the greater bill-of-material related to the additional electrical components in the propulsion chain, the weight of the system is expected to increase compared to a conventional propulsion system [21]. An improvement in overall aircraft efficiency can only be achieved if the increase in propulsion system efficiency and the enhancement in aero-structural-propulsive integration through the integration of turboelectric propulsion systems compensate the aforementioned negative effects.
In a serial system, fuel-cells and batteries are considered as means for generating electrical energy. Serial arrangements combining combustion engines, batteries and fuel-cells are also

considered [16] to draw the advantages of each of the system in order to achieve greater system performance to the detriment however of a greater system complexity.

2.1.2 Parallel Hybrid System

In a parallel system, the electric motor and the combustion engine are both mounted on the shaft of the propulsive device [20]. A common parallel system approach is realized by installing an electric motor on the low-pressure compressor shaft of a gas-turbine in order to support its operations [25–27]. The source of electrical energy and power to drive the electric motor can be provided by battery or fuel-cell. Parallel hybrid system powered by batteries will be the focus of aircraft sizing and integrated assessment in Section 5.3 and Section 5.4. If integrated to an existing gas-turbine, the concurrent utilization of the electric motor influences the operational characteristics of the gas-turbine. As a result the gas-turbine can be forced to operate into part-load leading to a degradation of its efficiency [27]. The change in gas-turbine efficiency due to different part-power operations resulting from the utilization of an electric motor is demonstrated in Section 5.3. In addition, the change in the operating line of the gas-turbine components can reduce the surge margin. Moreover, detailed system integration analysis are required for the implementation of an electric motor in the environment of a gas-turbine.
Another recent approach for a parallel system is the so-called “integrated system” [28, 29]. It consists of electrifying part of the core cycle of a gas-turbine. For instance, the electrification of the high-pressure compressor stages of a gas-turbine was proposed by Schmitz and Hornung [30]. Still in a pioneering phase, few publications are currently available on this topic.

2.1.3 Partial Hybrid System

In a partial hybrid system, at least one propulsive device is driven conventionally by a combustion engine while the other propulsive devices are driven directly by electrical motors [20]. In order to overcome the challenges related to the operation and integration of a parallel system, a partial parallel hybrid system was proposed by Pornet and Isikveren [31]. The electric motor and the propulsive device named “electrical fan” is integrated in addition to the combustion based engines as indicated in Figure 2.2. Fuel-cells or batteries can be selected as energy and power source to drive the electric motors. The integrated performance analysis of this partial parallel hybrid system is assessed in Section 5.5. In view of improving the overall vehicular efficiency, the electrical fans can be distributed to take advantage of distributed propulsion technology through tight aero-propulsive-structural integration. In addition to the potential benefits gained by distributing the electrical fans, this approach offers numerous advantages compared to mounting the electric motor on the low-pressure shaft of the gas-turbine. In this partial parallel hybrid system, the design and the operation of the conventional and electrical system are independent. The complex implications resulting from the interactions between the electric motor and the gas-turbine operations are consequently avoided. Moreover, the overall efficiency of the propulsion system can be optimized by operating the conventional and the electrical system close to their peak efficiencies. Finally,

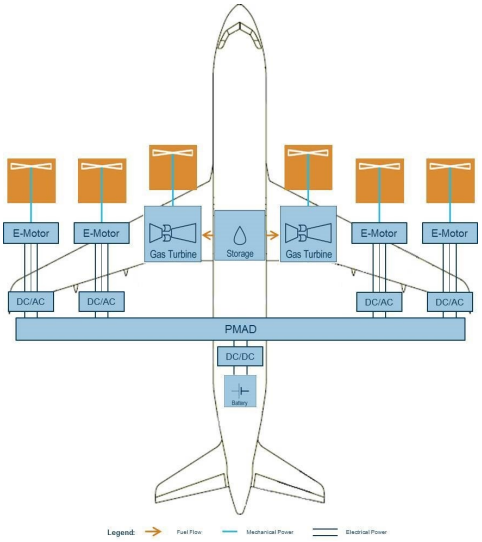

Figure 2.2: Partial parallel hybrid system

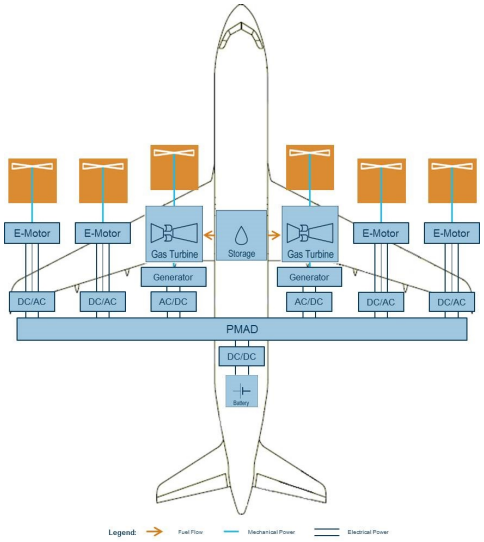

Figure 2.3: Partial turboelectric system [15]

it reduces the system complexity and beneficially avoids the integration challenges of the electric motor within the gas-turbine environment.

An evolution of this topology is a partial turboelectric system. Instead of having a complete independent electrical system, part of the electrical energy is produced by the gas-turbines through generators driven by mechanical power off-takes. The generators provide electrical energy to one or several electric fans. A schematic representation of this arrangement is illustrated in Figure 2.3. The additional provision of the electric power reduces the technological level requirement imposed to the electro-chemical energy sources. It enables also the deployment of optimum energy management schemes considering charge sustaining and charge depleting strategies of the batteries [32, 33]. Charge sustaining strategy enables for instance to operate the gas-turbine close to its optimum efficiency by utilizing any excess power to drive the generator and to recharge the battery during the mission.

2.2 Electrical Propulsion System Components

The pre-design evaluations of hybrid-electric propulsion system at aircraft level proposed in Chapter 5 are based on first-order linear models of the electrical components. These models rely on the following characteristics.

- The gravimetric specific power, p, the amount of power delivered per unit of mass, is a relevant parameter for sizing as it determines the mass of the components according to the power requirement.
- The volumetric specific power (or power density), ρ, the amount of power delivered per unit of volume, is a relevant parameter for integration as it defines the volume displacement required to install the component.

- The efficiency of the components, η, ratio of the useful power to the input power, is a relevant parameter for the system performance as it enables to quantify its overall efficiency and its losses.
- For energy sources, the gravimetric specific energy denoted as e, the amount of energy contained per unit of mass, is another important sizing parameter as it defines the mass of an energy source or of an energy storage required to deliver a given amount of energy.

The technological level assumed for these characteristics are reviewed for each components constituting the electrical system in the following sections.

2.2.1 Electric Motor

For aircraft application, high gravimetric specific power and efficiency of electric motors are of importance along with high volumetric specific power. Current conventional electric motors for aircraft application exhibit specific powers up to 5 kW/kg [34] and efficiency value around 95% [35]. When considering application requiring several megawatts, HTS technology is one interesting option [7, 8]. The characteristic of HTS technology is discussed in 2.3.1. Replacing the rotor and/or the stator of the electric motor architecture with HTS material leads to a significant increase in specific power [7] as well as improvement in efficiency. In contrast to conventional electric motors whose specific power remains nearly independent of the size, HTS electric motor specific power increases with power [36]. HTS electric motors are expected to achieve specific power exceeding 15 kW/kg and efficiency above 99% (cooling system not included) in the power and rotational range speed required for transport aircraft [6, 7, 37, 38]. HTS technology is assumed for the electric motor architecture constituting the hybrid-electric propulsion systems investigated in Chapter 5.

2.2.2 Power Management and Distribution System

The distribution and the management of the electrical energy from the energy source to the multiple electric consumers on-board the aircraft is performed by the PMAD system. This system is generally composed of:

- Cables that transmit the power through the electrical system. While using conventional technology for the power cables would result in heavier weight, HTS cables are projected to reach a specific weight of 9.2 kg/m [39] and by dropping the resistivity to zero offer a transmission efficiency of almost 100% (see Section 2.3.1). An important design consideration is the influence of the pressure change on breakdown voltage according to the Paschen's law [40] which determines the amount of insulation and shielding required.
- Circuit breakers, which protect the system from short circuits. In any high power system, semiconductor devices known as solid state power controller (SSPC) are used to control the power supplied to a load and to prevent fault current. State-of-the-art

SSPC yields specific power of around 28 kW/kg [41]. Projecting the evolution of the technology towards 2030, a specific power level of 44 kW/kg can be assumed with an efficiency of 99.5% [42].

- Converters, rectifiers and inverters which are used to convert the current between direct current and alternate current. State-of-the-art converter or inverter exhibit specific powers of 11 kW/kg and an efficiency of 97% [43]. By extrapolating the conventional technology evolution pace, a projected specific power value of 20 kW/kg in year 2030 was predicted by Vratny [42]. A model of a cryogenic inverter including cryocooler quoted by Brown [6] yields a specific power value of 25 kW/kg and an efficiency value of 99.5%.
- Controllers monitor functions to identify overload of electric device like the electric motor or the battery (also called the battery controller unit). Identical value in terms of specific weight and efficiency as cited for the converter or inverter can be assumed for the state-of-the-art [43] and for the projected value [38, 42].

The layout of the PMAD architecture is a complex task as it requires considering any abnormal modes to ensure provision of the electric energy to the vital, essential and non-essential systems. Moreover, the operations of the PMAD require the establishment of control strategies for power allocations schedule and distribution protocols. The final architecture selection results from an optimization process whose objectives are the minimization of system weight, volume and bill of material while maximizing the system efficiency for a given or a bandwidth of power requirements under the constraint of abnormal modes, system complexity and maintenance.

2.2.3 Electric Energy and Power Device

Besides utilizing a generator driven by a conventional combustion engine to convert mechanical energy into electrical energy, the two main devices considered for hybrid-electric propulsion system for transport aircraft are batteries and fuel-cells. The characteristics of these devices and their potential development are detailed in the following sections.

2.2.3.1 Battery

Batteries are expected to play a decisive role in advanced electric propulsion systems to provide electric energy at a high efficiency. The evolution of specific energy and specific power will determine the feasibility of a battery based electric propulsion system for commercial air transportation. The specific energy and specific power of batteries are not independent characteristics and will be determined during the battery design [44]. As a result, the combined enhancement of the specific energy and the specific power turns out to be a greater technological challenge than the single criterion optimization. Additional aspects such as specific energy density, efficiency, deterioration behaviour over time, life-cycle, operating temperature, discharge behaviour, safety, reliability and environmental sustainability need

also to be considered when selecting the battery technology [45]. Lithium battery technology is regarded as the most promising option for aircraft application. State-of-the-art lithium battery offers specific energy of circa 200 Wh/kg at cell-level [46]. In terms of power capability, specific power of around 2000 W/kg can be delivered [46]. Scaling up lithium battery technology in view of application in aircraft propulsion system is challenging due to the high power and high energy requirements. Extensive research activities are expended to develop the performance of batteries. The efforts focus mainly on improving the electrodes characteristics, notably by working on material properties and morphology, as well as enhancing the electrolyte properties [45, 47]. Specific energy of around 400 Wh/kg is predicted to be achieved at cell-level through future progress in lithium battery technology [48].
Through combinatorial association of potential advanced cathode and anode materials, achieving specific energy at cell-level in the range of 1000 Wh/kg to 1500 Wh/kg was declared feasible by Kuhn et al. [16][49] in the mid- to long-term. Future breakthrough in battery technology might also be achieved by re-thinking entirely the battery concept as indicated by the development of open battery systems like zinc-air, aluminium-air and lithium-air [47, 50]. Lithium-air battery demonstrates the highest theoretical specific energy with a estimated value of 1000 Wh/kg at cell-level [48, 51]. However, significant technological progress needs to be achieved to overcome the associated challenges and to mature the technology for industrial application. Long term strategy establishes a market readiness for a horizon of year 2030 [52].
The achievement of required voltage and current output levels is obtained by connecting the battery cell in series and in parallel into a so-called battery pack [42]. Additional weight for the housing and wiring of the battery cells into the battery pack needs to be taken into account for integration at aircraft level. The gravimetric specific values at system level are consequently reduced compared to the values quoted at cell-level. Theoretical analysis indicating housing and wiring weights accounting up to 30% of the battery pack can be found in [48].
Batteries are considered as a means to provide electrical energy and power for hybrid-electric system. The high efficiency level of a battery is the main advantage for its utilization. However, as the gravimetric specific energy of advanced batteries is expected to remain eight times lower than fossil fuel based on complete system exergy analysis [53], the integration of a battery system at aircraft level results in large detrimental weight sizing cascading effects which degrade the vehicular efficiency. The integrated performance implications of batteries as an electrical energy and power device for the propulsion of transport aircraft are thoroughly investigated in Chapter 5.

2.2.3.2 Fuel-Cells

Fuel-cells are electrochemical devices that convert the chemical energy contained in fuels into electrical energy. The different types of fuel-cells are categorized by the chemical reactions occurring at the anode and the cathode as well as by the type of electrolyte. The fuel-cells considered for aircraft application are the commercially available proton exchange membrane powered by hydrogen and the under development solid oxide fuel-cells. When supplied by

hydrogen, fuel-cells do not emit any carbon dioxide as the product of the chemical reaction is only water and heat, making fuel-cells applications to aircraft propulsion attractive for the achievement of the aviation goals introduced in Section 1. The required output power is reached by assembling the fuel-cells into a stack [54]. The suitable operational conditions for fuel-cells are provided by auxiliary systems referred to as the balance of plant. According to different sources compiled by Gradwohl [55], the balance of plant results in an 75% increase of the fuel-cells stack mass for state-of-the-art technology [56] while for advanced fuel-cells it could represent 50% of the fuel-cells stack mass [57]. The main disadvantage of fuel-cells is the relatively low specific power. As summarized by Gradwohl [55], the specific power for state-of-the-art fuel-cells related to continuous power is 1.24 kW/kg at stack level and 0.71 kW/kg at system level [55]. According to technological projection of advanced fuel-cells, specific power related to continuous power is estimated to reach 1.5 kW/kg at stack level and 1.0 kW/kg at system level [57]. In terms of efficiency, advanced fuel-cells are projected to exhibit an efficiency of 55% at system level [16]. However in addition to the low power density of fuel-cells stack, the challenges of integrating fuel-cells in aircraft propulsion system lays in the operations with hydrogen as a fuel. The safety issues related to the utilization of hydrogen, the detrimental integration impact of hydrogen tanks at aircraft level and the infrastructural complexity to supply hydrogen to airport remain as drawbacks. Consequently, the unique utilization of fuel-cells to provide the propulsive power requirement of transport aircraft is viewed as challenging [58].

2.3 Enabling Technologies for Hybrid-Electric Propulsion System

Technologies considered as key enablers for the deployment of electric drives to the propulsion system of transport aircraft are discussed in this section. It follows the argumentation published by Pornet [15]. The application of superconductivity to electric propulsion system is first reviewed in Section 2.3.1 followed by a discussion about distributed propulsion technology in Section 2.3.2.

2.3.1 Superconducting Technology

In view of the large electrical power requirement for propulsion system, superconductivity is seen as an enabling technology for electric drive application [8, 24, 59]. Superconducting materials exhibit a theoretical absence of electrical resistance when operated below critical temperature [60]. The utilization of HTS materials enables to improve gravimetric specific power and efficiency of the electrical components which explains the interest of implementing HTS technology in aircraft propulsion systems. The most common application of HTS materials at this point in time is for electric motors [5, 7, 59] and for the transmission cables [6, 22]. Malkin and Pagonis [61] debated also the development need of fully superconducting network (including the fault management, protection and switching implications). For HTS material, the critical temperature lies between 60 K and 77 K [62]. Operation at cryogenic

temperatures requires consequently a cooling system which typically features either cryogenic stored liquid hydrogen or nitrogen used as coolant [59] or a cryocooler [6, 38]. The operation at cryogenic temperature leads to many challenges related to the application of superconducting technology to transport aircraft. Besides handling safety related issues [63], the negative integration impacts of the cryogenic tank on aircraft design [64] and the infrastructural modifications required to supply the liquid hydrogen to the operated airports are issues that remain challenging [65, 66]. Implementing superconducting technology at aircraft level will result from a trade between performance, efficiency and system weight as well as complexity, reliability and maintenance.

2.3.2 Distributed Propulsion and Boundary Layer Ingestion Technology

The nature of the electric energy which can be easily distributed among different consumers makes distributed propulsion and boundary layer ingestion (BLI) [67, 68] key technologies for hybrid-electric aircraft. The level of aero-structural benefits through tightly coupled integration of the propulsive device with the airframe gained by distributed propulsion [69–76] and by BLI technology [23, 37, 77–81] will be decisive to leverage the drawbacks associated with electric propulsion systems.

2.4 Hybrid-Electric Technology Application to Aircraft Propulsion

The development of hybrid-electric aircraft has already started in the domain of the general aviation and it concerns mostly one to two-seater aircraft in the experimental category. A growing interest of leading industrial players towards hybrid-electric propulsion technology is evident with initiatives supported notably by Airbus and Siemens [82]. Application of hybrid-electric propulsion to general aviation enable to gain experimental data on key electrical component characteristics and system behaviour, to mature the technology and to learn about scaling potentiality. Hybrid-electric propulsion technology will evolve with respect to the maturation and the development of electric technology towards application for commuter, regional and narrow-body transport aircraft [69]. The pace at which the integration of hybrid-electric technology will occur, depends on the rhythm of technological improvement and breakthrough as well as the scaling pattern of the electrical components. The evolution of the electrical component technology will determine the feasibility of hybrid-electric propulsion system to transport aircraft application.
The introduction of hybrid-electric technology has dramatically opened the design space in aircraft design due notably to the expansion of combinatorial possibilities at system and at aircraft level which is expected to change the contemporary aircraft design paradigm [69]. Hybrid-electric technology is still in its pioneering age. On the one hand, knowledge about electric components technology for propulsion application and scaling laws need to be further gained. On the other hand the methodological approaches, modelling capabilities, program analysis and tools to scrutinize the design space, to perform the trade studies and to define

optimum integrated system configurations are still yet to be developed. An added complexity to the application of hybrid-electric technology is the possible synergistic implications in combination to other technology like distributed propulsion through greater integrated airframe and propulsion system interface and other aircraft systems like the secondary power system. The lack of methods and the highly interlaced complex context help to explain that up to this date only a few assessments of advanced aircraft concepts employing hybrid-electric propulsion technology have been published. When reviewing the compendium of hybrid-electric transport aircraft concept published by Pornet [14] hybrid-electric aircraft concept utilizing battery-fuel system either in serial or parallel topology were proposed with the NXG-50 [83] and the Sugar-Volt [25]. Turboelectric distributed approach were investigating on a blended wing body (BWB) configuration with the BW-11 [77] and the N3-X [23] concepts. No clear evidence can be drawn in view of defining the optimum hybrid-electric system architecture, optimum integration at aircraft level or optimum aircraft configuration. It reinforces the need for the development of methodology and framework for hybrid-electric aircraft analysis to assess the full potential of this technology.

Chapter 3

Methods for Sizing and Performance of Hybrid-Electric Aircraft

The conceptual design methods developed for sizing and performance of hybrid-electric aircraft are presented in this chapter. This construct relies on traditional methods employed for the design of conventional kerosene fuel-based aircraft. To fully understand the departure of the developed methods, the conventional methods are reviewed first in Section 3.1. Conventional design methods for sizing and performance analysis of fuel-based aircraft are offered in many textbooks [84–91]. The objective of this chapter is therefore not to provide a complete description of the traditional methods but rather to emphasize on the characteristics which lay the foundation for the design methods of hybrid-electric aircraft. The extension of the methods for sizing and performance analysis of hybrid-electric aircraft are then presented in Section 3.2.

3.1 Traditional Sizing and Performance Methods

Sizing is the process of finding a constrained balance between size, thrust and energy requirements of an aircraft under the objective of fulfilling all its transport tasks specified in the aircraft top-level requirements (ATLRS) and of the compliance with the airworthiness regulations. Further definitions of the aircraft sizing process can be found in the compendium proposed by Nam [92]. At least two main categories of requirements can be itemized for the sizing and performance of an aircraft:

- performance constraint requirements which relate the thrust to the size of the aircraft in order to fulfil point performance requirements,
- mission performance requirements which relate the amount of energy to the size of the aircraft in order to transport a design payload along a specified design mission.

A third category of requirements deals with operating economics objectives to offer a competitive product to the market. As highlighted in Chapter 1, further requirements of future

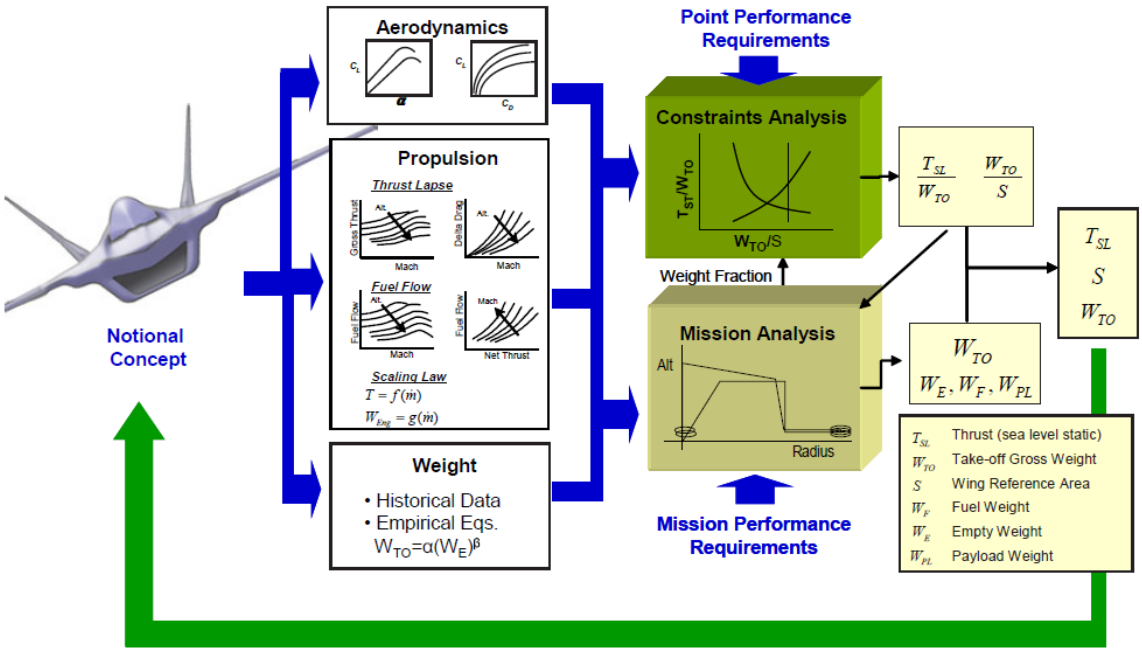

Figure 3.1: Traditional sizing and performance process according to Mattingly [90]

aircraft products will need to respect environmental regulations expressing, for instance, limitations in terms of emissions.
An illustration of the traditional sizing and performance process proposed by Mattingly et al. [90] is represented in Figure 3.1. Referring to this figure, the conventional methods will be described in the following. It is worthwhile noting that the two aforementioned itemized categories are represented in Mattingly's design process under the titles "constraints analysis" and "mission analysis". As indicated in Figure 3.1, the aircraft performance assessment relies on the determination of aircraft aerodynamic quality, propulsion characteristics and weight properties. The representation of these disciplines in conceptual design is discussed in the following paragraphs.

3.1.1 Geometric Properties

From an initial cloud of concepts, the most promising candidate, named in Figure 3.1 the "notional concept" or often refer to as the "baseline", is selected following a qualitative and/or a semi-quantitative downselection process. An initial estimation of the geometrical properties of the main components such as the fuselage, the wing, the empennage, the propulsion system and the landing gears is the first step in the process. The detailed geometrical description of each component and their arrangement serve as inputs for the methods used to estimate the aerodynamic and weight characteristics of the concept. Initial geometric data are generally based on known aircraft referred as reference aircraft.
In the context of the hybrid-electric aircraft concepts investigated in Section 5, traditional geometrical descriptions of aircraft components were utilized. For the parallel hybrid propul-

sion systems investigated in Section 5.3 and in Section 5.4, the integration of the electric motor was assumed not to change the geometrical properties of a conventional turbofan nacelle. Generic geometric properties of a short-duct fan cowling were applied for the integration of the electrical fans in the case of the partial parallel hybrid system assessed in Section 5.5. Classical geometrical constraints were set such as the minimum engine ground clearance which affects the design of the landing gear for under-wing mounted engines.
The outer mould-line of the fuselage was kept identical to the reference aircraft. Since the electro-chemical sources being stored within the cargo area, the cargo volume was set as a new geometrical constraint for the storage of the energy system as discussed in Section 5.1. The electric components of the PMAD were assumed to be contained within the fuselage and the wing volume.

3.1.2 Aerodynamic Properties

The drag polar determines the total drag of an aircraft according to a given flight state and operating lift condition. An accurate prediction of the drag polar is essential to determine the aerodynamic quality of the aircraft and its performance. As illustrated in Figure 3.1, it is typically characterized by the operating coefficient of lift (C_L) versus the coefficient of drag (C_D) curve. A decomposition of the total drag can be elaborated in profile drag, lift-induced drag, interference drag, wave drag and trim drag. In conceptual design, component build-up functions are commonly used for the calculation of the profile drag [86, 87]. Simplified lifting line theory is generally implemented for the calculation of the lift-induced drag contribution. The wave drag computation can be determined using methods developed by Gur et al. [93]. Interference drag is generally determined according to the arrangement of the components [86, 87].
The integration of the hybrid-electric propulsion system evaluated in Chapter 5 does not rely on tight aero-airframe couplings nor on BLI technology. The traditional "thrust-drag" bookkeeping is consequently kept for aircraft performance evaluations. Besides the traditional components sizing effects on the aircraft drag computation, the integration of hybrid-electric propulsion system at aircraft level implies capturing incremental profile drag including nacelle profile drag of additional electrical fans. According to conventional aerodynamic methods [86, 87], the nacelle drag contribution of the electrical fans was added by component build-up functions to the drag of the overall propulsion system.

3.1.3 Propulsion System Properties

In traditional performance programs, the propulsion system properties are interfaced using multi-dimensional tables comprising the thrust and the fuel flow characteristics as shown in Figure 3.1. The thrust tables determine the maximal thrust available at a given flight state defined by the International Standard Atmosphere deviation (ΔISA), the Altitude (Alt) and the Mach number (M). They are established with respect to the different engine ratings typically maximum take-off rating (MTO), maximum climb rating (MCL), maximum cruise rating (MCR) and maximum continuous rating (MCO). The fuel flow table determines the

fuel consumption of the engine according to the flight state ΔISA, Alt, M and the thrust (T). A single fuel flow table covering the complete flight envelope is implemented and is used for each segment of a mission. The traditional method restricts consequently the powerplant integration to propulsion system based on fuel only. It is an example of a limitation that needs to be levered in order to assess hybrid-electric propulsion systems which rely on electricity as an additional energy source. The thrust and energy characteristics of hybrid-electric propulsion system need consequently to be captured according to the properties of the conventional turbomachinery and the electrical components composing the propulsion chain. This is in the focus of the methods developed in Section 3.2.3.
The thrust tables and the fuel flow table of conventional propulsion systems are generally created in expert modules using, for example, gas turbine simulation software, such as the Numerical Propulsion System Simulation (NPSS) [94], the GasTurb performance software (GasTurb) [95] and the PRopulsion Object Oriented SImulation Software (PROOSIS) [96], or, by using simplified analytical methods as summarized by Nita [97]. A rubberised engine model is generally implemented in conceptual design phase for purposes of sizing. In concrete terms, this modelling approach assumes that the thrust lapse behaviour and the fuel flow characteristics remain unchanged with respect to the size of the engine in a given thrust or power range.

3.1.4 Weight and Balance Properties

The weight and balance properties of an aircraft include the determination of its mass, centre of gravity and inertia. In conceptual design, the mass of aircraft components is typically estimated using semi-empirical and empirical equations based on regression models built on historical data of existing aircraft as indicated in Figure 3.1. These methods are found in classical aircraft design text books [84, 86, 87, 98] and are very efficient to quickly investigate small to modest departure from the seed aircraft used to build the regression models. According to the estimated weight and with respect to the geometrical properties of the components and their spatial arrangement the centre of gravity and inertia of the aircraft can be determined.
Weight modelling of electrical components for propulsion chain is not available in traditional aircraft environment. The mass of each electrical components composing the electric propulsion system needs consequently to be calculated and interfaced at aircraft level. Methods for estimating the mass of the electrical components are detailed in Section 3.2.3. At aircraft level, the mass of the electrical components is mapped to the overall propulsion system mass using weight component build-up methods. The spatial allocation of the electrical components and systems affects the computation of the aircraft centre of gravity and inertia.

3.1.5 Aircraft Performance Analysis

Knowledge of the aerodynamics, propulsion system and weight properties of the aircraft enables the resolution of flight mechanical equations for aircraft performance analysis. The "constraints analysis" consists of point performance computations to assess the fulfilment

of performance requirements. The outcome of the performance constraints analysis determines a design that best fulfills a given sets of performance requirements emanating from the airworthiness regulations and from the ATLRS. In the conceptual design phase, the main criteria analysed for low-speed performance are the take-off and landing field length as well as the regulatory climb gradients (second segment climb, approach climb and landing climb). For high-speed performance, the residual rate-of-climb at top-of-climb (usually 300 fpm residual specific excess power) and at en-route cruise condition (usually 100 fpm residual specific excess power), the drift-down performance during climb or cruise in the event of an engine failure as well as the 1.3 g buffet onset limitation are considered. In addition, the aircraft flight envelope is defined by investigating the different flight performance limitations such as stall limitation, ceilings and maximum speed operation limitation as for instance the dive speed (VD)/dive Mach number (MD), the maximum operating speed (VMO)/maximum operating Mach number (MMO), the flaps extended speed (VFE) and the landing gear operating speed (VLO)/landing gear extended speed (VLE). In conceptual design the plot of thrust loading versus wing loading represented in Figure 3.1 is of great interest as it enables to establish the design space by drawing the constraints emanating from the performance requirements according to combinations of thrust and wing loading. At a given flight state and for a given weight and drag, the performance constraints analysis relies on the mapping of the available thrust. The methods to interface the thrust characteristics of hybrid-electric propulsion system are established in Section 3.2.4.1. The analysis of the performance constraints of hybrid-electric aircraft are discussed in Section 3.2.5.
The item named "mission analysis" consists of evaluating the integrated performance of an aircraft along set of specified missions. It determines the evolution of the aircraft weight during the different segments of the mission according to the propulsion system characteristics and the resulting fuel consumption. The main result of the mission analysis is the total fuel weight required to perform the aircraft missions. The assessment of hybrid-electric aircraft requires the mapping of the electrical energy consumption during the mission analysis. The methods to interface the energy characteristics of hybrid-electric propulsion system are developed in Section 3.2.4.3. The mission analysis is discussed in Section 3.2.5. The design mission enables sizing the aircraft according to the stage length and the design payload defined for a given flight technique in the ATLRS according to the process detailed in the following paragraph. The analysis of the off-design mission performance enable notably the construction of the payload-range diagram which describes the working capacity of the aircraft.

3.1.6 Aircraft Sizing Process

According to an initial maximum take-off weight (MTOW), wing-loading ($MTOW/S_{ref}$) and power-to-MTOW ($P/MTOW$) (or thrust-to-MTOW ($T/MTOW$)), the sea-level static thrust or power of the conventional system P_{SLS} and the wing reference area (S_{ref}) are determined. Concerning the P_{SLS} and with respect to the design and off-design performance and efficiency characteristics of the combustion engine, the thrust tables and the fuel flow table are generated for different engine ratings. Depending on the wing reference area S_{ref}, the sizing strategies of the aircraft components and with respect to the implemented scaling

laws and semi-empirical equations the weight of the aircraft components is determined. According to the size of the aircraft, the drag polar characteristics of the aircraft are computed. Knowing the aerodynamic efficiency, the aircraft weight and the propulsion system characteristics, the mission performance and the point performance requirements are analysed. The mission analysis module determines the total fuel mass required to fulfil the design mission. If the total fuel mass is higher than the first estimated fuel mass, the MTOW is increased by iteration. If the performance constraints are not fulfilled, the aircraft sizing parameters namely $P/MTOW$ and $MTOW/S_{ref}$ are adjusted through iteration. Once the mission performance requirement and the performance constraints are fulfilled, the aircraft is finally sized for its transport task.
The consideration of hybrid-electric propulsion system disrupts the traditional sizing process. In particular, the introduction of an additional electric propulsion chain requires the establishment of new design variables to determine the power and energy split between the conventional and the electrical system as described in Section 3.2.1. The total fuel mass is currently the single energy-based constraint assessed in the traditional methods. An additional energy constraint needs to be established in the aircraft sizing process to take into account the electrical energy available and in order to size subsequently the electric energy and power devices as discussed in Section 3.2.6. Moreover the presence of electrical components constituting to the propulsion requires the development of components sizing methods and principles as established in Section 3.2.7.

3.2 Methods for Sizing and Performance of Hybrid-Electric Aircraft

The traditional methods presented in the previous section are adequate for the sizing of conventional transport aircraft. Proprietary or commercially available aircraft performance programs or design environments such as the FLight Optimization System (FLOPS) [99], the Aircraft Performance Program (APP) [100], the aircraft analysis tool Piano (Piano) [101] and the PACELab Aircraft Preliminary Design (PACELab APD) [102] rely on these conventional methods. However, the integration of novel propulsion systems such as hybrid-electric propulsion system disrupts the conventional sizing and integrated performance analysis process. The methods need to be extended to capture the specifics of the nature of hybrid-electric propulsion system within the aircraft sizing and performance environment.
Due to the integration of an electrical system contributing to the propulsion, new system design parameters come into place. The design variables specific to the sizing of hybrid-electric propulsion systems need to be identified and implemented within the sizing process of the aircraft. The design parameters for the sizing of hybrid-electric aircraft are defined in Section 3.2.1. In the traditional design environment electrical system components are not available. The characteristics of the electrical system components need consequently to be modelled and interfaced to the aircraft sizing environment. The electrical propulsion components characteristics are described at system level in Section 3.2.3. The mapping of the components and the integration within the design environment are discussed in Section 3.2.4.

Besides weight and volume of the systems, the design and off-design thrust characteristics within the operational envelop are of importance for integrated performance analysis. The modelling of the thrust capabilities of hybrid-electric propulsion systems is described in Section 3.2.4.1.
Another challenge to consider for the integration of hybrid-electric propulsion systems in traditional performance programs is the mapping of the electric energy within the integrated mission performance computation. As indicated previously, the traditional methods present a limitation as the fuel flow table can only take into account fuel flow characteristics. The method proposed to extend the implementation of the propulsion system properties in order to interface the electric energy is discussed in Section 3.2.4.3. In addition, the presence of multiple energy and power systems which contribute each to the propulsion of the aircraft requires the establishment of power management strategies. Power sharing strategies enable managing the energy pathways between different sources of the hybrid-electric propulsion system. As only one common fuel flow table is implemented to represent the characteristics of the propulsion system for the complete mission, the establishment of power management strategies according to the different operational settings of the hybrid-electric propulsion system cannot be considered within the traditional approach. The extension of the method to determine the energy characteristics of hybrid-electric propulsion system are discussed in Section 3.2.4.3. The interfacing of the hybrid-electric propulsion characteristics in terms of thrust and energy requirement with the flight performance module is described in Section 3.2.5.
The sizing characteristics of electric components are elaborated in Section 3.2.6 and the overall sizing process of hybrid-electric aircraft is described in Section 3.2.7. According to the physical behaviour of the components constituting the hybrid-electric propulsion architecture, the new constraints emanating from the specificities of hybrid-electric propulsion system are highlighted in the sizing process.
Finally, metrics for vehicular efficiency assessment have to be introduced as the consumption of electric energy needs to be taken into account in the total energy evaluation of the aircraft. New figures-of-merit for the evaluation of vehicular efficiency and for the establishment of optimum flight techniques of hybrid-electric aircraft are derived in Chapter 4.

Beyond the state-of-the-art in traditional conceptual design methods, several pre-design methods for the sizing of hybrid-energy aircraft have been published to this date. A review of the published literature which contributed to the development of pre-sizing methods for hybrid-electric aircraft can be found in Perullo and Mavris [12]. These methods rely mainly on first-order equations for the modelling of the aircraft and the propulsion system. The method is based on linear scaling laws assuming constant gravimetric and constant efficiency values irrespective of scale and operational conditions. As the result these methods cannot account for detailed secondary effects such as the interactions between the operations of the electrical system and the conventional propulsion system; for instance, the efficiency change of the gas-turbine forced to operate into part power due to the concurrent utilization of an electric motor in a parallel topology. The aim of this chapter is the development of conceptual design methods which resolve the identified shortcomings of the contemporary methods and which offer higher fidelity modelling than pre-design methods through the use of efficiency

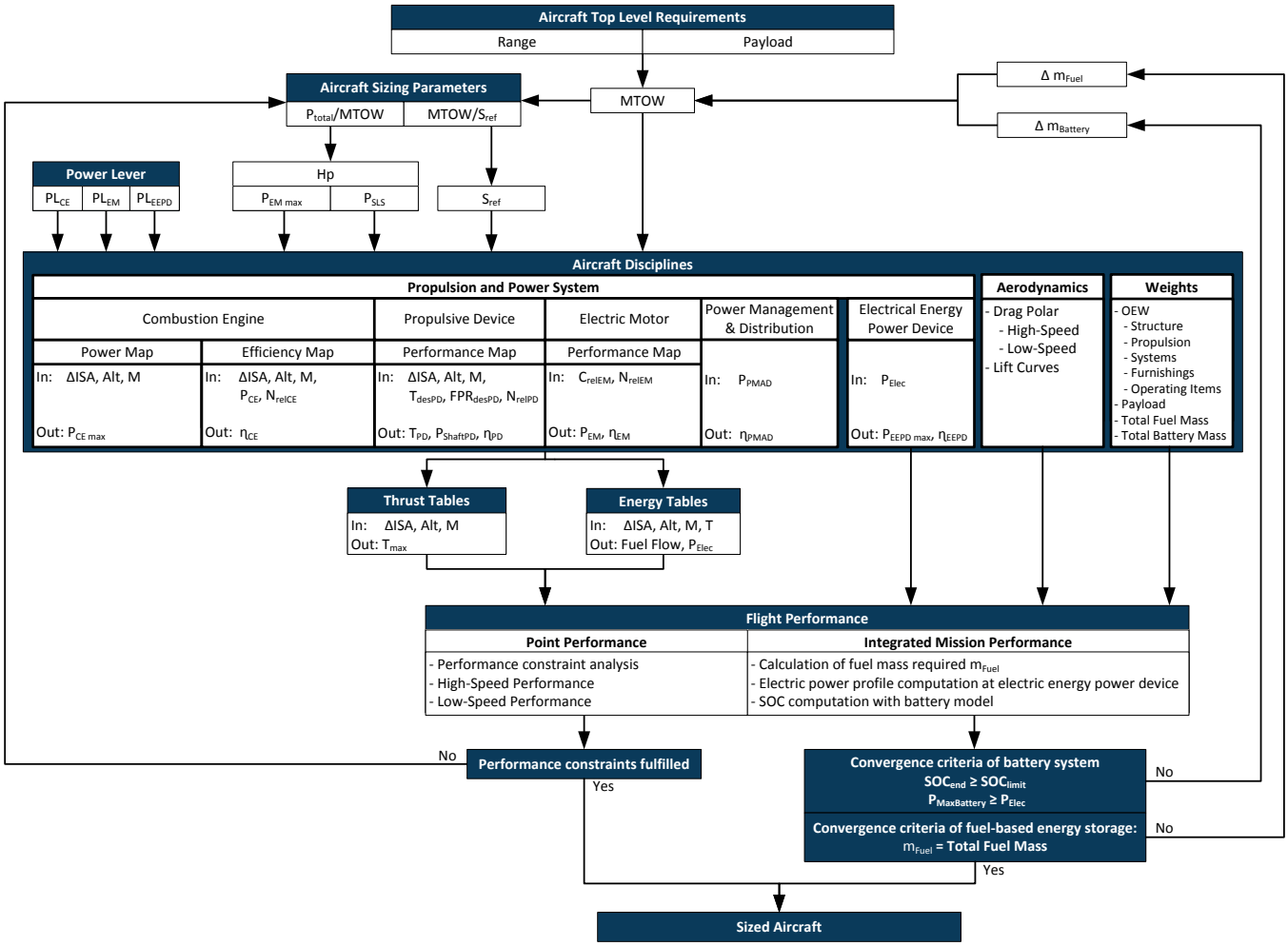

Figure 3.2: Synthesis procedure for hybrid-electric aircraft. Adapted from Pornet et al. [27].

and performance maps as well as physics-based models to determine the behaviour of the hybrid-electric propulsion system components. However, due to the utilization of legacy programs in industry, the methods are developed with the constraint of being implemented in a traditional sizing and performance program environment. The synthesis of the methods developed, adapted from Pornet et al. [27], is illustrated in Figure 3.2. It represents graphically the introduced design parameters for the design of hybrid-electric aircraft, the characteristics of the hybrid-electric propulsion components and subsequent integration within the aircraft sizing environment, the process for the integrated performance analysis as well as the iteration scheme for the sizing of hybrid-electric aircraft.

Figure 3.2 will be described in the subsequent sections to present in detail the overall hybrid-electric aircraft design and sizing procedure. The procedure is applicable to each of the hybrid topologies discussed in Section 2.1. In the case of a partial parallel hybrid system, a more practical procedure can be represented. This approach followed for the integrated perform-

ance evaluation of a partial parallel hybrid system in Chapter 5 is represented in Figure A.1. The application of the methods will be exemplified on a serial, parallel and partial parallel hybrid system topology. In order to illustrate the parameters that will be used in the description of the methods, a lay-out of these topologies is represented in Figure 3.3, Figure 3.4 and Figure 3.5 respectively.

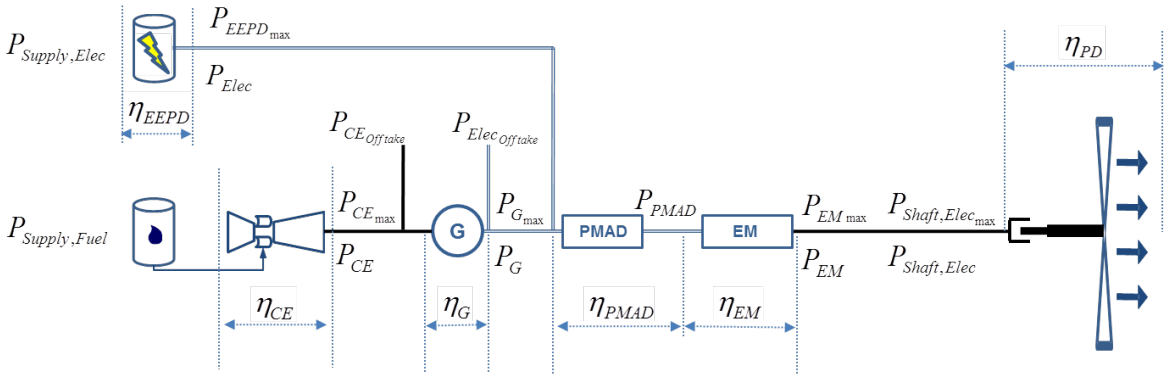

Figure 3.3: Serial hybrid propulsion system

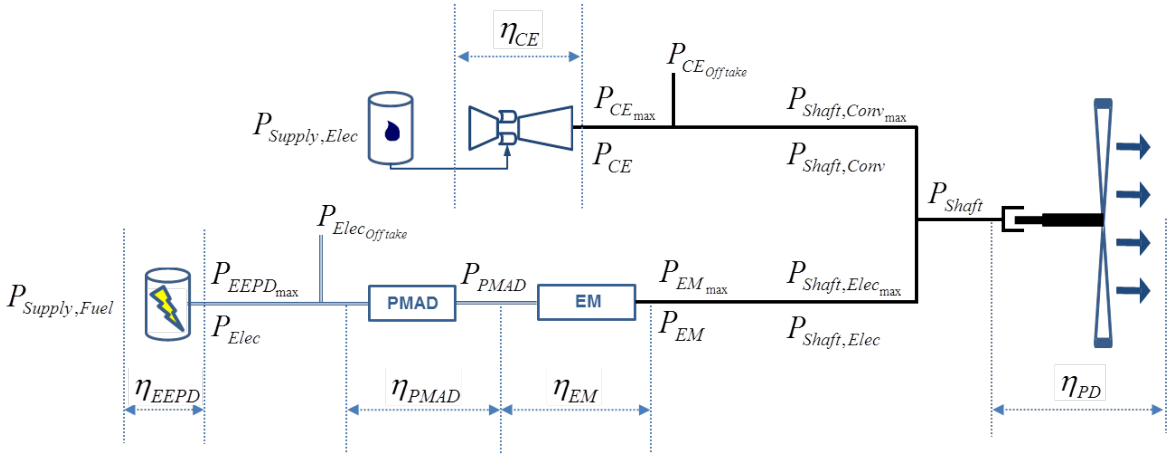

Figure 3.4: Parallel hybrid propulsion system. Adapted from Pornet et al. [27].

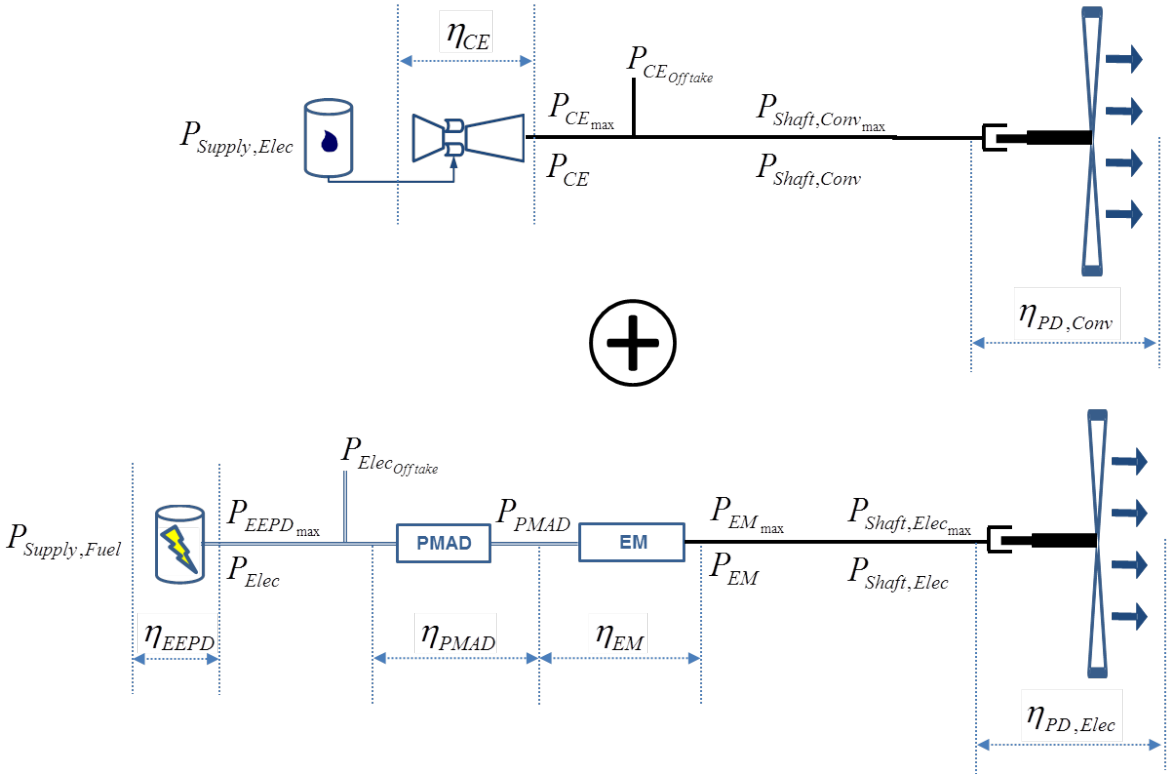

Figure 3.5: Partial parallel hybrid propulsion system

3.2.1 Design Variables

The design variables for hybrid-electric propulsion system need to be established within the sizing process. It was demonstrated that the parametric description of a dual energy propulsion system requires the establishment of two fundamental algebraic parameters namely the degree-of-hybridization for power (H_P) and the degree-of-hybridization for energy (H_E) [13, 103]. The parameter H_P describes the amount of electric power relative to the overall total power. Commonly, the installed power or the useful power (power measured at the propulsive device) is quoted. The convention chosen herein is to denote the degree-of-hybridization for power referring to the useful power with the parameter H_{Puse}. The degree-of-hybridization for power is a new design variable in the sizing process as it determines according to the overall power requirement, the sizing power of the electrical power system. The design parameter H_P and H_{Puse} are consequently represented in Figure 3.2 and in Figure A.1 respectively. The methods for sizing the hybrid-electric propulsion system according to H_P are described in Section 3.2.6.
The parameter H_E is the ratio of electrical energy consumed over the total energy; it characterizes the so-called energy split. The quantity H_E is evaluated along a specified segment or mission. The parameter $H_{E\text{block}}$ refers, for instance, to the block mission. For a given hybrid-electric propulsion system architecture, H_E is the outcome of the sizing as well as the energy and power management strategy defined for the hybrid system along a selected

mission.
H_P and H_E will be used to draw design charts while investigating the design space of hybrid-electric aircraft concepts as illustrated in Chapter 5. Different cases can be considered to exemplify the value bounds of these parameters. A conventional kerosene-based gas-turbine propulsion system is characterized by an H_P and an H_E equal to zero. A pure serial hybrid-electric architecture where only electric power is provided at the propulsive devices but the energy storage is solely kerosene based is described by an H_P equals to 1 and H_E equals to 0. Finally an universally electric aircraft where the energy storage is batteries only is denoted by an H_P of 1 and an H_E of 1.

3.2.2 Methods for System Integration at Aircraft Level

The approach selected for the integration at aircraft level of the component and system is based on the utilization of multidimensional tables which represent the main physical characteristics of the model. A multidimensional table consists of a matrix of dimensions $l \times c$. The dimension c is given by the sum of the number of inputs n and the number outputs m. The outputs are computed through full-factorization of the inputs values. The l dimension of the matrix is obtained by multiplying the vector length by the n input. These multidimensional tables are typically generated by engineering expert modules outside of the aircraft design environment and often given the moniker “map” or “deck”. The inputs and outputs are selected such that the characteristics and physical behaviours of the system are properly modelled and interfaced at aircraft level. Within the aircraft environment the values of the output parameters are calculated using interpolation techniques. The determination of the input vector dimensions and the use of appropriate interpolation methods to capture the sensitivity of the system at aircraft level rely on engineering judgement. This interfacing technique was selected as it is already part of the legacy aircraft programs notably to determine the propulsion system characteristics. This technique has to be seen as a solution to interface the systems. It does not have any implications in the way the process for sizing of hybrid-electric aircraft is established. Other techniques can be entertained, such as, using co-simulation by linking the expert modules directly to the aircraft sizing and environment. Another avenue is the implementation of dynamic-link libraries which represents an executable of the expert modules interfaced within the aircraft platform. The selection of the interfacing methods depends upon the integration flexibility of the aircraft environment to enable the couplings as well as the extent of computational effort.

3.2.3 Methods for Propulsion Components Integration

The components and the topological combinations considered in the layout of hybrid-electric propulsion systems for transport aircraft application were established in Section 2.1. The quality of the assessment at aircraft level relies on the capability of capturing the component physical behaviour and scaling sensitivity. The objective of this section is consequently to describe the methods to interface the components characteristics at aircraft level. As illustrated in Figure 1.1, modelling of component characteristics is performed in external engineering

modules. They are referenced in the following sections for readers interested in knowing the details of the physics implemented in these models.

3.2.3.1 Methods for Turbofan Integration

The layout of hybrid-electric propulsion systems relies on conventional powerplants. For commercial transport aircraft, the most commonly used powerplant system is the turbofan. The relevant design parameters as well as the design and off-design performance of turbofans can be determined by using gas-turbine performance programs. In this thesis, advanced geared turbofan models were produced using the commercial software GasTurb [95]. The geared turbofans were sized at top-of-climb (TOC) under the conditions *ISA*, flight level (FL) 350 and M 0.78 at a MCL rating. In the context of integrated aircraft assessment presented in Chapter 5, a projected year entry-into-service (YEIS) of 2035 was considered. Cycle temperature and compression levels, component efficiencies as well as duct pressure losses reflect consequently the technology settings for the YEIS 2035. For consideration of turbine cooling, component efficiency and size impact, typical design laws were applied [104, 105]. Zero power off-take and zero bleed were assumed for flow path sizing due to the implementation of an all-electric non-propulsive power systems as discussed in Section 5.2.2. Off-design simulation was based on GasTurb [95] standard component maps. With respect to H_{Puse}, the turbofans are sized for varying levels of design thrust as illustrated in Figure A.1. Consequently, for more detailed modelling of the influence of the engine size on the thrust lapse and fuel flow characteristics, the sensitivity against the design thrust was considered.

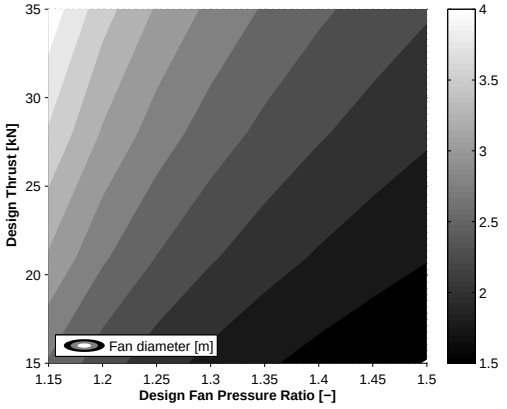

Figure 3.6: Fan diameter versus design thrust and design fan pressure ratio. Geared turbofan sized at *ISA*, FL 350, M 0.78.

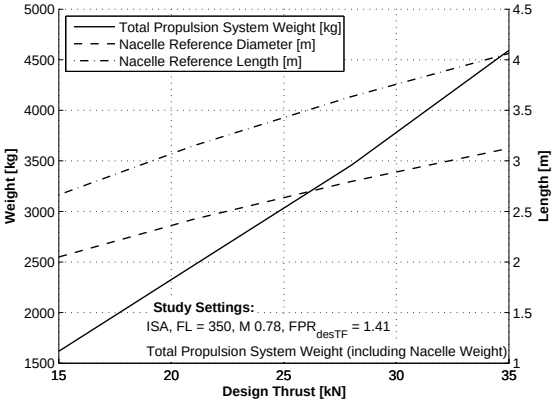

Figure 3.7: Propulsion system weight and geometry versus design thrust. Geared turbofan sized for design FPR 1.41 at *ISA*, FL 350, M 0.78.

A "design deck" was created to interface the main design parameters of the conventional powerplant at aircraft level with respect to the design thrust of the turbofan ($T_{des,TF}$) and the design fan pressure ratio of the turbofan ($FPR_{des,TF}$). The evolution of the fan diameter of the turbofan ($D_{Fan,TF}$) against $T_{des,TF}$ and $FPR_{des,TF}$ is drawn in the contour plot

in Figure 3.6. The weight of the engines was predicted according to geometric component dimensions and performance parameters based on conceptual design methods developed by Seitz et al. [104]. Figure 3.7 represents the evolution of the total propulsion system weight (including the nacelle weight) versus the $T_{des,TF}$ for a geared turbofan sized at a $FPR_{des,TF}$ of 1.41. The nacelle reference diameter and length, illustrated in Figure 3.7, were estimated based on a typical slenderness ratio of a generic turbofan nacelle.
For each of the engines, the maximum thrust and fuel flow characteristics were provided in form of multi-dimensional tables in order to interface the conventional powerplant characteristics at aircraft level. In the approach adopted, the thrust and fuel flow tables are a function of the design thrust. The integration of these tables within the aircraft sizing environment is illustrated in Figure A.1. The maximum thrust characteristics at MCL rating are illustrated in Figure 3.8 for a geared turbofan sized at a $T_{des,TF}$ of 21 kN. The design at *ISA*, FL 350, M 0.78 conditions and at a MCL thrust setting yielded to a thrust specific fuel consumption ($TSFC$) of 13.24 g/kN/s for the engine designed at a $T_{des,TF}$ of 35 kN, and, of 13.30 g/kN/s for the engine designed at a $T_{des,TF}$ of 15 kN. This demonstrates the relatively small scale effect on the engine efficiency. The $TSFC$ characteristics of the geared turbofan models are represented in Figure 3.9 at cruise condition *ISA*+10°C, FL 350 and M0.76 against the thrust setting for each design thrust. It can be observed that the scale effect has also a small influence on the $TSFC$ characteristics. The so-called $TSFC$ bucket extends in these models from around 70% to 100% of the maximum thrust. This characteristic is important as it determines the efficiency evolution of the geared turbofan in part load operation during cruise. Within the bucket, the geared turbofan runs close to its maximal efficiency under the given flight conditions.

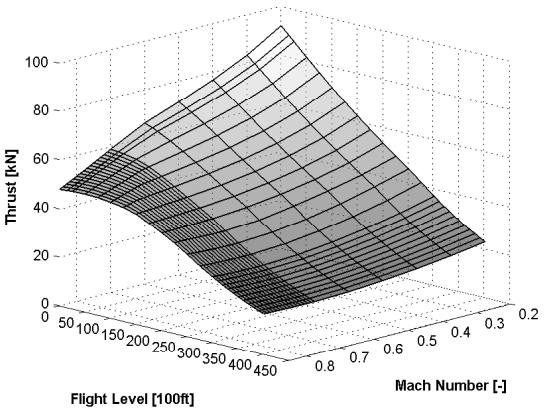

Figure 3.8: Thrust characteristics under MCL rating. Geared turbofan sized for a design thrust of 21 kN and a design FPR of 1.41 [31].

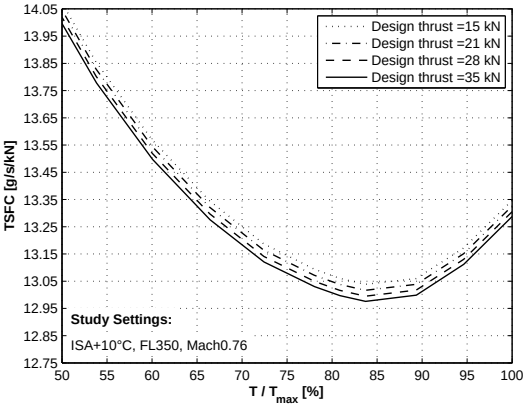

Figure 3.9: TSFC characteristics of the geared turbofans sized for a design FPR of 1.41 at cruise condition *ISA*+10°C, FL 350 and M 0.76 [31].

3.2.3.2 Methods for Propulsive Device Integration

The relevant design parameters of the propulsive device can be determined by using gas-turbine performance software. The characteristics of the propulsive device implemented in this thesis are discussed based on a zero-dimensional performance model of a ducted fan developed by Steiner et al. [106]. The model relies on classical gas dynamic theory and standard compressor theory. Based on this model, a design deck of the propulsive device was created to determine the main design parameters with respect to the design thrust of the propulsive device ($T_{des,PD}$) and the design fan pressure ratio of the propulsive device ($FPR_{des,PD}$). The flow path sizing was performed at TOC design conditions *ISA*, FL 350, M 0.78. According to the design thrust and the $FPR_{des,PD}$, the geometry of the propulsive device is generated. The evolution of fan diameter of the propulsive device ($D_{Fan,PD}$) is represented as a contour plot in Figure 3.10.

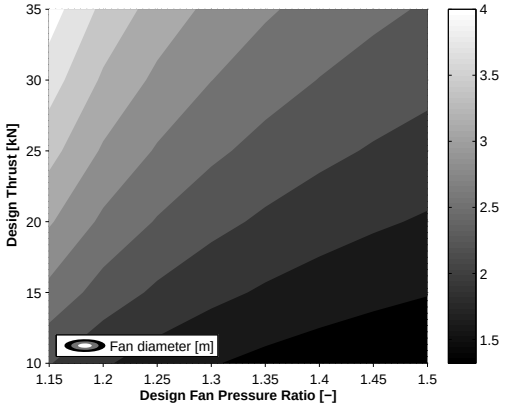

Figure 3.10: Ducted fan diameter versus design thrust and design fan pressure ratio. Ducted fan sized at ISA, FL 350, M 0.78.

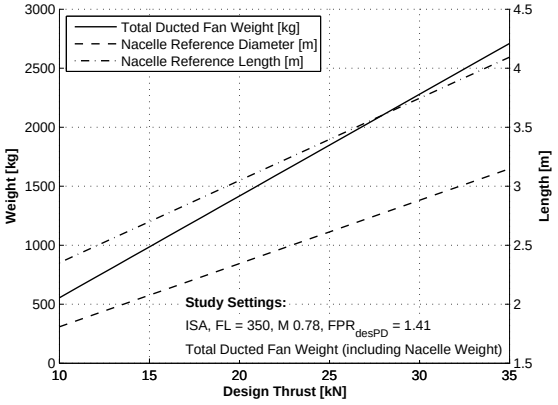

Figure 3.11: Ducted fan weight and geometry versus design thrust. Ducted fan sized at ISA, FL 350, M 0.78 and design FPR 1.41.

For the integration of a ducted propulsive device, the nacelle reference length and diameter are determined and interfaced with the geometric module of the aircraft environment. These parameters can be determined by correlations developed in [107, 108] or by using scaling methods of a known reference nacelle geometry. For sake of consistency the correlations used for the sizing of the short-duct fan cowling of the turbofan were also implemented for the sizing of the ducted-fan nacelle geometrical properties. The nacelle geometrical reference parameters are represented in Figure 3.11 versus $T_{des,PD}$. The geometry of the ducted propulsive device is also interfaced at aircraft level with drag component build-up functions to determine profile drag generated by the nacelle. Based upon the geometrical properties of the propulsor and nacelle, the weight of the system can be predicted using weight correlations as published in [107, 109], or, on conceptual design methods as developed by Seitz et al. [104] which were used for the prediction of the ducted fan weight as represented in Figure 3.11.
Besides geometrical dimensions and weight modelling, the determination of the design and off-

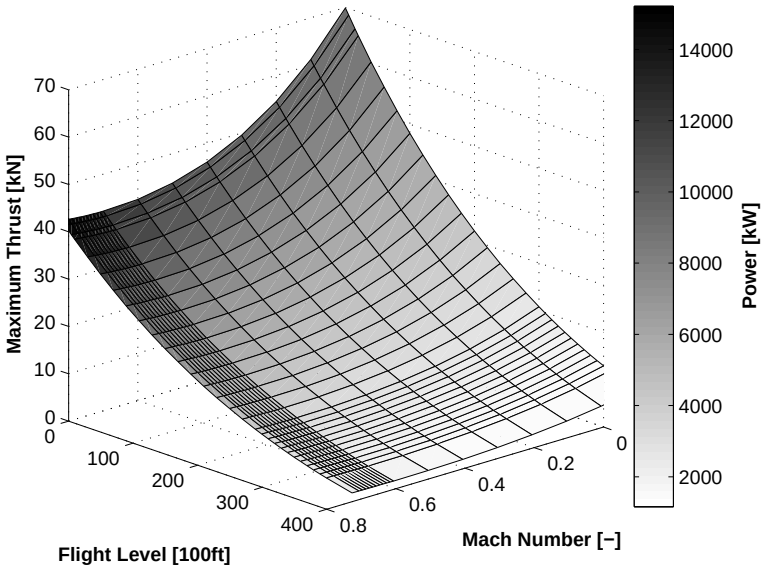

Figure 3.12: Maximum thrust of ducted-fan sized for 10 kN at ISA, FL 350, M 0.78 and design FPR 1.41

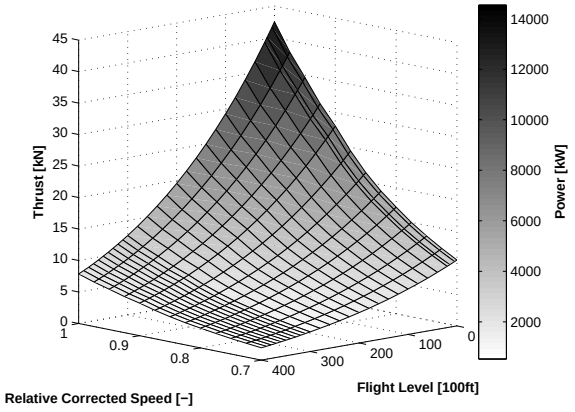

Figure 3.13: Ducted fan off-design thrust characteristics versus altitude at M 0.78

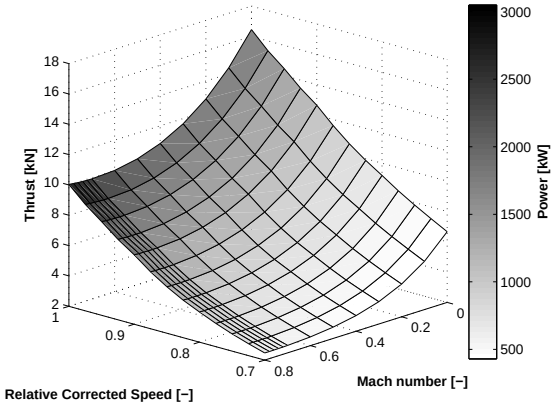

Figure 3.14: Ducted fan off-design thrust characteristics versus Mach at FL 350

design performance characteristics of the propulsive device are of importance for integration at aircraft level. A standard component map of the fan was incorporated from GasTurb [95] for performance calculations. At a given flight state according to the conditions ΔISA, Alt and M, the available thrust T, the shaft power required (P_{Shaft}) and the efficiency of the propulsive device, η_{PD}, need to be interfaced at aircraft level. P_{Shaft} is related to the efficiency of the propulsive device (η_{PD}) according to Equation 3.1. The determination of η_{PD} implies the evaluation of the propulsive and transmission efficiencies of the propulsive device [104]. The transmission efficiency is composed of the fan polytropic efficiency, as well as the intake, ducting and nozzle losses [106].

$$P_{Shaft} = \frac{T \cdot M \cdot a}{\eta_{PD}} \tag{3.1}$$

The maximum thrust characteristics and the required shaft power are illustrated in Figure 3.12 for a ducted-fan model sized at ISA, FL 350 and M 0.78, for a design thrust of 10 kN and a fan design pressure ratio of 1.41 [31]. The thrust level is controlled by the variation of the relative corrected speed of the propulsive device ($N_{rel,PD}$). Per definition, $N_{rel,PD}$ is equal to 1.0 at the design point. At a given flight state and $FPR_{des,PD}$, the thrust level decreases when reducing $N_{rel,PD}$. The variation of thrust according to $N_{rel,PD}$ is representing for varying altitude in Figure 3.13 for M 0.78 and for varying Mach number in Figure 3.14 at FL 350. The setting of $N_{rel,PD}$ is a function of the power available at the shaft of the ducted fan P_{shaft}. In other words, the level of thrust achievable depends upon the amount of power delivered at the shaft of the ducted fan. If not enough shaft power is delivered at the shaft by the power system, the relative speed of the fan is decreased in order to match the shaft power requirement according to the off-design power characteristics of the ducted fan model. As a result of the reduction in $N_{rel,PD}$, the available thrust decreases. These characteristics are determining for the sizing of the electric motor as discussed in Section 3.2.6.2 and applied in Section 5.5. The propulsive device characteristics are mapped at aircraft level with the parameters ΔISA, Alt, M, $T_{des,PD}$, $FPR_{des,PD}$ and $N_{rel,PD}$ as inputs, and, T, P_{Shaft} and η_{PD} as outputs. This map interfaces the performance characteristics of the propulsive device to the aircraft sizing and performance environment as illustrated in Figure 3.2.

3.2.3.3 Methods for Combustion Engine Integration

The layout of hybrid-electric propulsion system for transport aircraft commonly combines an electrical system with a conventional system driven by a combustion engine installed either in a serial or in a parallel arrangement as discussed in Section 2.1. The geometry, weight and performance characteristics of a combustion engine need consequently to be modelled. For transport aircraft application, a ducted gas-turbine is most likely to be implemented. A geometrical description of turbo-engine components based upon the parametrisation of the engine flow path can be modelled according to methods developed by Seitz [110]. For the prediction of component weights, semi-empirical methods are based upon the geometrical description as described in [110]. For the mapping of the performance characteristics of the combustion engine, the development of the required maps is discussed in the following

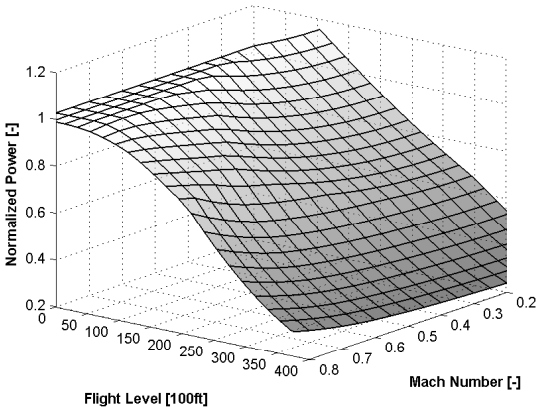

Figure 3.15: Normalized power characteristics of a generic turbo-engine in ISA condition

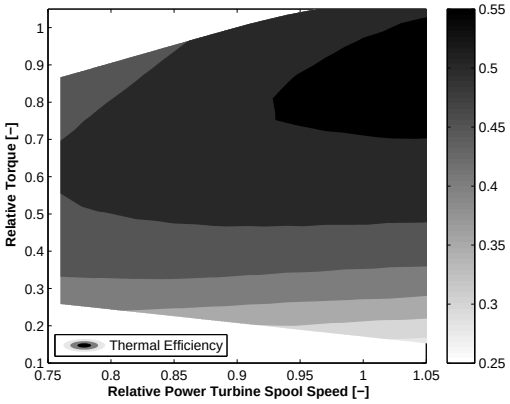

Figure 3.16: Efficiency contour characteristics of a generic turbo-engine at ISA, FL 350 and M 0.78

based on a generic model of a turboshaft. This model was implemented in the context of the integrated aircraft performance assessment of a parallel system in Section 5.3. The fuel consumption characteristics of the turbo-engine are directly coupled with the efficiency of the combustion engine (η_{CE}). As expressed in Equation 3.2, the fuel flow (FF) is directly related to the η_{CE} via the shaft power of the combustion engine (P_{CE}) and the fuel heating value (FHV).

$$FF = \frac{P_{CE}}{FHV \cdot \eta_{CE}} \tag{3.2}$$

As illustrated in Figure 3.2, two performance maps were generated, the power map and the efficiency map. The performance modelling requires determining the maximum power available which can be produced at a given flight state (ΔISA, Alt, M). The maximum power of the combustion engine ($P_{CE,max}$) is a function of the intrinsic power lapse characteristic of the engine according to ΔISA, Alt and M. For purpose of sizing, a rubberised engine modelling approach can be followed by normalizing $P_{CE,max}$ with a reference power typically chosen as the sea-level maximum static power (P_{SLS}) as discussed in Section 3.1.3. The normalised power map of the implemented turboshaft model is represented in Figure 3.15 at *ISA* condition versus the altitude and the Mach number. By normalizing the map, the assumption is made that within a given power range, the power lapse characteristics remain invariant with the engine size. When sizing the engine (varying P_{SLS}), different levels of power can be achieved in order to match the power requirement of the propulsive device to produce the required thrust.

The thermal efficiency characteristics of the implemented turboshaft model are illustrated against the relative torque and the relative power turbine spool speed. In view of interfacing the fuel consumption characteristics at aircraft level, the η_{CE} is mapped as a function of the flight state ΔISA, Alt, M, the relative corrected speed of the combustion engine ($N_{rel,CE}$)

and P_{CE} with the efficiency map. It is integrated within the aircraft design environment as shown in Figure 3.2. Following the rubberised engine modelling approach, by normalizing P_{CE} with a reference power, the efficiency characteristics of the engine are assumed to be independent of the engine size in a given power range.

3.2.3.4 Methods for Electric Motor Integration

In contrast to air-breathing machines, the performance of an electric motor is independent of the flight state. The characteristics of an electric motor can be represented in a torque and speed diagram (for a given direct current voltage value) as illustrated in Figure 3.17 [38]. The operational envelope is drawn according to three limitations: the maximum torque limitation being represented by the region I; the maximum power and the maximum rotational speed limitations indicated by the region II. These boundaries depend upon the technology of the machine and the design point selected. Methods for the calculation of the geometrical characteristics of the electric motor can be elaborated based on the electric motor components design as detailed by Vratny et al. [38]. Based upon the geometric properties of the components, the total weight of the electric motor is calculated using component build-up methods.

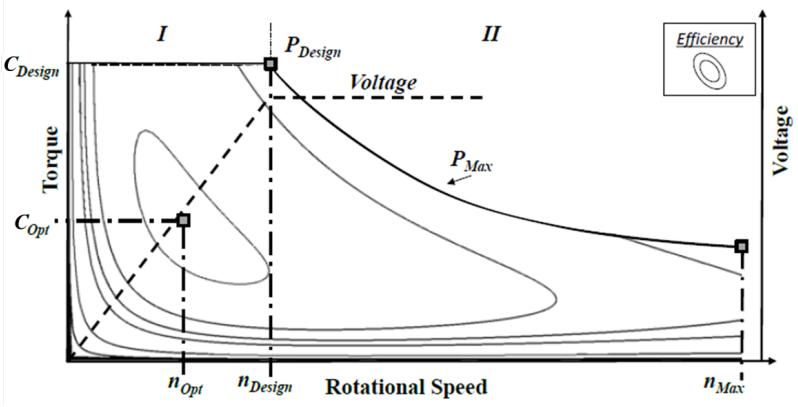

Figure 3.17: Generic design and efficiency chart of a conventional electric motor from [38].

The design and off-design power of an electric motor can be mapped at aircraft level according to the relative torque of the electric motor ($C_{rel,EM}$) and the relative speed of the electric motor ($N_{rel,EM}$) measured against the design point. With $C_{rel,EM}$ and $N_{rel,EM}$ the power of the electric motor (P_{EM}) is defined. Thermal limitations are considered using a thermal model to determine the achievable performance of the machine within the operating environment. The efficiency contours of a conventional electric motor are represented in the torque and speed diagram in Figure 3.17. Considering the different losses occurring within an electric motor namely the copper losses, iron losses, aerolic and frictions losses of the rotor, the efficiency of the electric motor (η_{EM}) can be mapped out for each operational point [38]. The efficiency and power characteristics of the electric motor can be consequently interfaced at aircraft level using a multidimensional table with $C_{rel,EM}$ and $N_{rel,EM}$ as inputs

and as outputs P_{EM} and η_{EM}. The interfacing of the electric motor performance using a performance map is represented in Figure 3.2.

In the framework of this thesis, HTS technology was assumed for the electric motor design. Simplified pre-design methods were implemented for the modelling of the electric motor. First order estimate of the weight and volume of the HTS motor were evaluated using linear scaling laws based on gravimetric and volumetric specific power values as discussed in Section 2.2.1. The sizing criterion of the electric motor was based on the power requirement at the selected design point. The matching of the electric motor with the propulsive device relies consequently on the power characteristics only. The torque and speed limitations were not considered in the design of the electric motor. Under the premise that the thermal environmental conditions of the electric motor are correctly managed by the cooling system, it was assumed that the maximum power of the electric motor ($P_{EM,max}$) is available at each point of the aircraft flight envelope. $P_{EM,max}$ drives consequently the thrust performance of the ducted fan according to the fan shaft power requirement as discussed in Section 3.2.3.2. The power requirement to maintain the HTS material below critical temperature were assessed based on relations established by Vratny et al. [38].
In the applications investigated in Chapter 5, the HTS electric motor is operated constantly or close to $P_{EM,max}$. The off-design efficiency characteristic of an HTS electric motor presented in [60] and [38] indicates that the efficiency of an HTS electric motor remains nearly constant in a range of rated part power from 5% to 100% and rated torque from 20% to 100% [104]. Hence, the efficiency of the HTS motor was assumed constant for all its operations. Appropriate values of electric motor efficiencies were taken from Section 2.2.1. This simplification is, however, only suitable for electric motors based on HTS technology.

3.2.3.5 Methods for Power Management and Distribution System Integration

In conceptual design, weight, volume and efficiency of the PMAD components are the most relevant parameters for the integration at aircraft level. These characteristics need to be established for each component constituting the PMAD system.
In this thesis, first order estimations of weight and volume were implemented based on linear scaling according to gravimetric and volumetric specific power. According to the layout of the PMAD and its sizing power-criterion, the total weight of the PMAD system is obtained by summing up the weight of each of its components. The efficiency of the PMAD components was assumed constant during the operations. The overall efficiency of the PMAD was determined by the product of each components efficiency. The efficiency of the power management and distribution system (η_{PMAD}) is mapped in the design environment according to power required at the PMAD (P_{PMAD}) as indicated in Figure 3.2.
With the availability of physics-based models of the PMAD components, the fidelity of the components modelling can be improved. For instance, off-design efficiency characteristics with respect to power variation can be interfaced at aircraft level. This is notably demonstrated by the physics-based models of an inverter and a controller developed by Vratny et al. [38] which enable to map the efficiency of these components within the required power range of the electric motor. More accurate weight predictions can be also achieved with the

development of component weight methods based on the number of switches constituting the inverter and controller [38].

3.2.3.6 Methods for Electric Energy and Power Device Integration

The methods for the integration of electric and energy power device (EEPD) in the aircraft sizing and performance process are discussed in the following. In view of determining the energy requirement, the efficiency characteristics of the EEPD need to be modelled according to the evolution of the electric power requirement at the EEPD, P_{Elec}. In addition, the maximal power which can be delivered by the EEPD is of importance to size the system with respect to the maximal power requirement occurring within the operating flight envelope. As represented in Figure 3.2, the EEPD performance are interfaced according to P_{Elec} as input and with the efficiency of the electrical energy and power device (η_{EEPD}) and the maximum power of the electrical energy and power device ($P_{EEPD,max}$) as outputs. Referring to Section 2.2.3, battery and fuel cell systems are considered as electric energy and power device in the layout of hybrid-electric propulsion system for transport aircraft. The modelling characteristics of the battery and fuel cell in view of generating these interfaces are described in Section 3.2.3.6.1 and in Section 3.2.3.6.2 respectively.

3.2.3.6.1 Methods for Battery System Integration The capability to deliver the energy and power requirement is related to the sizing of the battery system. The determination of $P_{EEPD,max}$ requires the description of the battery system sizing approach. By sizing the battery system, the total battery mass required to fulfil the energy and power requirements at aircraft level is determined according to the battery characteristics. In the following, the fundamental characteristics involved in battery system sizing are established first by assuming a constant efficiency of the battery system (η_{Bat}). In view of considering a variable η_{Bat} in the sizing of the battery system, a more sophisticated scheme using a physics-based model of a battery is then discussed. The latter approach is implemented in this thesis for the integrated evaluation of hybrid-electric propulsion systems.
The battery gravimetric specific energy at system level ($e_{Bat,Syst}$) and the battery gravimetric specific power at system level ($p_{Bat,Syst}$) are the key parameters in conceptual design for the sizing of the battery mass. According to the energy and power requirements at aircraft level, either the specific energy or the specific power is the sizing criterion for the battery mass. Assuming that the power profile of the electric power required at the battery system characterized by the parameter, P_{Elec}, is known, the total battery mass required is the maximum of the battery mass obtained either by the energy requirement criterion or by the power requirement criterion as formulated in Equation 3.3.

$$m_{Battery} = \max(m_{Battery\,energy}; m_{Battery\,power}) \tag{3.3}$$

where $m_{Battery\,energy}$ denotes the mass of the battery sized according to the energy requirement and $m_{Battery\,power}$ characterizes the mass of the battery sized according to the power

requirement.
Adapted from Vratny et al. [111] the sizing of the battery mass according to the electrical energy requirement is expressed in Equation 3.4 assuming a constant η_{Bat}. By integrating P_{Elec} over time, the total electrical energy required by the battery system is determined. As P_{Elec} is the electric power required by the battery system, this parameter does not include the efficiency of the battery itself. Consequently, η_{Bat} is considered in Equation 3.4 in order to compute the electrical energy supply. The amount of energy available in a battery is characterized by the battery state-of-charge (SOC). The SOC expresses the amount of energy available in percent of the total energy. To protect the battery from irremediable damage, the battery must not be discharged below a certain limit. The SOC limit is taken into account in Equation 3.4 with the term SOC_{limit}.

$$m_{Battery\,energy} = \frac{1}{\eta_{Bat} \cdot e_{Bat,Syst} \cdot (1 - SOC_{limit})} \int_{t_{initial}}^{t_{end}} P_{Elec}(t) \cdot dt \tag{3.4}$$

The maximal power required along the mission profile can turn out to be the criterion for sizing of the battery system mass. In particular, the high power requirement during takeoff or climb can represent the sizing case for the battery mass for transport aircraft sized for short design mission range [10]. The power which can be delivered by a battery is a function of the $p_{Bat,Syst}$. As a result, delivering a certain power level requires the installation of a given total battery mass, as formulated in Equation 3.5. In other terms, according to the total battery mass and $p_{Bat,Syst}$, Equation 3.5 determines $P_{EEPD,max}$.

$$m_{Battery\,power} = \frac{\max(P_{Elec})}{\eta_{Bat} \cdot p_{Bat,Syst}} \tag{3.5}$$

Assuming a constant η_{Bat} is suitable in conceptual design phase [111]. However, in order to enhance the level of fidelity of the battery modelling, the sensitivity of η_{Bat} was modelled in this thesis based upon a physics-based battery model developed by Vratny et al. [111]. Considering the evolution of η_{Bat} for a given power demand and SOC implies the evaluation of the voltage level and electric current. The input required by the battery model is the power profile which determines the electric power required P_{Elec} to be delivered by the battery system. According to the required electrical power and the battery SOC, the available output voltage at required discharge rate is calculated using the discharge characteristics of the battery cell [111]. With respect to the discharge rate fulfilling the power requirements, the battery SOC is calculated at each time step. In this way, the battery SOC at the end of the mission is determined. As indicated in Figure 3.2, if the SOC of the battery calculated at the end of the mission for an initial battery mass is below the SOC_{limit}, the battery mass is increased iteratively until the SOC constraint is met. The battery mass sized at aircraft level according to the energy requirements is consequently determined by iteration. The description of the iterative sizing loop is detailed in Section 3.2.7.
The sizing power criterion of the battery is evaluated with Equation 3.5 according to the

efficiency value of the battery calculated by the physics-based battery model. The battery mass interfaced with the aircraft model is finally determined by Equation 3.3. According to the sizing of the battery system, the integration of the physics-based battery model enables determining $P_{EEPD,max}$ and η_{EEPD} with respect to P_{Elec}.

3.2.3.6.2 Methods for Fuel Cells Integration The integration of a fuel cell as an energy and power device in hybrid-electric propulsion systems require the determination of the maximum power of the fuel cell system ($P_{FC,max}$) and the efficiency of the fuel cell system (η_{FC}) according to the electrical power requirement P_{Elec}. A first order approximation based upon an invariant efficiency value, gravimetric and volumetric specific power as highlighted in Section 2.2.3.2 can be used in first instance. Higher fidelity representation of the characteristics of the fuel-cells can be achieved with the integration of physics-based models. The mapping of η_{FC} can be established for instance on the basis of an analytical model of a fuel cell system developed by Gradwohl [55] according to the work published by Haji [112]. Considering the different types of losses namely the activation losses, the ohmic losses and the concentration losses, the voltage characteristics of a fuel cell is modelled according to the level of current [55]. As a result, the efficiency of the fuel cell is computed according to the amount of losses. In addition, the efficiency of the balance of plant is taken into account to establish the overall efficiency of the fuel cell system [55]. The output power of the fuel cell is calculated as the product of the current and the voltage. According to this analytical model, a multi-dimensional table can be produced with the electrical power required at the fuel cell system as input P_{Elec} and the efficiency of the fuel cell system as output η_{FC}. According to η_{FC}, the fuel flow of the fuel cell (FF_{FC}) required to provide the electric power during the mission is computed with Equation 3.6.

$$FF_{FC} = \frac{P_{Elec}}{\eta_{FC} \cdot FHV} \tag{3.6}$$

The maximal electrical power produced by the fuel cell system during the mission or within the flight envelope sets the fuel cell maximum power requirement $P_{FC,max}$ as shown in Equation 3.7.

$$P_{FC,max} = \frac{\max(P_{Elec})}{\eta_{FC}} \tag{3.7}$$

$P_{FC,max}$ determines the number of cells composing the fuel cell stack [55]. The weight of the fuel cell can be calculated according to methods developed by Gradwohl [55] considering the number of cells and the additional estimated mass resulting from the components of the balance of plant. The coupling of a physics-based model of a fuel cell enables the computation of $P_{EEPD,max}$ and η_{EEPD} according to P_{Elec} to interface the fuel cell performance with the aircraft environment as indicated in Figure 3.2.

3.2.4 Methods for Propulsion System Integration

In the previous section, the component models constituting the hybrid-electric propulsion system were considered independent of each other. According to a given hybrid-electric topology, the component characteristics need to be linked together to interface the performance of the propulsion system to the aircraft design environment. The calculation of the maximum thrust available and the determination of the energy consumed during the mission are the main aspects that the methods have to address as detailed in Section 3.2.4.1 and Section 3.2.4.3 respectively. The methods are described for the serial, parallel and and partial parallel hybrid topologies.

3.2.4.1 Thrust Characteristics

The determination of the maximum available thrust is the focus of the mathematical relations developed in the following paragraphs. According to the characteristics of the hybrid-electric propulsion system, the maximum thrust is computed at each flight state (ΔISA, Alt and M) for the different ratings MTO, MCL, MCR and MCO. The commonality with a traditional sizing and performance program is provided by the utilization of an identical thrust table format with ΔISA, Alt and M as inputs and T_{max} as output. This table enables the interfacing of the propulsion system thrust characteristics with the flight performance module as illustrated in Figure 3.2. The calculation of the maximum thrust for parallel, serial and partial parallel hybrid-electric propulsion system is detailed in Section 3.2.4.1.1, Section 3.2.4.1.2 and Section 3.2.4.1.3 respectively.

3.2.4.1.1 Parallel Hybrid System The equations provided for the parallel system were published by Pornet et al. [27]. The formulation of the mathematical relations is based upon the generic parallel propulsion system illustrated in Figure 3.4. For a hybrid-electric parallel system, the maximum thrust is determined by the sum of the maximum shaft power delivered by the conventional system ($P_{Shaft,Conv,max}$) and the maximum shaft power delivered by the electrical system ($P_{Shaft,Elec,max}$) available at the shaft of the propulsive device at each flight state as established in Equation 3.8,

$$T_{max} = \eta_{PD} \cdot \frac{P_{Shaft,Conv,max} + P_{Shaft,Elec,max}}{M \cdot a} \tag{3.8}$$

where η_{PD} is computed according to the propulsive device performance map described in Section 3.2.3.2. $P_{Shaft,Conv,max}$ is determined by Equation 3.9. The power lever of the combustion engine (PL_{CE}) determines the power setting of the combustion engine according to the maximum power available, $P_{CE,max}$ as expressed in Equation 3.10. PL_{CE} is introduced in the equation in view of conducting energy management strategy to adapt the utilization of the combustion engine according to the segment of the mission. In addition, the power off-take at the combustion engine ($P_{CE,Offtake}$) is taken into account in the determination of

$P_{Shaft,Conv,max}$. $P_{CE,max}$ is obtained according to the performance map of the combustion engine as established in Section 3.2.3.3.

$$P_{Shaft,Conv,max} = PL_{CE} \cdot P_{CE,max} - P_{CE_{Offtake}} \tag{3.9}$$

$$PL_{CE} = \frac{P_{CE}}{P_{CE,max}} \tag{3.10}$$

$P_{Shaft,Elec,max}$ is determined with Equation 3.11 by the limiting power between the power of the electrical motor P_{EM} and the $P_{EEPD,max}$ delivered at the shaft of the electrical motor. In this equation the efficiency chain determined by η_{EM} times the η_{PMAD} is considered. In addition, the electrical power off-take ($P_{Elec,Offtake}$) is taken into account. The maximal power output of the electric energy and power device is set by a controller. The regulation of the controller can be expressed in terms of a power lever of the electrical energy and power device (PL_{EEPD}).

$$P_{Shaft,Elec,max} = \min(P_{EM}, \eta_{PMAD} \cdot \eta_{EM} \cdot (PL_{EEPD} \cdot P_{EEPD,max} - P_{Elec,Offtake})) \tag{3.11}$$

P_{EM} is determined in Equation 3.12 according to the power lever of the electric motor (PL_{EM}) and $P_{EM,max}$. $P_{EM,max}$ is calculated according to the power map of the electric motor as described in Section 3.2.3.4.

$$P_{EM} = PL_{EM} \cdot P_{EM,max} \tag{3.12}$$

η_{EM} is determined according to the performance map of the electric motor as detailed in Section 3.2.3.4. η_{PMAD} is calculated according to the layout of the PMAD system as highlighted in Section 3.2.3.5. The maximum power available at the electrical energy and power device is determined in the case of a battery system according to the maximum power of the battery system ($P_{Bat,max}$) which can be established by the terms expressed in Equation 3.5. For a hybrid-electric propulsion system equipped with fuel cells, the maximum power of the fuel cell system $P_{FC,max}$ is determined according to the number of cells as discussed in Section 3.2.3.6.2.

3.2.4.1.2 Serial Hybrid System The mathematical relations for the determination of the maximum thrust of a serial hybrid-electric propulsion system are formulated in this paragraph. They are based upon a generic serial hybrid-electric propulsion system illustrated in Figure 3.3. In contrast to a parallel system, the maximum thrust of a serial system depends

besides η_{PD} and the true airspeed only on the maximum shaft power delivered by the electrical system $P_{Shaft,Elec,max}$ as expressed in Equation 3.13.

$$T_{max} = \eta_{PD} \cdot \frac{P_{Shaft,Elec,max}}{M \cdot a} \tag{3.13}$$

The maximum power of the electrical system is determined in Equation 3.14. It is expressed according to the power of the electric motor as established in Equation 3.12 and the amount of electrical power delivered at the shaft of the electric motor which is a function of the maximum power of the generator ($P_{G,max}$), $P_{EEPD,max}$ and $P_{Elec,Offtake}$.

$$\begin{aligned} P_{Shaft,Elec,max} = \min(&P_{EM}, \\ &\eta_{PMAD} \cdot \eta_{EM} \cdot (P_{G,max} - P_{Elec,Offtake} + PL_{EEPD} \cdot P_{EEPD,max})) \end{aligned} \tag{3.14}$$

$P_{G,max}$ is formulated in Equation 3.15. It is a function of the power delivered by the combustion engine according to $P_{CE,max}$, the power setting PL_{CE}, $P_{CE,Offtake}$ and the efficiency of the generator (η_G). η_G is calculated according to the efficiency map as discussed for the electric motor in Section 3.2.3.4.

$$P_{G,max} = (PL_{CE} \cdot P_{CE,max} - P_{CE,Offtake}) \cdot \eta_G \tag{3.15}$$

3.2.4.1.3 Partial Parallel Hybrid System In a partial parallel hybrid system as illustrated in Figure 2.3, the maximum thrust available is consequently obtained according to Equation 3.16.

$$T_{max} = \frac{\eta_{PD_{Conv}} \cdot P_{Shaft,Conv,max} + \eta_{PD_{Elec}} \cdot P_{Shaft,Elec,max}}{M \cdot a} \tag{3.16}$$

where $\eta_{PD_{Conv}}$ and $\eta_{PD_{Elec}}$ characterize the efficiency of the propulsive device of the combined conventional and electrical system respectively. The $P_{Shaft,Conv,max}$ and the $P_{Shaft,Elec,max}$ are calculated similarly as in parallel system as highlighted in Equation 3.9 and Equation 3.11 respectively.

3.2.4.2 Summary of Thrust Characteristics

In view of summarizing the determination of thrust characteristics of hybrid-electric propulsion systems, a table recapitulating the calculation of the maximum thrust is presented in Table 3.1 according to the hybrid-electric propulsion system topologies considered.

Topology	Equations for the computation of T_{max}	Equation
Parallel	$T_{max} = \eta_{PD} \cdot \frac{P_{Shaft,Conv,max} + P_{Shaft,Elec,max}}{M \cdot a}$	(3.8)
Serial	$T_{max} = \eta_{PD} \cdot \frac{P_{Shaft,Elec,max}}{M \cdot a}$	(3.13)
Partial parallel	$T_{max} = \frac{\eta_{PD_{Conv}} \cdot P_{Shaft,Conv,max} + \eta_{PD_{Elec}} \cdot P_{Shaft,Elec,max}}{M \cdot a}$	(3.16)

Topology	Equations for the computation of $P_{Shaft,Conv,max}$	Equation
Serial, Parallel, Partial parallel	$P_{Shaft,Conv,max} = PL_{CE} \cdot P_{CE,max} - P_{CE_{Offtake}}$	(3.9)

Topology	Equations for the computation of $P_{Shaft,Elec,max}$	Equation
Parallel, Partial parallel	$P_{Shaft,Elec,max} = \min(P_{EM}, \eta_{PMAD} \cdot \eta_{EM} \cdot (PL_{EEPD} \cdot P_{EEPD,max} - P_{Elec,Offtake}))$	(3.11)
Serial	$P_{Shaft,Elec,max} = \min(P_{EM}, \eta_{PMAD} \cdot \eta_{EM} \cdot (P_{G,max} - P_{Elec,Offtake} + PL_{EEPD} \cdot P_{EEPD,max}))$	(3.14)

Table 3.1: Summary of maximum thrust computation for hybrid-electric propulsion system

3.2.4.3 Energy Characteristics

Dealing with several energy sources in hybrid-electric propulsion systems requires the definition of energy management strategies. The energy consumption characteristics need consequently to be mapped within the aircraft sizing and performance environment. In the context of hybrid-electric aircraft, the fuel power and the electric power required at the energy source, P_{Elec}, need to be determined at each given flight state (ΔISA, Alt, M) according to the thrust level T. To provide commonality with traditional performance analysis programs, the same format as the fuel flow table is selected with the flight state ΔISA, Alt and M and the current engine net thrust T as inputs and the FF as output. In addition,

P_{Elec} is added as a second output parameter. This table which contains the FF and P_{Elec} as outputs enables to determine the energy consumption of the aircraft and is consequently renamed the energy table. The energy management strategies are inherently contained in the energy table. In contrast to the use of a single fuel flow table covering the overall operating flight envelope, the methods are extended to enable the creation of an energy table for each of the mission segments. This implementation enables different operational settings of the hybrid-electric propulsion system according to the flight phases. As a result, energy tables are created for takeoff, climb and cruise. For takeoff and climb, the tables are calculated with the operational settings utilized for the computation of the thrust table ratings MTO and MCL. Moreover if different energy management strategies are envisaged for the reserves and contingency, energy tables for the loiter and the diversion can be created. A consequence of this implementation approach is the fact that the management of the energy can be optimized only with respect to each mission segment. High-level optimizers can be used to control the parametrization of the energy table calculation and to determine the energy management by segment. However this method precludes point-to-point optimization during a mission. A more generalized approach for energy management optimization is proposed by [12].
The flight performance module, which will be detailed in Section 3.2.5, selects the thrust table and the energy table with respect to the segment of the mission flown. P_{Elec} is computed in the performance analysis module to determine the electrical power profile required at the EEPD and to determine the energy consumed by integration of the power over time. It is important to emphasize that P_{Elec} represents the power output which needs to be delivered by the EEPD. This electrical power does not take into account yet the efficiency of the electrical energy source device itself. The reason is that the efficiency evolution of the electrical energy source device is not known at this stage as it is for instance in the case of battery a function of the power required and the SOC. It depends consequently of the integrated mission computation. The efficiency of the electrical energy source device is computed along the mission profile by the performance analysis module according to the battery model (see Section 3.2.5 and Section 3.2.7). In the following, the computation of the FF and the P_{Elec} is exemplified for a parallel, serial and partial parallel hybrid topology respectively.

3.2.4.3.1 Parallel Hybrid System According to the energy management strategies elaborated for the different segments of the mission, the energy table is calculated with respect to the power settings PL_{CE}, PL_{EM} and PL_{EEPD}. For a given flight state (ΔISA, Alt, M) the thrust is determined according to the propulsive device fan speed $N_{rel,PD}$ as detailed in Section 3.2.3.2. During cruise, the resulting required shaft power, P_{Shaft}, is obtained from the propulsive device performance map as shown in Figure 3.2. Recalling Equation 3.11, if the power of the EEPD considering the electrical power off-take is not limiting, the shaft power required at the combustion engine is determined according to the electric motor power as expressed in Equation 3.17.

$$P_{CE} = P_{Shaft} - PL_{EM} \cdot P_{EM,max} \tag{3.17}$$

During takeoff and climb the maximal thrust is provided according to the thrust ratings. Rearranging Equation 3.10, the power of the combustion engine is given by Equation 3.18.

$$P_{CE} = PL_{CE} \cdot P_{CE,max} \tag{3.18}$$

The fuel power supply ($P_{Supply,Fuel}$) is formulated in Equation 3.19 according to the efficiency of the combustion engine η_{CE}. The efficiency η_{CE} is obtained from the efficiency map described in Section 3.2.3.3.

$$P_{Supply,Fuel} = \frac{P_{CE}}{\eta_{CE}} \tag{3.19}$$

According to the fuel heating value FHV, the fuel flow of the combustion engine, first output of the energy table, is calculated according to Equation 3.20.

$$FF = \frac{P_{Supply,Fuel}}{FHV} \tag{3.20}$$

The second output of the energy table, P_{Elec}, is formulated in Equation 3.21.

$$P_{Elec} = \frac{PL_{EM} \cdot P_{EM,max}}{\eta_{PMAD} \cdot \eta_{EM}} + P_{Elec,Offtake} \tag{3.21}$$

If the power of the EEPD turns to be limiting in Equation 3.11, the power of the combustion engine is determined by Equation 3.22.

$$P_{CE} = P_{Shaft} - (PL_{EEPD} \cdot P_{EEPD,max} - P_{Elec,Offtake}) \cdot \eta_{PMAD} \cdot \eta_{EM} \tag{3.22}$$

In this case the P_{Elec} is formulated in Equation 3.23.

$$P_{Elec} = PL_{EEPD} \cdot P_{EEPD,max} \tag{3.23}$$

3.2.4.3.2 Serial Hybrid System For a given flight state (ΔISA, Alt, M) and according to a required thrust, the electric power required at the electric motor is determined according to Equation 3.24.

$$P_{EM} = \frac{T \cdot M \cdot a}{\eta_{PD}} \tag{3.24}$$

The power delivered by the generator (P_G) is calculated as a function of P_{EM} and $P_{EEPD,max}$ according to Equation 3.25.

$$P_G = \frac{P_{EM}}{\eta_{PMAD} \cdot \eta_{EM}} - PL_{EEPD} \cdot P_{EEPD,max} \tag{3.25}$$

P_{Elec} is determined according to Equation 3.23.

The power required at the combustion engine P_{CE} is expressed in Equation 3.26 according to P_G under the consideration of the electric power off-take at the generator $P_{Elec,Offtake}$ and the power off-take at the combustion engine $P_{CE,Offtake}$.

$$P_{CE} = \frac{P_G + P_{Elec,Offtake}}{\eta_G} + P_{CE,Offtake} \tag{3.26}$$

The fuel power supplied and the corresponding amount of fuel flow, first output of the energy table, are determined according to Equation 3.19 and Equation 3.20 respectively.
For takeoff and climb, the energy table is computed according to the power lever settings PL_{CE} and PL_{EEPD} set for the creation of the respective thrust table. The power of the combustion engine is calculated according to Equation 3.18. The resulting fuel flow is computed with Equation 3.19 and Equation 3.20. P_{Elec} is the result of Equation 3.23.

3.2.4.3.3 Partial Parallel Hybrid System In a partial parallel hybrid system, the conventional and the electrical system are independently computed. The calculation of the FF and of P_{Elec} formulated in Equation 3.27 and Equation 3.28 is a function of the shaft power required at the conventional system ($P_{Shaft,Conv}$) and of the shaft power required at the electrical system ($P_{Shaft,Elec}$). $P_{Shaft,Conv}$ and $P_{Shaft,Elec}$ are determined with respect to the propulsive device model according to the flight state conditions (ΔISA, Alt, M) and the thrust determined according to the propulsive device fan speed $N_{rel,PD}$ as discussed in Section 3.2.3.2.

$$FF = \frac{P_{Shaft,Conv}}{FHV \cdot \eta_{CE}} \tag{3.27}$$

$$P_{Elec} = \frac{P_{Shaft,Elec}}{\eta_{PMAD} \cdot \eta_{EM}} \tag{3.28}$$

In the case of a partial parallel hybrid system, the energy management is directly an outcome of the propulsion system sizing and more specifically of H_P. The methods for the sizing of partial parallel hybrid system are described in Section 3.2.6. Two different energy management strategies for an aircraft concept equipped with a partial parallel hybrid system are investigated in Section 5.4.

3.2.4.4 Summary of Energy Characteristics

The mapping of the energy consumption within the aircraft design environment needed to establish the energy characteristics of hybrid-electric propulsion system is summarized in Table 3.2.

Topology	Equations for the computation of FF	Equation
Parallel	$FF = \frac{1}{FHV \cdot \eta_{CE}} \cdot (P_{Shaft} - PL_{EM} \cdot P_{EM,max})$	(3.19), (3.20) and (3.17)
Serial	$FF = \frac{1}{FHV \cdot \eta_{CE}} \cdot (\frac{P_{Elec,Offtake} + \frac{P_{EM}}{\eta_{EM} \cdot \eta_{PMAD}} - PL_{EEPD} \cdot P_{EEPD,max}}{\eta_G} + P_{CE,Offtake})$	(3.19), (3.20), (3.25) and (3.26)
Partial parallel	$FF = \frac{P_{Shaft,Conv}}{FHV \cdot \eta_{CE}}$	(3.27)

Topology	Equations for the computation of P_{Elec}	Equation
Parallel	$P_{Elec} = \frac{PL_{EM} \cdot P_{EM,max}}{\eta_{PMAD} \cdot \eta_{EM}} + P_{Elec,Offtake}$	(3.21)
Serial	$P_{Elec} = PL_{EEPD} \cdot P_{EEPD,max}$	(3.23)
Partial parallel	$P_{Elec} = \frac{P_{Shaft,Elec}}{\eta_{PMAD} \cdot \eta_{EM}}$	(3.28)

Table 3.2: Summary of energy characteristics calculation for hybrid-electric propulsion system

3.2.5 Methods for Flight Performance Analysis

Flight performance analysis requires the knowledge of the propulsion system performance and efficiency characteristics. These properties are provided to the flight performance module through the thrust and energy tables discussed in Section 3.2.4.1 and Section 3.2.4.3 respectively. Moreover, the aerodynamics and the weight properties of the aircraft need to be interfaced with the flight performance module. The aerodynamic characteristics are provided in terms of the drag polars computed at low- and high-speed conditions as well as the lift curves. The determination of the aircraft weight properties results from component mass build-up methods of the different aircraft systems. The propulsion total weight includes the weight of the conventional and electrical propulsion system as discussed in Section 3.2.3.

The flight performance analysis as represented in Figure 3.2 is composed of two modules, the integrated mission performance module and the point performance module. The integrated mission performance analysis consists of determining the amount of energy an aircraft must carry on-board to accomplish its design mission. The calculation includes the energy requirement for the mission as well as for the reserves to comply with operational regulations. The required thrust is computed by resolving the flight mechanics equations at each discretized point of the mission segments according to the flight state ΔISA, Alt and M, the aircraft gross-weight and the aerodynamic efficiency delivered by the drag polar. With respect to the flight state and the computed thrust, the value of the FF is calculated by interpolating in the energy table according to the rating corresponding to the segment of the mission. The computation of the FF is performed at each discretized point of the segment. The integration of the FF over time enables the computation of the fuel mass consumed and correspondingly the change in aircraft gross-weight over time.
Concurrently, the electric power required to produce the thrust, P_{Elec}, is interpolated in the energy table at each discretized point of the segment according to the flight state. The required electrical power P_{Elec} is the input for the electric energy and power device model. P_{Elec} defines the required electric power profile. In the case, of an electrical system powered by fuel cells, the required FF_{FC} is determined according to P_{Elec} and the computed fuel cell efficiency η_{FC} as formulated in Equation 3.6. The FF_{FC} is integrated over time to determine the fuel mass consumed and the change in aircraft gross-weight along the mission. If the EEPD is a battery system, the available output voltage at the required discharge rate is calculated using the discharge curve of the battery model according to P_{Elec} and the SOC of the battery as highlighted in Section 3.2.3.6.1. According to the discharge rate fulfilling the power requirements, the SOC is calculated at each discretized point of the mission segment. As a result, the SOC of the battery at the end of the mission can be determined. The knowledge of the battery SOC at the end of the mission enables the sizing of the battery mass according to the energy requirement as described in Section 3.2.7. In addition, the maximal electrical power occurring in the profile, $max(P_{Elec})$, is assessed in order to determine the sizing criterion of the battery mass.

3.2.6 Methods for Hybrid-Electric Propulsion System Sizing

Freeman et al. [18] highlighted that the sizing of hybrid-electric propulsion system should proceed from the propulsive device back to the electric energy and power device. It is explained by the fact that the sizing of the upstream components (close to the production of thrust) influences the power required of all-downstream elements according to the efficiency value chain. The same strategy is followed in this thesis for the sizing of the hybrid-electric propulsion systems. The sizing characteristics of the propulsive device and of the electric motor vary according to the investigated hybrid-electric propulsion system topology. Consequently, the sizing specificities are discussed with respect to the topologies investigated.

3.2.6.1 Propulsive Device Sizing

The flow path sizing of the propulsive device is determined by the design point which occurs typically for medium-to-large commercial transport aircraft at TOC conditions [104]. The total thrust requirement at the design point is distributed among the number of propulsive devices, N_{PD}. The sizing $T_{des,PD}$ is consequently obtained with Equation 3.29 with respect to the total design thrust (T_{des}).

$$T_{des,PD} = \frac{T_{des}}{N_{PD}} \tag{3.29}$$

For a partial parallel hybrid system, the characteristics of the propulsive device driven by the conventional and the electrical system have to be analysed independently. In the following, the conventional propulsion system is denoted as the turbofan (TF). According to the total design thrust requirement, T_{des}, and the specification of a level of H_{Puse}, the $T_{des,TF}$ and the design thrust of the electrical fan ($T_{des,EF}$) are determined with Equation 3.30 and with Equation 3.31 respectively.

$$T_{des,TF} = \frac{T_{des} \cdot (1 - H_{Puse})}{N_{TF}} \tag{3.30}$$

$$T_{des,EF} = \frac{T_{des} \cdot H_{Puse}}{N_{EF}} \tag{3.31}$$

N_{TF} and N_{EF} represent the installed number of turbofans and electric fans respectively. The knowledge of the design thrust $T_{des,TF}$ and $T_{des,EF}$ enables the characterization of the geometrical dimensions and weight properties of propulsion system as highlighted in Section 3.2.3.1 and in Section 3.2.3.2. As represented in Figure A.1, $T_{des,TF}$ enables the computation of the thrust and fuel flow characteristics of the turbofans. $T_{des,EF}$ is used in the performance map of the propulsive device for the calculation of the thrust characteristics of the electric fan.

3.2.6.2 Electric Motor Sizing

By recalling the description of a parallel system in Figure 3.4, the electric motor is mechanically linked to the shaft of the gas-turbine. By specifying a level of H_P, the maximal power of the electric motor is formulated in Equation 3.32,

$$P_{EM,max} = H_P \cdot P_{SLS} \tag{3.32}$$

H_P is consequently a design parameter which can be optimized according to the selected objective function. An integrated investigation of the implication of the level of H_P on block fuel consumption is analysed in Section 5.3 for the retrofit of a narrow-body transport aircraft equipped with a parallel hybrid-electric propulsion system. For a parallel hybrid-electric propulsion system whose electrical motor is used to drive by itself the shaft of the propulsive device during some segments of the mission profile, the electric motor can be sized with Equation 3.32. However, a more practical sizing case is given by sizing the electric motor according to the maximal shaft power required by the propulsive device during the selected mission segment or at any other selected sizing point in the flight envelope. The level of H_P becomes an outcome of the sizing process. This method was used for the sizing of a narrow-body transport aircraft, presented in Section 5.4, which features a parallel hybrid-electric system whose electric motor drives the shaft of the propulsive device during cruise only.
Considering a serial system, the electric motor drives the shaft of the propulsive device. As the result, the electric motor is sized to meet the required aircraft performance within the flight envelope. Recalling Equation 3.24, the electric motor power is sized for the maximal power occurring within the flight envelope as defined in Equation 3.33.

$$P_{EM,max} = \max(\frac{T_{PD} \cdot M \cdot a}{\eta_{PD}}) \tag{3.33}$$

For a partial parallel hybrid system, the sizing depends on the shaft power characteristics of the propulsive device. If the electric motor is sized according to the propulsor shaft power required at TOC, the installed power of the electric motor limits the ducted fan performance at lower altitude as the power demand of the ducted fan increases with decreasing altitude. The evolution of the power requirement of a ducted-fan with varying altitude and Mach number was represented for maximum thrust in Figure 3.12. As a result the fan speed is reduced during take-off and climb limiting the available thrust. The decrease of the installed thrust with reduction of the relative corrected fan speed $N_{rel,PD}$ was represented in Figure 3.13 for varying altitudes at M 0.78 and in Figure 3.14 for varying Mach number at a FL 350.
The sizing implications on the ducted fan off-design speed characteristics are represented generically in Figure 3.18. It illustrates the variation of the normalized power load of the electric motor PL_{EM} and $N_{rel,PD}$ throughout a given mission for an electric motor sized for the shaft power requirement at TOC. From takeoff which starts at around 7 min and the end of climb which finishes at around 30 min, the operations of the electric fan are limited by the installed power of the electric motor. $N_{rel,PD}$ is less than 1.0 while the electric motor runs at its maximum installed power. During climb $N_{rel,PD}$ increases as the required fan power decreases with altitude to reach the value of 1.0 at TOC. In this example the design point of the electric motor was set at FL350 and M 0.78. The fact that the TOC and the cruise were flown at M 0.75 the electric motor power requirement is slightly less than 1.0 at TOC and during the cruise segment which has a duration of 125 min. During the descent phase, the electric fan is not used which explains the zero values for PL_{EM} and $N_{rel,PD}$. Beyond 150 min of the operation, the diversion is represented including the climb and cruise segment.

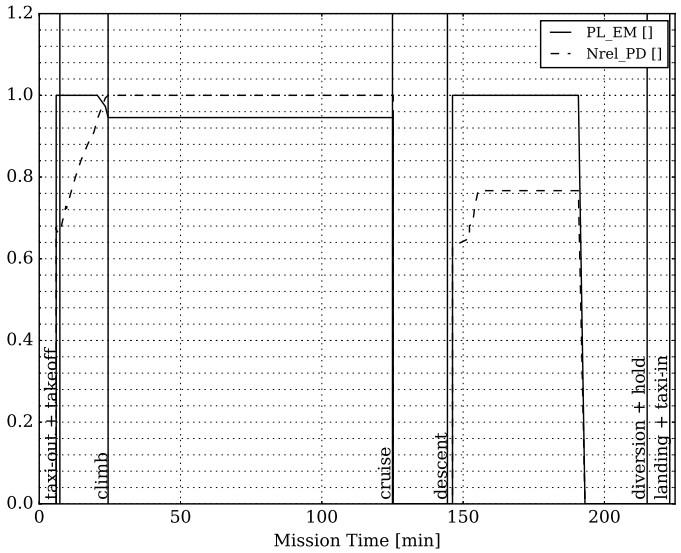

Figure 3.18: Part-load power of the electric motor and relative corrected ducted fan speed versus mission time

The diversion descent is performed without the electrical fan. As the diversion is flown at a lower altitude than cruise, the required fan shaft power is larger than at the design TOC point. The power of the electric motor limits consequently the performance of the electric fan during diversion. As indicated in Figure 3.18, the electric motor runs at maximal power while $N_{rel,PD}$ achieves a value around 0.76 during the diversion cruise segment.

From this analysis, it could be concluded that the electric motor should be sized at relevant take-off conditions such that take-off and initial climb performance requirements are met. But in fact, the critical sizing case of the electric motor depends on the level of H_{Puse}. At low values of H_{Puse}, the turbofan still delivers a large proportion of the thrust at take-off. Consequently, the sizing case for the electric motor is at TOC. According to $T_{des,EF}$, η_{PD} and the flight speed conditions at TOC, the electric motor power is sized according to Equation 3.34.

$$P_{EM,max} = \frac{T_{des,EF} \cdot M \cdot a}{\eta_{PD}} \tag{3.34}$$

The available take-off thrust of the turbofan results from the sizing of the turbofan at TOC according to Equation 3.30. It depends on the thrust lapse characteristics of the turbofan and on the temperature limitation setting at take-off. The de-rating of the turbofan can be adjusted to improve the life-cycle of the turbofan according to the electric fan maximal thrust available at take-off. The available take-off thrust of the electric fan depends on the installed electric motor according to the sizing resulting from Equation 3.34 and the thrust lapse characteristics of the electric fan as shown for a generic ducted-fan in Figure 3.12.

With growing levels of H_{Puse}, the role of the electric fan in providing the required thrust during take-off and climb becomes more predominant. As a result the sizing of the electric motor is constrained by take-off and climb performance such that the electrical fan delivers the required thrust. Typically the take-off field length (TOFL), the climb gradient requirements as well as the time-to-climb become the sizing constraints. In order to minimize the impact of the electrical system weight, the sizing of the electric motor is set as an optimization scheme whose constraints are the take-off and climb performance requirements. The critical sizing cases of an electric motor equipping a partial parallel hybrid-electric propulsion system are discussed in the integrated performance analysis of a narrow-body aircraft featuring a quad-fans arrangement in Section 5.5.
In this context, it is worthwhile highlighting that for a universally electric aircraft, the electric motor has to be sized for take-off conditions which results in a large propulsion system weight [10]. This sizing criterion results in an oversized electric motor in cruise condition as in contrast to a gas-turbine the electric motor maximal power remains invariant with flight speed and altitude assuming it is suitably thermally managed. For a hybrid-electric aircraft, according to the topology and the utilization of the hybrid-electric propulsion system, the electric motor power does not have to be sized to the take-off power requirement diminishing the impact of the electric motor sizing on the propulsion system weight.
According to $P_{EM,max}$, the weight and volume of the electric motor are determined applying scaling laws based on gravimetric and volumetric specific power or relying on physics-based model as discussed in Section 3.2.3.4. The weight of the electric motor is interfaced with the components weight build-up methods within the aircraft sizing environment for the computation of the overall propulsion system weight.

3.2.6.3 Power Management and Distribution System Sizing

The PMAD is sized according to the highest power requirement occurring in the electrical system under consideration of abnormal modes. With respect to the power resulting from the sizing case and the layout of the PMAD system, the weight and volume of the PMAD are calculated according to the methods indicated in Section 3.2.3.5. The weight of the PMAD is linked to the weight component build-up methods of the propulsion system. According to the representation of the PMAD in Figure 3.4 and Figure 3.3, the sizing case for P_{PMAD} is given by Equation 3.35.

$$P_{PMAD} = \frac{P_{EM,max}}{\eta_{EM}} \tag{3.35}$$

3.2.7 Methods for Sizing of Hybrid-Electric Aircraft

The overall procedure for the sizing of hybrid-electric aircraft illustrated in Figure 3.2 is described in this paragraph. First of all, the transport tasks and the complete set of performance requirements to be achieved are stipulated in the ATLRS. For a transport aircraft, the

design mission is determined by the two main following parameters: the design payload and the design range. According to an initial estimated MTOW and with respect to initial values for the main sizing parameters of the aircraft namely $MTOW/S_{ref}$ and $P_{total}/MTOW$, the total power required P_{total} and the wing reference area S_{ref} are determined. With the specification of a degree of hybridization for power H_P, P_{SLS} and $P_{EM,max}$ are computed so that the total aircraft power requirement P_{total} is fulfilled as detailed in Section 3.2.6.2.
As illustrated in Figure A.1, in case of a partial parallel hybrid-electric propulsion system, instead of expressing the power-to-weight ratio $P_{total}/MTOW$, a more practical approach is to specify the ratio of $T/MTOW$. Similarly, the total design thrust requirement T_{des} is calculated according to an initial value of MTOW. With the formulation of a degree of hybridization for useful power H_{Puse}, the design thrust of the conventional system $T_{des,TF}$ and of the electrical system $T_{des,EF}$ is computed as demonstrated in Section 3.2.6.1.
The sizing characteristics of the propulsive device were discussed for a serial, a parallel and a partial parallel hybrid system in Section 3.2.6.1. The particularities of the electric motor sizing were formulated in Section 3.2.6.2. The geometrical properties of the propulsion system are linked to the drag component build-up functions to determine the complete drag polar of the aircraft. The overall weight of the electrical propulsion system is determined by summing up the weight of the electrical components. The electrical propulsion system weight is mapped as an additional item to the propulsion weight of the aircraft.
According to the hybrid-electric propulsion system topology selected and with respect to the design and off-design performance characteristics of the components, the thrust tables and the energy tables are computed according to the different mission segment as detailed in Section 3.2.4.1 and Section 3.2.4.3 respectively.
By interpolating within the energy table according to the flight state and the thrust, the FF is calculated. The fuel mass required is calculated by integrating the FF along the integrated mission. Concurrently, the electric power required at the electric energy and power device, P_{Elec}, is interpolated within the energy table. P_{Elec} serves as input for the sizing of the electric energy and power device.
If a fuel cell system is implemented as electric energy and power device, the number of fuel cells required is sized according to the maximum electric power occurring within the flight envelope as highlighted in Section 3.2.3.6.2. According to P_{Elec}, the efficiency of the fuel cell system is evaluated based for instance on the physics-based model of a fuel cell as discussed in Section 3.2.3.6.2. The determination of the fuel cell efficiency enables the computation of the FF_{FC} according to Equation 3.6. By integrating the FF_{FC} of the fuel cell over time, the total fuel mass supply of the fuel cell system to provide the electric energy and power over the mission is determined.
Utilizing batteries as an energy and power device, the total battery system mass required to provide the electric energy and power has to be determined. According to the battery model, the SOC is computed along the mission as detailed in Section 3.2.5. To protect the battery from any damage and to prolong design service goal suitable for use in aerospace, the battery must not be discharged below SOC_{limit} typically set at 20%. This is represented generically in Figure 3.19 for the mission power profile discussed in Figure 3.18.

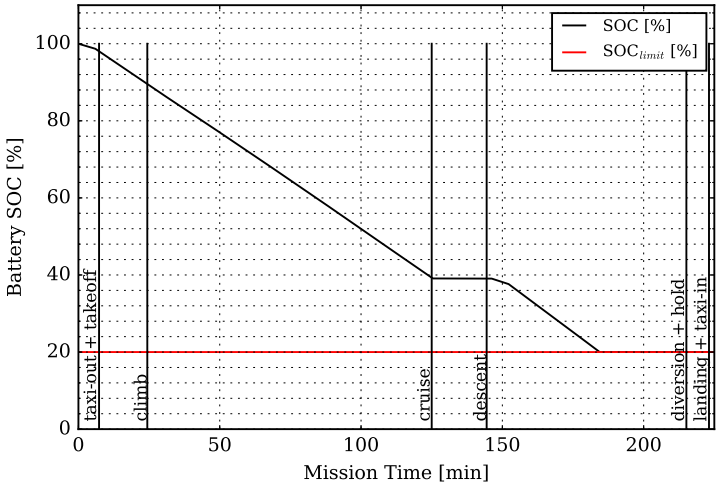

Figure 3.19: Battery SOC profile versus mission time

If the computed SOC at the end of the mission is below SOC_{limit}, the installed battery mass is increased by iteration. The SOC_{limit} of the battery represents consequently an additional constraint in the sizing of hybrid-electric aircraft compared to a fuel-based only aircraft. Even if the energy required of a commercial transport aircraft is generally the sizing criterion for the battery mass, the electrical power required might be the sizing constraint according to the specific power of the battery and the operational utilization of the battery. Consequently, as described in Section 3.2.3.6 both criteria must be verified for the sizing of the battery mass. In addition, if the total fuel mass calculated is above the initial estimated fuel mass, the fuel mass is increased by iteration. The iteration for the fuel mass and the battery mass calculation needs to be both conducted until the convergence criteria are met.
The main aircraft sizing parameters namely $MTOW/S_{ref}$ and $P_{total}/MTOW$ are determined by iteration with respect to the analysis of the point performance constraints for low- and high-speed performance. When the performance constraints and the integrated mission performance are fulfilled, the aircraft is sized for its design transport task.

3.2.8 Summary of Hybrid-Electric Propulsion System Sizing Principles

The sizing principles of hybrid-electric propulsion system developed in Section 3.2.6 and Section 3.2.7 are summarized in Table 3.3.

Topology	Equations for propulsive device sizing	Equation
Parallel, Serial	$T_{des,PD} = \frac{T_{des}}{N_{PD}}$	(3.29)
Partial parallel	$T_{des,TF} = \frac{T_{des} \cdot (1 - H_{Puse})}{N_{TF}}$	(3.30)
	$T_{des,EF} = \frac{T_{des} \cdot H_{Puse}}{N_{EF}}$	(3.31)

Topology	Equations for electric motor sizing	Equation
Parallel	$P_{EM,max} = H_P \cdot P_{SLS}$	(3.32)
Serial	$P_{EM,max} = \max(\frac{T_{PD} \cdot M \cdot a}{\eta_{PD}})$	(3.33)
Partial parallel	$P_{EM,max} = \frac{H_{Puse} \cdot T_{des} \cdot M \cdot a}{\eta_{PD} \cdot N_{EF}}$	(3.31) and (3.34)

Topology	Equation for PMAD sizing	Equation
Serial, Parallel, Partial parallel	$P_{PMAD} = \frac{P_{EM,max}}{\eta_{EM}}$	(3.35)

	Equations for batteries sizing	Equation
	$m_{Battery} = \max(m_{Battery\,energy}; m_{Battery\,power})$	(3.3)
	$m_{Battery\,energy} = \frac{1}{\eta_{Bat} \cdot e_{Bat,Syst} \cdot (1 - SOC_{limit})} \int_{t_{initial}}^{t_{end}} P_{Elec}(t) \cdot dt$	(3.4)
	$m_{Battery\,power} = \frac{\max(P_{Elec})}{\eta_{Bat} \cdot p_{Bat,Syst}}$	(3.5)

	Equation for fuel-cells sizing	Equation
	$P_{FC,max} = \frac{\max(P_{Elec})}{\eta_{FC}}$	(3.7)

Table 3.3: Summary of sizing principles for hybrid-electric propulsion system

Chapter 4

Methods for Flight Technique Optimization of Hybrid-Electric Aircraft

The establishment of figures-of-merit to evaluate the vehicular efficiency of an aircraft is essential in conceptual design. Related to their instantaneous form, they are used for flight technique optimization to determine optimum altitude-speed technique as a function of the aircraft gross-weight, the aerodynamic efficiency and the overall propulsion system efficiency. As an integrated form along a given mission, the metrics are used to assess the overall efficiency of the vehicle to perform its transport task and to compare the vehicular efficiency of different investigated concepts.

4.1 Traditional Figure-of-Merits for Flight Technique Optimisation

Traditionally, the vehicular efficiency assessment of fuel-based aircraft is evaluated by the specific air range (SAR) as indicated in Equation 4.1 [113]. It characterizes the distance travelled per unit of fuel consumed.

$$\mathrm{SAR} = \frac{M \cdot a \cdot L/D}{TSFC \cdot W} \tag{4.1}$$

where M is the Mach number, a is the sound velocity, W is the aircraft gross-weight, L/D is the aerodynamic efficiency of the aircraft and $TSFC$ is the thrust-specific fuel consumption which characterizes the fuel flow per amount of thrust.
Optimizing an aircraft for maximum SAR results in minimizing its fuel consumption. The speed which results in flying at maximum SAR is defined as the maximum range cruise (MRC). Instead of MRC, commercial transport aircraft typically operate at long range cruise (LRC) which is defined by the speed reached under the condition of 99% of maximum SAR. Using the SAR as metric for flight technique optimization focuses only on fuel consumption. However airlines are interested in minimizing their operating costs along given routes. The cost of fuel is not the only factor contributing to the total operating cost of an aircraft. Fixed

costs and time dependent costs need to be also taken into account. As the fixed costs are independent of the speed-altitude characteristic, they are irrelevant for optimization purposes. However, the time-related cost needs to be considered to determine the economical Mach number for which the total cost is minimized. To operate their aircraft fleet for minimum overall cost, the airlines base their operation on so-called cost index (CI) [114] which relates the cost of time to the cost of fuel as highlighted in Equation 4.19.

$$CI = \frac{c_{Time}}{c_{Fuel}} \tag{4.2}$$

with c_{Time} and c_{Fuel} representing the specific cost of time and the specific cost of fuel respectively. By computing the CI for different flight conditions and for varying aircraft gross-weight, the optimum economical Mach number can be determined for used in the aircraft performance calculation. An example of the utilisation of the CI for evaluation of the optimum economical Mach number is discussed in Section 5.3.4.

4.2 Figure-of-Merits for Flight Technique Optimisation of Hybrid-Electric Aircraft

The mathematical construct of SAR is based on a mass-flow due to the term $TSFC$ in Equation 4.1. Its utilization is consequently limited to aircraft whose operations are based on a fuel energy only (e.g. kerosene, diesel or hydrogen). With the consideration of electric energy, the metric SAR becomes inadequate for the determination of optimum flight technique for hybrid-electric aircraft. New figure-of-merits reflecting the specific characteristics of hybrid-electric propulsion system need to be developed. The definition of optimum speeds needs to be revisited according to the newly introduced metrics. Similarly, only the cost of fuel is considered in the mathematical expression of the CI described in Equation 4.19. Consequently, the derivation of CI for hybrid-electric aircraft is necessary to cover the identification of optimum economical flight profile. The methods developed for optimum flight techniques of hybrid-electric aircraft presented in this chapter were published by Pornet et al. [115].
A generalization of the SAR metric based on the energy consumed was proposed by Seitz et al. [104]. The energy specific air range (ESAR) metric expressed in Equation 4.3 characterizes the energetic vehicular efficiency. In concrete terms, it represents the distance travelled for a given amount of energy.

$$\text{ESAR} = \frac{M \cdot a \cdot L/D}{TSPC \cdot W} \tag{4.3}$$

with the term thrust specific power consumption ($TSPC$) which relates the power of the energy supplied to the thrust requirement [104]. For speed sensitivity analysis, the speed at which maximum ESAR occurs was characterized as the maximum ESAR range cruise (MERC) by Pornet et al. [115]. The long ESAR range cruise (LERC) was defined as the speed at which 99% of the maximum ESAR occurs mirroring the definition of the LRC speed [115]. Using ESAR, as a figure-of-merit for flight technique optimization results in minimum

energy consumed during a mission. When an aircraft utilizes more than one energy source, as for instance hybrid-electric aircraft, optimizing the flight profile according to SAR results in an optimum in terms of fuel consumption, minimizing the CO_2 emissions. Optimizing with respect to ESAR results in a flight profile where the total energy (the combination of fuel and electric energy) consumed is minimized for a given stage length. However, these optima may not represent minimum energy cost due to the different prices of the energy market prices. The cost specific air range (COSAR) metric is established in Section 4.3 as a new figure-of-merit to optimize the flight profile of hybrid-energy aircraft for minimum energy cost. Moreover as airlines base their fleet operations on CI for operational economics optimization, CI formulations are derived in Section 4.4 to enable optimized flight profile based on economics objective for hybrid-electric aircraft.

4.3 The Cost-Specific Air Range

For a single energy source aircraft, the optimization according to both SAR and ESAR leads to minimum energy cost. However, when multiple energy sources with different market prices are used simultaneously, this relation is not valid anymore. From this consideration, a figure-of-merit related to the price of the energy sources involved in a hybrid-energy aircraft is more appropriate for flight technique optimization. A new figure-of-merit, COSAR, is proposed. Incorporating the specific cost of each energy source, c, COSAR is established as:

$$\text{COSAR} = \frac{M \cdot a \cdot L/D}{(\sum_i TSPC_i \cdot c_i) \cdot W} \tag{4.4}$$

According to the definition COSAR determines the distance which can be travelled by an aircraft per amount of energy cost. For hybrid-energy aircraft, $TSPC$ can be expressed according to Equation 4.5.

$$TSPC = \frac{\sum_i P_i}{T_{Total}} = \sum_i TSPC_i \tag{4.5}$$

The power P_i represents the power extracted at the energy source. P_i, is summed up for each energy supply considered, which is equivalent to the summation of each respective $TSPC$. COSAR can be applied to any given combination of energy sources under the requirement that the specific price of the energy is known. For the particular case of a hybrid-electric aircraft using, for instance, fuel and battery as energy sources, the $TSPC$ can be written as in Equation 4.6.

$$TSPC = \frac{P_{Supply,Fuel} + P_{Supply,Elec}}{T_{Total}} = TSPC_{Supply,Fuel} + TSPC_{Supply,Elec} \tag{4.6}$$

with the electrical power supply ($P_{Supply,Elec}$) and ($P_{Supply,Fuel}$), the fuel power supplied. The fuel power provided by the combustion engine is equal to the FF multiplied by the fuel heating value FHV.

$$P_{Supply,Fuel} = FF \cdot FHV \tag{4.7}$$

$$\text{COSAR} = \frac{M \cdot a \cdot L/D}{(TSPC_{Supply,Fuel} \cdot c_{Fuel} + TSPC_{Supply,Elec} \cdot c_{Elec}) \cdot W} \tag{4.8}$$

where, c_{Elec} is the specific cost of electricity. It is worthwhile highlighting the fact that if the electricity price is negligible versus the fuel price, the COSAR speed-altitude optimum will be equivalent to the one given by the SAR metric.
In order to relate COSAR to the design parameters introduced in Section 3.2.1, H_E can be expressed as the ratio of the instantaneous electric power supply over the total instantaneous power requirement at the energy sources as established in Equation 4.9.

$$H_E = \frac{P_{Supply,Elec}}{P_{Supply,Total}} \tag{4.9}$$

The COSAR figure-of-merit can be formulated as a function of H_E according to Equation 4.10.

$$\text{COSAR} = \frac{M \cdot a \cdot L/D}{\frac{P_{Supply,Total}}{T_{Total}}((1 - H_E) \cdot c_{Fuel} + H_E \cdot c_{Elec}) \cdot W} \tag{4.10}$$

By defining the combined cost of energy in Equation 4.11,

$$c_{Energy} = (1 - H_E) \cdot c_{Fuel} + H_E \cdot c_{Elec} \tag{4.11}$$

COSAR can finally be formulated as a function of ESAR according to Equation 4.12.

$$\text{COSAR} = \frac{\text{ESAR}}{c_{Energy}} \tag{4.12}$$

Due to the dependency of c_{Energy} on the flight condition, it is important to highlight that Equation 4.12 does not represent a proportional relation between COSAR and ESAR. Using COSAR as an objective function means optimizing the flight profile of hybrid-energy aircraft according to the current market energy price for minimum energy cost. The speed which maximizes COSAR was designated as the maximum COSAR range cruise (MCRC) while the long COSAR range cruise (LCRC) was defined as the speed which fulfils the 99% maximum COSAR condition [115] .

4.4 Operational Economics Optimization

The interest of airlines lies in minimizing their cash operating cost. In addition to the energy cost, fixed cost and time-related cost are relevant for operating cost optimization purposes. The utilization of COSAR as objective function leads to minimize the cost of energy for a given stage length. Thereafter, the time-related cost needs to be considered to determine the optimum economical Mach number for which the total cost is minimized. The derivation of the CI for hybrid-electric concepts is established in this paragraph.

A generalized cost function, C, can be expressed as in Equation 4.13.

$$C = C_0 + c_{Time} \cdot t + c_{Energy} \cdot E_{Supply,Total} \tag{4.13}$$

C_0 denotes the fixed cost of the airlines which represents the cost independent of the trip time. As a result, C_0 does not play any role in the speed-altitude optimization problem. c_{Time} includes flight crew, cabin crew and time-dependant maintenance. The time of the mission is represented by the variable t. The specific cost of energy c_{Energy} was established in Equation 4.11. $E_{Supply,Total}$ is the total energy consumed. The possible influence on c_{Time} due to the utilisation of unconventional propulsion system such as hybrid-electric is not considered in the following formulations.
For the particular application of a hybrid-electric aircraft, the function is formulated in Equation 4.14.

$$C = C_0 + c_{Time} \cdot t + c_{Fuel} \cdot E_{Supply,Fuel} + c_{Elec} \cdot E_{Supply,Elec} \tag{4.14}$$

In order to establish the cost per stage length, the cost function can be formulated as in Equation 4.15 considering a given stage length, R, and a block speed, V.

$$\frac{C}{R} = \frac{C_0}{R} + \frac{c_{Time}}{V} + c_{Fuel} \cdot \frac{P_{Supply,Fuel}}{V} + c_{Elec} \cdot \frac{P_{Supply,Elec}}{V} \tag{4.15}$$

Finally, according to the COSAR metric established in Equation 4.8, the cost function of a hybrid-electric aircraft is defined as:

$$\frac{C}{R} = \frac{C_0}{R} + \frac{c_{Time}}{V} + \frac{1}{COSAR} \tag{4.16}$$

The influence of the time-related cost on the optimum speed of a hybrid-electric aircraft can be evaluated by analysing Equation 4.16. On one hand with increasing Mach number the cost of time decreases for a given stage length. This leads to a cost economical Mach number which tends to be higher than MCRC. However, this increase in optimum speed is counteracted by the rise of COSAR at higher Mach number. On the other hand if the specific cost of time is negligible against the specific cost of energy, the economical Mach number coincides with MCRC.

In view of optimizing the flight profile of hybrid-electric aircraft with respect to the time-related cost and the cost of energy, a cost-index metric is derived in the following. Differen-

tiating Equation 4.13 with respect to the block time yields the cost increase per change in time as defined in Equation 4.17.

$$\frac{\mathrm{d}C}{\mathrm{d}t} = c_{Time} + c_{Fuel} \cdot \frac{\mathrm{d}E_{Supply,Fuel}}{\mathrm{d}t} + c_{Elec} \cdot \frac{\mathrm{d}E_{Supply,Elec}}{\mathrm{d}t} = 0 \tag{4.17}$$

A local minimum leads to establish the condition of having Equation 4.17 equals to zero.

Rewriting Equation 4.17 as a function of the design parameter H_E in Equation 4.18 results in the general definition of the CI for hybrid-electric aircraft in Equation 4.19.

$$\begin{aligned}\frac{\mathrm{d}C}{\mathrm{d}t} &= c_{Time} + \\ &(c_{Fuel} \cdot (1 - H_E) + c_{Elec} \cdot H_E) \cdot \frac{\mathrm{d}E_{Supply,Total}}{\mathrm{d}t} + E_{Supply,Total} \cdot (c_{Elec} - c_{Fuel}) \cdot \frac{\mathrm{d}H_E}{\mathrm{d}t}\end{aligned} \tag{4.18}$$

$$CI = \frac{c_{Time} + E_{Supply,Total} \cdot (c_{Elec} - c_{Fuel}) \cdot \frac{\mathrm{d}H_E}{\mathrm{d}t}}{c_{Fuel} \cdot (1 - H_E) + c_{Elec} \cdot H_E} = -\frac{\mathrm{d}E_{Supply,Total}}{\mathrm{d}t} \tag{4.19}$$

The application of the CI is demonstrated in the following for three different hybrid-electric propulsion system characterized namely by a constant degree of hybridization for energy, a constant electric power supply and a constant amount of electric energy consumption.

4.4.1 Constant Degree of Hybridization for Energy

For a hybrid-electric aircraft configuration equipped with a propulsion system whose operational utilization results in a constant H_E, the fractional change of H_E versus time in Equation 4.19 equals zero.

$$\frac{\mathrm{d}H_E}{\mathrm{d}t} = 0 \tag{4.20}$$

Combining Equation 4.19 and Equation 4.20, the expression of CI for constant H_E is obtained in Equation 4.21.

$$CI_{H_{Econst}} = \frac{c_{Time}}{c_{Fuel} \cdot (1 - H_E) + c_{Elec} \cdot H_E} \tag{4.21}$$

$CI_{H_{Econst}}$ becomes the ratio of c_{Time} and the specific cost of the energy weighted by H_E. A value of H_E tending to zero leads to the traditional cost index definition considering in this case the total energy supplied. For a fixed c_{Time} and a c_{Elec} far less than c_{Fuel}, the $CI_{H_{Econst}}$ optimization would lead to higher economical Mach number compared to the one obtained by using the traditional cost index. This effect will be even more pronounced for higher H_E values. An example of a hybrid-electric concept for the application of $CI_{H_{Econst}}$ is presented in Section 5.4. For this hybrid-electric aircraft concept, H_{Puse} is fixed at 50% during cruise. Under the assumption that the efficiency of the hybrid-electric propulsion system does not vary significantly during cruise, H_E remains constant.

4.4.2 Constant Electric Power Supply

In this section, the CI is derived for hybrid-electric propulsion system whose operations result in a constant electric power supply. The formulation of the CI for constant electric power supply is relevant for the hybrid-electric aircraft concept investigated in Section 5.3. In this context, the hybrid-electric propulsion system is composed of an electric motor power running at constant power during a given segment of the mission. Under the assumption that the efficiency chain of the electrical system from the electric energy and power device to the electric motor is invariable during the operation, the electric power supplied $P_{Supply,Elec}$ remains constant. Considering now H_E as a function of the flight conditions, the energies supplied can be written as:

$$E_{Supply,Elec} = P_{Supply,Elec} \cdot t \tag{4.22}$$

and

$$E_{Supply,Fuel} = E_{Supply,Total} - E_{Supply,Elec} = E_{Supply,Total} - P_{Supply,Elec} \cdot t \tag{4.23}$$

Equations 4.22 and 4.23 can be combined into Equation 4.17.

$$\frac{\mathrm{d}C}{\mathrm{d}t} = c_{Time} + c_{Fuel} \cdot (\frac{\mathrm{d}E_{Supply,Total}}{\mathrm{d}t} - P_{Supply,Elec}) + c_{Elec} \cdot P_{Supply,Elec} = 0 \tag{4.24}$$

Equation 4.24 yields to the definition of the CI for constant electric power as expressed in Equation 4.25.

$$CI_{P_{Electric,const}} = \frac{c_{Time} + P_{Supply,Elec} \cdot (c_{Elec} - c_{Fuel})}{c_{Fuel}} = -\frac{\mathrm{d}E_{Supply,Total}}{\mathrm{d}t} \tag{4.25}$$

As the cost for electricity, c_{Elec}, is in the numerator of Equation 4.25, an increase in c_{Elec} leads to a larger value of $CI_{P_{Electric,const}}$. As the result, the optimum economical flight speed increases with increasing electricity price. Moreover, $CI_{P_{Electric,const}}$, becomes zero under the specific price relation given by Equation 4.26.

$$c_{Fuel} = c_{Elec} + \frac{c_{Time}}{P_{Supply,Elec}} \tag{4.26}$$

This condition results in an economical Mach number which coincides with the ESAR optimum cruise speed as the term, $dE_{Supply,Total}/dt$, equals zero. Under the condition of a fuel price c_{Fuel} much greater than the electricity price c_{Elec}, Equation 4.25 yields the formulation:

$$CI_{P_{Electric,const_{(c_{Elec} << c_{Fuel})}}} = \frac{c_{Time}}{c_{Fuel}} - P_{Supply,Elec} \tag{4.27}$$

According to Equation 4.27, different scenarios can be discussed with respect to the relation between $P_{Supply_{Elec}}$ and the ratio c_{Time}/c_{Fuel} which reflects the conventional CI expressed in Equation 4.19.

- Values of $P_{Supply,Elec}$ less than the ratio c_{Time}/c_{Fuel} result in a $CI_{P_{Electric,const}}$ lower than the CI. This condition tends to lower the optimum flight speed. However, the resulting economical Mach number is still higher than MRC.
- Values of $P_{Supply,Elec}$ which equal the ratio c_{Time}/c_{Fuel} nullify Equation 4.27. Under this condition the optimum economical Mach number is equal to MRC.
- Values of $P_{Supply,Elec}$ larger than the conventional CI provide a negative $CI_{P_{Electric,const}}$. In this case, MRC is chosen as economical Mach number.

Similarly, if the fuel price c_{Fuel} is very large compared to c_{Time} and c_{Elec}, a negative $CI_{P_{Electric,const}}$ will be obtained as formulated in Equation 4.28. In this scenario, the economical speed corresponds to MRC.

$$\lim_{c_{Fuel}\to\infty} CI_{P_{Electric,const}} = -P_{Supply,Elec} \tag{4.28}$$

Another case to highlight is when c_{Elec} equals c_{Fuel}. This condition leads to the formulation of the traditional cost index definition however in this case with the total energy supplied considered. As a result the economical Mach number may be changed compared to the conventional case if the energy consumption characteristic is different.

$$CI_{P_{Electric,const_{(c_{Elec}=c_{Fuel})}}} = \frac{c_{Time}}{c_{Fuel}} = -\frac{\mathrm{d}E_{Supply,Total}}{\mathrm{d}t} \tag{4.29}$$

4.4.3 Constant Amount of Electrical Energy Consumption

For this third hybrid-electric application, the amount of $E_{Supply_{Elec}}$ stored is consumed irrespective of the flight speed. It represents, for instance, the case of a number of fully charged batteries installed on board of an aircraft whose capacity is consumed independently of the flight speed until the end of the mission according to a given state-of-charge. With respect to the specificity of this hybrid-electric propulsion system, the variation of the electric energy consumed at the energy source during the total mission time, t, is zero:

$$\frac{\mathrm{d}E_{Supply,Elec}}{\mathrm{d}t} = 0 \tag{4.30}$$

which leads to:

$$\frac{\mathrm{d}E_{Supply,Fuel}}{\mathrm{d}t} = \frac{\mathrm{d}E_{Supply,Total}}{\mathrm{d}t} - \frac{\mathrm{d}E_{Supply,Elec}}{\mathrm{d}t} = \frac{\mathrm{d}E_{Supply,Total}}{\mathrm{d}t} \tag{4.31}$$

Consequently, Equation 4.17 yields:

$$\frac{\mathrm{d}C}{\mathrm{d}t} = c_{Time} + c_{Fuel} \cdot \frac{\mathrm{d}E_{Supply,Fuel}}{\mathrm{d}t} = c_{Time} + c_{Fuel} \cdot \frac{\mathrm{d}E_{Supply,Total}}{\mathrm{d}t} = 0 \tag{4.32}$$

The CI definition obtained in Equation 4.33 is similar to the conventional CI established in Equation 4.19. As the electric energy consumption is independent of the time, it is like

considering the electrical cost as part of the fixed cost. Consequently, only the change in fuel consumption is relevant to determine the optimum economic Mach number.

$$CI_{E_{Electric,const}} = \frac{c_{Time}}{c_{Fuel}} = -\frac{\mathrm{d}E_{Supply,Total}}{\mathrm{d}t} = -\frac{\mathrm{d}E_{Supply,Fuel}}{\mathrm{d}t} \tag{4.33}$$

4.5 Summary of Cost-Index for Hybrid-Electric Aircraft

The cost-index equations established through Section 4.4 are summarized in Table 4.1.

Cost Index	Equation
$CI = \frac{c_{Time} + E_{Supply,Total} \cdot (c_{Elec} - c_{Fuel}) \cdot \frac{\mathrm{d}H_E}{\mathrm{d}t}}{c_{Fuel} \cdot (1 - H_E) + c_{Elec} \cdot H_E}$	(4.19)
Cost Index for Constant Degree of Hybridization for Energy	**Equation**
$CI_{H_{Econst}} = \frac{c_{Time}}{c_{Fuel} \cdot (1 - H_E) + c_{Elec} \cdot H_E}$	(4.21)
under the condition $\frac{\mathrm{d}H_E}{\mathrm{d}t} = 0$.	
Cost Index for Constant Electric Power Supply	**Equation**
$CI_{P_{Electric,const}} = \frac{c_{Time} + P_{Supply,Elec} \cdot (c_{Elec} - c_{Fuel})}{c_{Fuel}}$	(4.25)
under the condition $P_{Supply,Elec} = constant$.	
Cost Index for Constant Electrical Energy Consumption	**Equation**
$CI_{E_{Electric,const}} = \frac{c_{Time}}{c_{Fuel}}$	(4.33)
under the condition $\frac{\mathrm{d}E_{Supply,Elec}}{\mathrm{d}t} = 0$.	

Table 4.1: Summary of cost-index for hybrid-electric aircraft

Chapter 5

Integrated Performance of Hybrid-Electric Propulsion Systems

With regards to the potential evolution of battery technology discussed in Section 2.2.3.1, fuel-battery hybrid-electric system is viewed as a promising topology towards the achievement of the future aviation goals highlighted in Section 1. The feasibility and the potential benefits of fuel-battery propulsion system need to be assessed at aircraft level. The integrated performance of fuel-battery hybrid-electric propulsion system is examined in this chapter on the narrow-body transport aircraft segment represented by the class of the Airbus A320 or Boeing B737. By equipping the conventional gas-turbines with an electric motor powered by batteries, the retrofit of a narrow-body transport aircraft with a parallel hybrid-electric propulsion system is analysed first in Section 5.3. In order to gain more insights into the sizing heuristics and design axioms of hybrid-electric aircraft, the investigation of hybrid-electric narrow-body clean sheet designs are evaluated in Section 5.4 and in Section 5.5. In Section 5.4, the sizing and performance implications of a parallel hybrid-electric system are investigated by sizing the aircraft for increasing design ranges and according to different levels of battery technology. The integrated performance of a partial parallel hybrid-electric propulsion system is evaluated in Section 5.5 on a narrow-body transport aircraft featuring a quad-fan arrangement. The integrated performance are examined in terms of change in aircraft weight, potential block fuel reduction and change in vehicular efficiency. Moreover, the implications of hybrid-electric propulsion system on flight technique optimality are analysed. In view of the integrated performance, design heuristics and suitable market range segments are evaluated for the application of fuel-battery hybrid-electric narrow-body transport aircraft.

5.1 Aircraft Top-Level Requirements and Sizing Guidelines

The ATLRS, the design mission and the sizing guidelines specified for the design of the hybrid-electric transport concepts investigated in this chapter are highlighted in the following. For these aircraft studies, the YEIS is set to 2035. Consequently, the hybrid-electric propulsion

technology implemented in the aircraft concepts is projected to a YEIS 2035. Moreover, evolutionary technological improvements related to the disciplines of aerodynamics and structure are assumed to suitably reflect a YEIS 2035. The design payload of the aircraft is set at 180 passengers (PAX) assuming 102 kg per PAX. Compliance with the airworthiness regulations CS-25 and FAR 25 transport category is administered. Field performance is characterized by a TOFL at *ISA*, sea-level not being greater than 2200 m, and an approach speed less than 145 KCAS. Additionally, the time-to-climb to initial cruise altitude is limited to 25 min.

The defined mission profile consists of a taxi-out, take-off at sea level and *ISA*+10°C, climb at *ISA*+10°C with a speed schedule 250 KCAS / 300 KCAS / M0.76 until an initial cruise altitude at FL 350. The cruise, performed at M 0.76 and *ISA*+10°C, is followed by a mirrored descent, landing and taxi-in. Reserves fuel according to EU-OPS 1.255 accounts for 5% trip fuel contingency cruise, 30 minute hold at 1500 ft and 100 nm alternate. Only for the hybrid-electric aircraft concept assessed in Section 5.5, the mission reverves were adapted. Because of the use of electrical energy during contingency cruise, the account based on percentage of trip fuel was modified and expressed as an equivalent time criterion set at 10% of the block time.

For the design of the aircraft, the following sizing guidelines were applied. The wing is sized according to a constant wing loading of 645 kg/m^2 to retain similar en-route buffet onset characteristics as well as low-speed performance. It is also sized for a constant wing aspect ratio of 12.5. The flow-path sizing of the propulsive device is set at top-of-climb (*ISA*, FL350 and M0.78) for a residual rate-of-climb of 300 fpm. The sizing of the vertical and horizontal stabilizer is conducted according to constant volume coefficient. The fuselage geometry is kept fixed for all variations investigated. The cargo volume represents consequently a constraint for the storage of the batteries and for the conventional cargo. The volume constraint problem is analysed assuming a constant battery density of 1000 kg/m^3, which includes the volume of the battery and of the thermal management system. Detailed structural strengthening of the fuselage due to loading and de-loading of the battery in the cargo compartment are disregarded in these aircraft studies.

5.2 Propulsion and Power Systems

The propulsion and power systems commonly shared across the narrow-body transport aircraft concepts investigated are described in this section. Specificities related to the propulsion system are detailed in the respective section related to each aircraft concept.

5.2.1 Electric Propulsion System

For each hybrid-electric aircraft concept investigated in this chapter, an identical architectural layout for the electrical chain of the propulsion system was selected as illustrated in Figure 5.1.

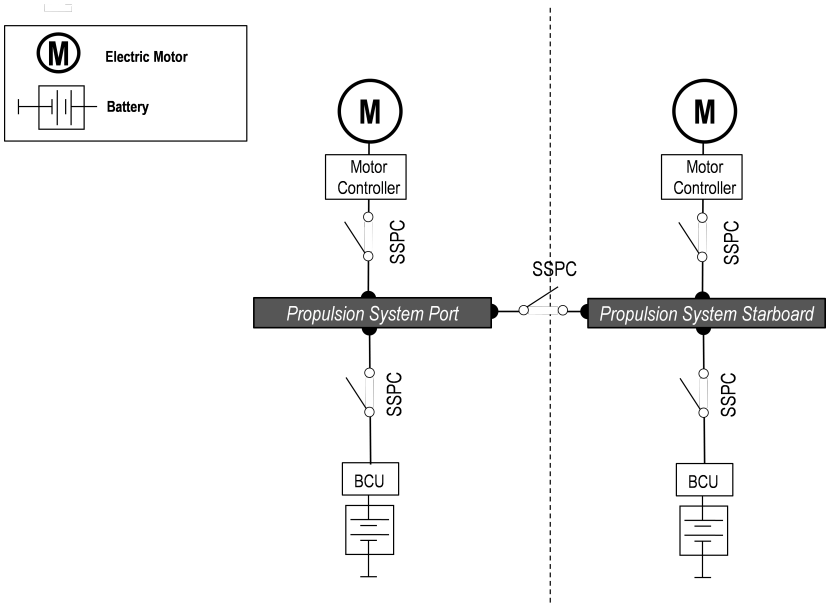

Figure 5.1: Electric propulsion system [27]

It is composed of an electric motor equipped with controller which are powered by batteries. According to the YEIS, HTS technology was assumed for the electric motor and for the electric cables. Each battery pack is controlled by a battery controller unit (BCU). The battery technological level is a key factor in determining the performance of the integrated hybrid-electric aircraft concepts. Consequently, sensitivity analysis based on the battery gravimetric specific energy are conducted at aircraft level. According to the prediction of the evolution of the battery technology indicated in Section 2.2.3.1, the battery gravimetric specific energy cell-level (e_{Bat}) is varied in the analysis between 750 Wh/kg and 1500 Wh/kg.

Component	Specific weight	Efficiency
Battery	750 - 1500 Wh/kg [9, 16]	90 - 95 %
HTS Motor	20.0 kW/kg [6]	99.5 %
HTS Cables	9.2 kg/m [39]	100 %
Controller	20.0 kW/kg [6]	99.5 %
Converter	18.0 kW/kg [6]	99.5 %
SSPC	44.0 kW/kg [42]	99.5 %

Table 5.1: Technology assumption for the electrical components of the propulsion system [27]

The PMAD enables the transmission and distribution of the electrical power through electrical buses. Protection in the system is provided by the implementation of SSPC. For the propulsion system architecture equipped with several electric motors, each electric bus dedicated to a propulsion system is interconnected via a SSPC to ensure redundancy in the system. The potential technological evolution of the electrical components beyond the state-of-the-art were discussed in Section 2.2. The technological level of the electrical components assumed in terms of specific weight and efficiency for aircraft level assessment are summarized in Table

5.1. The specific weights of the components are assumed invariant with scale. Except for the batteries, the efficiency of the components is assumed constant with the operating conditions. The efficiency of the electric propulsion system implemented in the aircraft models depends consequently only on the variation of the battery efficiency with respect to its discharge characteristic according to the battery model presented in Section 3.2.3.6.1 as well as the efficiency change of the propulsive device with the flight state and the power settings according to the model introduced in Section 3.2.3.2.

5.2.2 All-Electric Power System

The layout of the all-electric power system architecture implemented in the hybrid-electric aircraft concepts investigated in this chapter is illustrated in Figure 5.2.

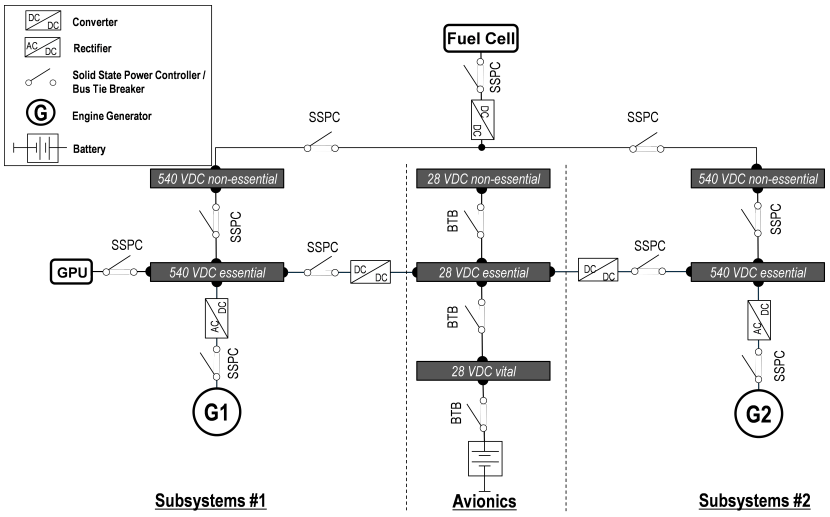

Figure 5.2: Layout of the all-electric power system architecture [27]

Following the trends already set by state-of-the-art aircraft such as the Boeing B787 [116], it consists of an all-electric subsystem architecture. The main operating voltage of the subsystems is 540 VDC, which was identified as the future operating voltage [117]. The Boeing B787 has already demonstrated a subsystem voltage level of 270 VDC [118]. The assumptions with regards to the specific weight of the components constituting the all-electric power subsystem are summarized in Table 5.2.

In addition to a zero-bleed architecture, it features zero-power off-take from the engine in normal modes as the power required by the subsystems is provided by proton exchange membrane fuel-cells operated with liquid hydrogen. The weight of the fuel cell system, including the liquid hydrogen and tank mass, was estimated according to [55]. The stored liquid hydrogen was also used as coolant to maintain the HTS materials of the electric motors and cables constituting the propulsion system below critical temperature. However, to ensure redundancy in the system, a generator is installed on each combustion engine to provide electric energy in abnormal modes. The weight of the generators was calculated according to [34].

Component	Power and weight estimation
Environmental control system	Number of PAX [119] according to a specific weight of 0.36 kW/kg [120]
Flight controls	Flight control area [67] according to a specific weight of 3.73 kW/kg [121]
Landing gear	Based on MTOW [122] according to a specific weight of 0.19 kW/kg [122]
Anti-icing	Scaled icing area based on B787 reference area [123]
Cables and busses	Based on maximum subsystem power according to [42]
Fuel cell system (incl. liquid hydrogen and tank mass)	Based on maximum subsystem power according to [55]
Generator	Based on maximum power according to a specific weight of 5 kW/kg [34]

Table 5.2: Technology assumption for the electric components of the power system [27]

The power demand and mass estimations of the important subsystems like environmental control system or flight controls are estimated according to methods described by Vratny [42]. The power demand for the cabin systems and the instruments is estimated according to the methods published by Xia [124]. For the controller, converter and SSPC the same technological level as summarized in Table 5.1 is assumed.

5.3 Parallel Hybrid Retrofit Aircraft

The retrofit of a narrow-body transport aircraft equipped with a fuel-battery hybrid-electric propulsion system was assessed by Pornet et al. [27]. The reference aircraft is sized for a design range of 3300 nm. The hybrid-electric propulsion system is composed of a HTS electric motor powered by batteries mounted on the low-pressure shaft of the gas-turbine to support its operation during some segments of the mission. Both gas-turbines are equipped with an electric motor. The layout of the electric propulsion system is illustrated in Figure 5.1. The hybridization approaches investigated are discussed in Section 5.3.2. The geometry of the reference aircraft is kept fixed. Possible increase of the nacelle wetted area due to the integration of the electric engine has not been considered in this aircraft study. It was decided not to downsize the combustion engine to give the capability to the aircraft to still fly medium range missions based on the conventional system only. The design mission in comparison to the reference aircraft was found to be reduced to 2770 nm because of the installation of the necessary electrical components.
Due to the nature of the retrofit, the installation of the additional electrical components is limited by the MTOW of the reference aircraft. In off-design, the reference aircraft is taking-off at a take-off weight (TOW) less than MTOW according to the block fuel required to fly the off-design mission. Off-design missions open consequently the possibility to install and to

size the hybrid-electric propulsion system under the constraint of MTOW. Aircraft market study targeting an YEIS 2035 [125] showed that a 900 nm stage length will cover 79% of all world-wide flights in the 180-200 seats segment. This stage length was identified as the maximum utilization stage length of the retrofitted aircraft. Aiming for minimum fuel burn consumption at maximum utilization stage length, this off-design range was selected to size the hybrid-electric propulsion system. An identical flight profile as described in Section 5.1 was attributes to the off-design mission. To maximize the benefits, the batteries are utilized only during the block mission. The mission reserves are flown with fuel only.

5.3.1 Hybrid-Electric Propulsion System Model

The aircraft is equipped with advanced geared turbofan engines. The geared turbofan model was developed according to the methods presented in Section 3.2.3.1. It features a bypass ratio of 18 at flow path sizing conditions occuring at TOC conditions under MCL rating. At *ISA*, FL350, $M0.78$ conditions and maximum thrust settings, the $TSFC$ yields 13.25 g/kN/s. In order to facilitate the flexibility required for the hybridization of the propulsion system, it was decided to decouple the integrated geared turbofan power plant model into a modular arrangement of a turboshaft engine and a geared ducted fan device that in combination feature the same properties as the reference geared turbofan. Therefore, a two-spool turboshaft engine model with a booster mounted to the power shaft was set up in GasTurb [95]. Turboshaft intake conditions were iterated to simulate the presence of the frontal geared fan, both, at design and off-design conditions. Turboshaft nozzle pressure ratio was iterated to yield adequate values of core residual thrust. The resulting turboshaft engine model was successfully verified against the reference geared turbofan model taking into account the temperature, pressure and corrected mass flow values at important thermodynamic stations. The turboshaft was integrated at aircraft level according to the methods described in Section 3.2.3.3. The geared ducted fan device was captured using the ducted fan model introduced in Section 3.2.3.2. As part of the integrated aircraft study, the ducted fan and turboshaft engine models were matched appropriately.

5.3.2 Sizing and Integrated Performance Analysis

The sizing and integrated performance of the retrofit aircraft equipped with a parallel hybrid-electric propulsion system is assessed in the following. The analysis aims at exploring the design space related to the implementation of the parallel hybrid-electric propulsion system at aircraft level. The objective is to size the system in order to achieve the largest reduction in block fuel against the reference aircraft. The design parameters and constraints involved in the sizing of the hybrid-electric propulsion system are indicated in Figure 5.3. In this figure, the relative change in block fuel compared to the reference aircraft is assessed by sizing and utilizing the electric motor for cruise only. The other segments like takeoff, climb and the reserves are performed with the conventional combustion engines only. The design parameters indicated are the total installed maximal power of the electric motor $P_{EM,max}$ and the power setting of the electric motor in cruise. 0% meaning that the electric motor is

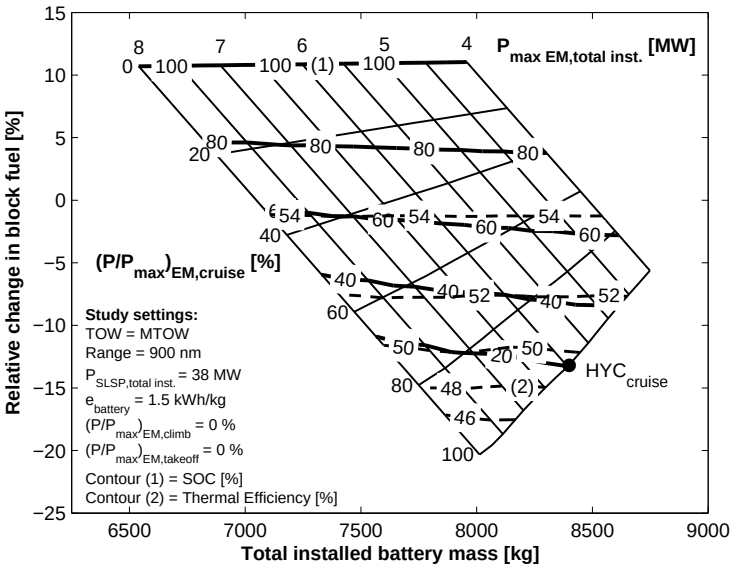

Figure 5.3: Design chart for hybrid-electric propulsion system in cruise [27]

not used whereas 100% means that the maximal power of the electric motor installed is used during cruise. The first contour line represents the battery state-of-charge. According to battery technology, the battery must not be discharged below a certain SOC limit commonly set at 20%. This additional constraint in the sizing of hybrid-electric aircraft was highlighted in Section 3.2.7. The design chart is consequently constrained by the 20% SOC limitation. In order to maximize the electrical energy available on board the aircraft, the TOW at 900 nm stage length is set equal to MTOW. Consequently, the total battery mass installed is an outcome of the study. As the MTOW is fixed, the total battery mass results from the trade between the additional electrical system weight which is mainly a function of the maximal power of the electric motor installed and the fuel mass required. Due to the MTOW limitation, an increase in system weight is directly traded by a decrease in the battery mass which can be installed on board of the aircraft.

Because of the resulting higher TOW compared to the reference aircraft, it is intuitive that the hybrid-electric retrofit aircraft requires more fuel than the reference aircraft if no electric energy is used as it can be observed at 0% power setting of the electric motor. As no electric energy is used, the battery SOC remains constant at 100%. The very slight change in fuel burn observed when increasing $P_{EM,max}$ is explained by the influence of the electrical system and battery installation on the centre-of-gravity of the aircraft affecting the lift-to-drag ratio of the aircraft according to the variation in trim drag.
By increasing the power setting of the electric motor, more electrical energy is used during cruise, leading to an increase in the potential fuel burn reduction. For an installed electric motor power of 6 MW, it can be observed that the electric motor needs to be used above 40% to achieve a block fuel reduction compared to the reference aircraft. The sizing of the electric motor power is critical in the search for minimum block fuel consumption. Installing

a too small electric motor limits the potential use of the electric energy during cruise which results in lower fuel burn reduction benefit. The fuel burn potential reduction increases when increasing the installed electric motor power as more electrical energy is utilized during cruise. However, the increase in the maximal power of the electric motor installed becomes then limited by the 20% SOC constraint.
The design axiom for minimum fuel-burn is consequently to select the electric motor which is utilized at its maximal power during cruise, as indicated by the power setting of 100% and which consumes the entire available electric energy of the batteries installed with respect to the 20% SOC constraint. For the hybrid-electric retrofit concept investigated, the optimal system sizing, indicated in the graphic with the notation "HYC_{cruise}", led to a total electrical motor power installed of 6MW and a total battery mass installed of 8400 kg. With this design, a fuel burn reduction of 13% is achieved compared to the reference aircraft along the 900 nm off-design mission stage length.
Due to the concurrent utilization of the electric motor, the operations of the turboshaft are impacted during cruise. As mentioned previously the turboshafts are not resized in this hybridization scheme. The additional power provided by the electric motor leads the turboshaft to run into part-power during cruise. The thermal efficiency of the turboshaft is consequently impacted by the electric motor operation. Illustrated in Figure 5.3 with the second contour line, the degradation of the thermal efficiency of the turboshaft becomes larger with increasing electric motor power setting and with increasing installed electric motor power. An efficiency degradation of about 4 percent point is noticed along the 20% SOC constraint compared to the case without the electric motor. This degradation penalizes the fuel burn consumption.

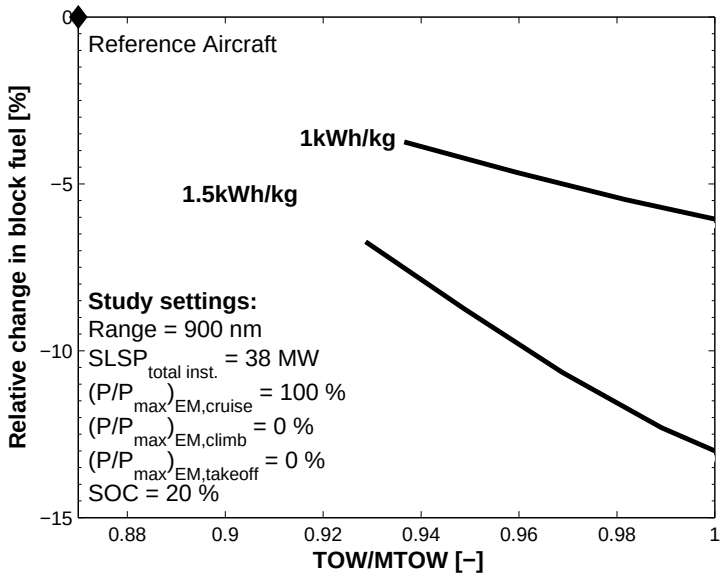

Figure 5.4: Sensitivity study against battery specific energy [27]

The fuel burn reduction potential indicated depends strongly on the e_{Bat} assumed in this

study at 1500 Wh/kg at cell-level. A sensitivity study related to the e_{Bat} is presented in Figure 5.4. In this study, the total battery mass installed is a design variable and the electric motor installed is used at 100% of its maximal power installed during cruise. In Figure 5.4, the aircraft concepts are sized according to a 20% SOC constraint. The block fuel reduction is measured against the reference aircraft performing an off-design mission of 900 nm. As indicated by Figure 5.4, the block fuel reduction is the highest when the MTOW condition is reached. This confirms the previous assumption made that the highest fuel burn reduction is achieved when maximizing the available electric energy on board of the aircraft as in Figure 5.3 drawn at MTOW constraint. Figure 5.4 shows that by decreasing the e_{Bat} from 1500 Wh/kg to 1000 Wh/kg, the potential fuel saving is reduced by around 50%.

In the above analysis, the electric motor was used during cruise only while the takeoff and the climb segments were still performed with the conventional gas-turbine only. The benefits of utilizing the electric motor during climb and cruise is now examined in Figure 5.5.

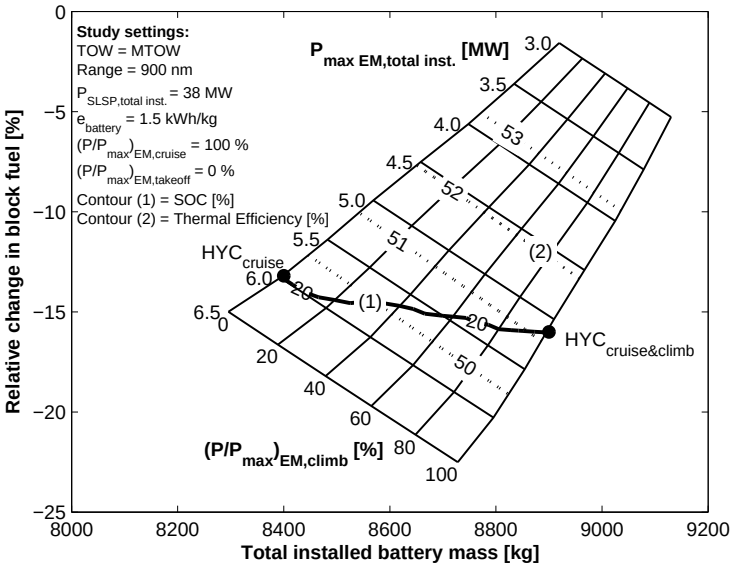

Figure 5.5: Design chart hybrid-electric propulsion system in climb and cruise [27]

In this assessment, the electric motor is used at 100% of its maximum power during cruise while the electric motor power is varied during climb from 0% to 100%. The optimum electric motor installation in view of minimizing the fuel consumption is investigated by varying the maximal electric motor power installed $P_{EM,max}$. The analysis of Figure 5.5 shows that the impact of using the electrical motor during the climb results to an additional -3% point at the optimum case denoted by the abbreviation "$HYC_{cruise\&climb}$". With respect to the SOC constraint, the electrical energy available is consumed completely along the 20% SOC line. As investigated previously in Figure 5.3, if no electric power is used during climb, the optimal design point is found with the installation of a 6000 kW total electric motor power which translates in an H_P of 16% and a battery system mass of 8400 kg. Limited by the MTOW constraint, the only way to use additional electrical energy during the climb,

while still utilizing the electric motor at 100% during cruise and respecting the 20% SOC constraint is to reduce the power of the electrical motor installed. The resulting design axioms for the hybrid-electric propulsion system utilized during climb and cruise are itemized in the following.

- Due to the reduced electrical energy utilized during cruise, the absolute cruise fuel consumption is higher. As shown in Table 5.3, the cruise fuel consumption is 10% higher in cruise, even if the efficiency of the gas-turbine during cruise is slightly improved as it runs into better part load. This is shown in Figure 5.5 with about 1 percent point efficiency gain during cruise between HYC_{cruise} and $HYC_{cruise\&climb}$.
- Installing a lower electric motor power results in reducing the electrical system weight which enables the increase of the battery mass installed (if at the same time, the block fuel burn remains constant or is reduced), leading to more electric energy available on board of the aircraft. In this case the block fuel is reduced by -3% as indicated in Table 5.3.
- The use of electrical energy during climb enables climb fuel burn reduction. Moreover, considering short off-design mission, the relative contribution of the climb in the block mission increases. Reducing fuel consumption during climb on short stage length has consequently a larger impact on the block fuel consumption. The fuel burn savings achieved during climb are -22% as represented in Table 5.3.

As a result, the fuel burn saved during the climb overcomes the increase in fuel during cruise resulting finally in a reduction of block fuel consumption. The selection of the electric motor power for minimum fuel burn follows the aforementioned design axioms. With respect to the objective of minimizing the fuel consumption, the optimum system design point is found by installing a total electric motor power of 5100 kW which results in an H_P of 13% and a total battery mass of 8900 kg. A block fuel reduction up to 16% against the reference aircraft is achieved by operating the electric motor during climb and cruise.

Segment	Taxi-out	Take-off	Climb	Cruise	Descent	Landing	Taxi-in	Block
Fuel Change	0%	0%	-22%	10%	0%	0%	0%	-3%

Table 5.3: Relative fuel consumption values between $HYC_{cruise\&climb}$ and HYC_{cruise} [27]

In summary, the sizing of the hybrid-electric propulsion system is the outcome of an interplay between the maximum electric motor power, which determines mainly the weight of the associated electrical system, the control setting of the electric motor, the total mass of the battery required and the potential reduction in fuel consumption. The sizing is constrained by the SOC of the battery and due to the specificity of the retrofit by the MTOW.

5.3.3 Aircraft Mass Breakdown

The hybrid retrofit aircraft utilizing the hybridization approach during climb and cruise is compared against the reference conventional aircraft for an off-design mission of 900 nm in

Table 5.4. The TOW of the reference aircraft to operate this off-design mission is 68697 kg and the release fuel which includes the block fuel and the reserves is 6453 kg. In order to maximize the electric energy on-board the aircraft, the hybrid retrofit aircraft operates the 900 nm stage length at MTOW with 78990 kg. It is a 15% increase in TOW compared to the reference aircraft. The propulsion system of the hybrid aircraft is increased by 6% due to the installation of the electric motors sized for a total power of 5100 kW. The installation of the electric propulsion system results in a 31% increase in electrical system weight and an additional 8900 kg of batteries. The decrease in release fuel of 10% is less than the previously quoted block fuel reduction of 16% as the reserves flown with fuel only are accounted for in the release fuel.

Aircraft mass breakdown	Unit	Reference Aircraft	Hybrid Aircraft	Δ Ref.
Structure	[kg]	20819	20819	0%
Propulsion system	[kg]	8991	9501	6%
- Conventional powerplant	[kg]	8991	8991	0%
- Electric motors (incl. controllers)	[kg]	NA	510	NA
Equipment	[kg]	14073	15593	11%
- Furnishing	[kg]	4435	4435	0%
- Hydraulic system (anti-icing)	[kg]	173	173	0%
- Electrical system	[kg]	4941	6461	31%
- Instruments	[kg]	944	944	0%
- Operational items	[kg]	3580	3580	0%
OEW	[kg]	43883	45913	5%
Payload	[kg]	18360	18360	0%
Release fuel (block and reserves)	[kg]	6453	5818	-10%
Total battery	[kg]	NA	8900	NA
TOW	[kg]	68697	78990	15%

Table 5.4: Mass breakdown of the reference and hybrid-electric aircraft for an off-design mission of 900 nm [27]

The retrofitting of an aircraft with a hybrid-electric system enables to gain insights into the design parameters, constraints and behavior of the propulsion system as well as to establish first design heuristics. However, in view of examining the sizing effects resulting from the integration of hybrid-electric propulsion at aircraft level and of investigating the potential market range application for hybrid-electric narrow-body transport aircraft, the integrated performance of clean sheet designs need to be assessed.

5.3.4 Optimum Flight Technique

The optimum flight technique for the retrofit aircraft equipped with a parallel hybrid-electric propulsion system is analysed in this paragraph. It was published by Pornet et al. [115]. The optimum altitude-speed schedule is assessed according to the vehicular efficiency metrics introduced in Chapter 4. The relative value of SAR and ESAR are illustrated in Figure

5.6 and Figure 5.7 respectively. COSAR depends on the specific market price of the energy sources. The relative value of COSAR is evaluated assuming a fuel price of 6 USD/USG, an electricity price of 0.07 USD/kWh in Figure 5.8 and an electricity price of 0.16 USD/kWh in Figure 5.9. The aircraft weight condition of 98% of MTOW represents a typical aircraft weight at TOC.

The analysis of Figure 5.6 indicates that maximum SAR occurs at a Mach number close to 0.7 and a FL of 350. The evaluation of maximum ESAR in Figure 5.7 shows that it evolves towards higher Mach number value. Recalling Section 4.2, ESAR takes into account the overall energy consumption of the aircraft. In addition to the fuel energy, which is exclusively considered in SAR, the electric energy consumption is comprised in the ESAR metric. The increase in Mach number is rooted in the operational characteristics of the hybrid-electric propulsion system and especially the management of the electrical energy. As the electric motor runs continuously at its maximal power during cruise, the operation of the electric motor is independent of the flight conditions. However, the flight speed influences the flight time and as a result the amount of electrical energy consumed during cruise. For a given mission, increasing the Mach number reduces the electric energy requirement. As a result, the Mach number value for maximum ESAR increases. However, this change is counteracted by the higher fuel consumption occurring at higher flight speed. With a Mach number of 0.71, the speed for optimum ESAR is consequently slightly higher than the Mach number of 0.7 for optimum SAR. This operational characteristic explains also the optimum SAR trend. Lowering the operating Mach number increases the flight time and as a result leads to higher electric energy consumption. This effect amplifies the influence of decreasing Mach number on fuel consumption. Consequently, optimum fuel consumption occurs at rather low Mach numbers.

When analysing the optimum COSAR trend, the specific cost of each energy sources needs to be taken into account. Recalling Equation 4.11, H_E weights the specific cost of each energy involved in the hybrid-energy propulsion system. For an instantaneous point performance computation, H_E is a constant value. However, it is interesting to note that during cruise, the instantaneous value of H_E tends to increase. Assuming that the efficiency of the conventional and electrical system remains about constant during cruise, this evolution of H_E is explained by the operation of the electric motor during cruise at its maximal power while the power requirement of the turbofans diminishes as a result of the aircraft weight reduction during cruise. In Figure 5.8, the specific price of the electric energy represents roughly 40% of the specific price of the fuel. The cost of fuel dominates consequently the energy cost relation leading to a flight schedule tending to minimize the fuel energy consumption. It results in an COSAR speed optimum which lays between the SAR and ESAR speed optimum while being closer to the SAR optimum. For a specific electricity price of 0.16 USD/kWh, the electric price equals about the fuel specific price. As demonstrated by Equation 4.12, COSAR is equivalent to the ESAR metric under this price condition. As the result the optimum flight technique for maximum ESAR and maximum COSAR in terms of speed and altitude are identical and the contour of Figure 5.9 coincides with the one of Figure 5.7.

In the modelling of the hybrid-electric propulsion system, the influence of altitude on the efficiency of the electric motor was neglected in first instance assuming an appropriate thermal

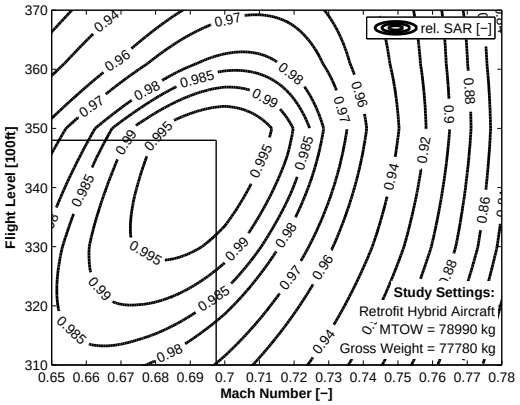

Figure 5.6: Altitude and speed sensitivity of relative SAR for a gross-weight at 98% of MTOW [115]

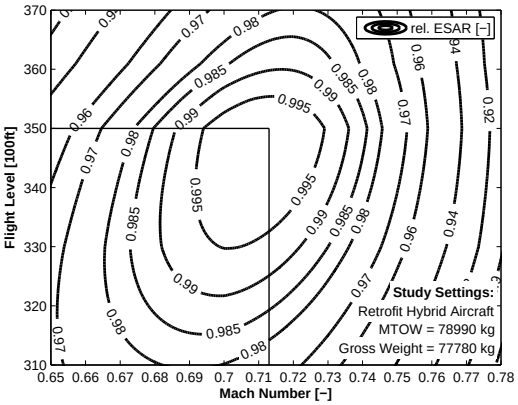

Figure 5.7: Altitude and speed sensitivity of relative ESAR for a gross-weight at 98% of MTOW [115]

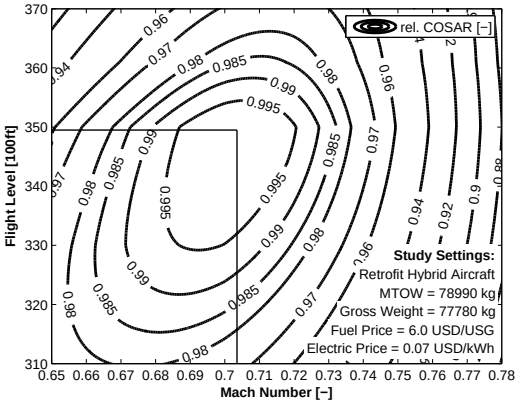

Figure 5.8: Altitude and speed sensitivity of relative COSAR for a gross-weight at 98% of MTOW and a specific electricity price of 0.07 USD/kWh [115]

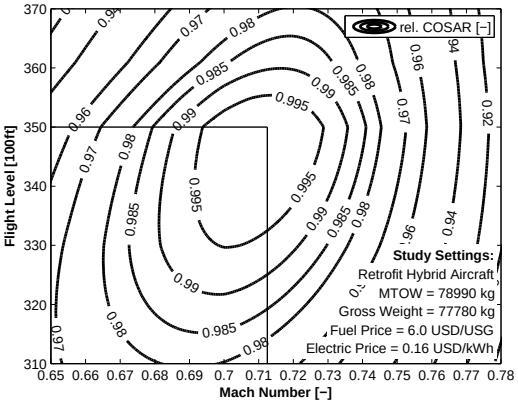

Figure 5.9: Altitude and speed sensitivity of relative COSAR for a gross-weight at 98% of MTOW and a specific electricity price of 0.16 USD/kWh [115]

management will be effected. Consequently, the altitude optimization is not influenced by the choice of the objective functions.

The speed sensitivity with respect to the metrics SAR, ESAR and COSAR of the retrofit hybrid-electric aircraft concept is investigated in Figure 5.10 at an altitude of 35000 ft against a variation in aircraft gross-weight. The increase in COSAR value with reduction in aircraft gross-weight and the reduction in optimum speed with decreasing gross-weight to adapt the lift coefficient in order to operate close to the maximum lift-to-drag ratio (L/D) are expected result. The increase in optimum speed between MRC and MCRC resulting from the operating condition of the electric motor as detailed previously is noticeable. For a gross-weight of

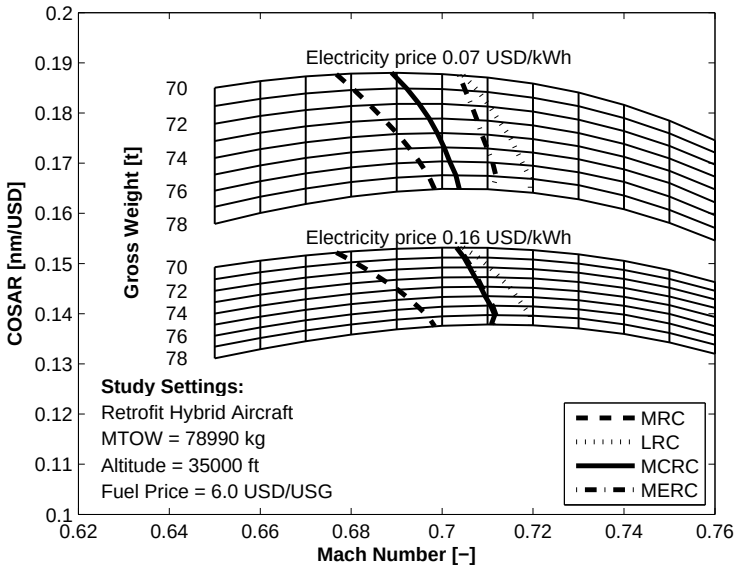

Figure 5.10: Optimum speed sensitivity versus gross-weight according to SAR, ESAR and to COSAR at an altitude of 35000 ft [115]

70000 kg, a flight profile optimized according to maximum SAR would lead to a MRC below 0.68 whereas using COSAR as objective function would result in a MCRC of 0.69 assuming a specific electricity price of 0.07 USD/kWh. The increase in MCRC with increasing electricity price is also identifiable. Assuming a specific electricity price of 0.16 USD/kWh, MCRC is above 0.7. As analysed in previously, MERC is higher than MCRC at an electricity price of 0.07 USD/kWh, whereas it coincides with MCRC for 0.16 USD/kWh. It can also be noted that LRC is in both cases higher than MCRC.
The change in COSAR with respect to gross-weight according to the different specific electricity price is worthwhile noticing. The analysis of Figure 5.10 shows that the sensitivity of COSAR is more pronounced for lower specific electricity price. This is again the result of the operational strategy of the electric motor during cruise. As the electric motor operates at maximum power during cruise, it is independent of the flight power demand. In other words the electric energy consumed during cruise in independent of the gross-weight variation. For a higher electricity price, the contribution of the fuel energy price is less preponderant to COSAR, thus reducing the sensitivity of COSAR versus the gross weight change.

The sensitivity of the optimum economical Mach number for the retrofit hybrid-electric aircraft is assessed in Figure 5.11 according to a variation of c_{Time}. The cost index is evaluated according to Equation 4.25 which was derived for the case of a constant electric power utilization independent of the flight state. According to Equation 4.25, higher cost of time results in increasing CI. The trend towards higher optimum economical Mach number with increasing c_{Time} is clearly noticeable in Figure 5.11. For a c_{Time} of zero, Equation 4.25 becomes negative with a value of -2 kWh/min. With this condition the line of optimum MCRC coincides exactly with the optimum Mach number defined by c_{Time}. As c_{Time} is negligible,

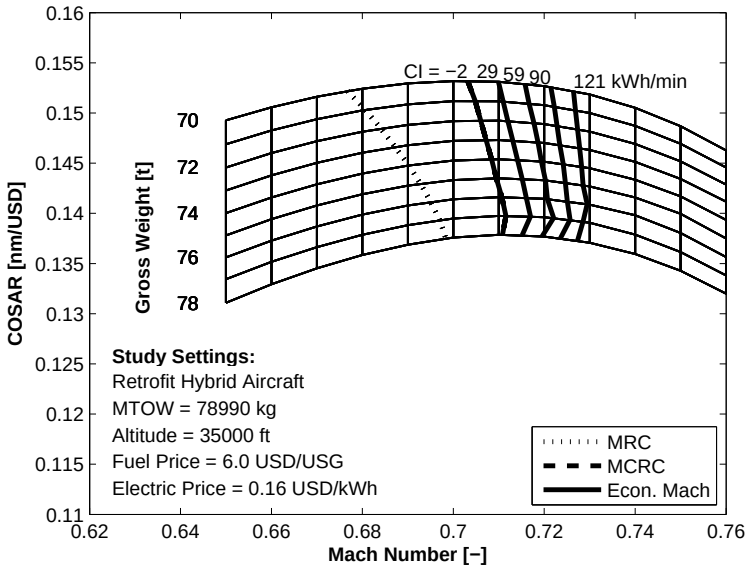

Figure 5.11: Optimum speed sensitivity versus gross-weight according to SAR, COSAR and minimum cost at an altitude of 35000 ft [115]

the most economical flight technique results in minimizing the energy cost in other words in maximizing COSAR. With increasing value of CI, c_{Time} becomes more preponderant. In order to minimize the cost, the optimum economical Mach number increases. The line with a CI of 121 kWh/min represents consequently the lowest block time condition.

5.4 Parallel Hybrid Clean-Sheet Design

In view of assessing the sizing implications of fuel-battery propulsion systems on aircraft design and overall aircraft performance as well as of identifying suitable market segments for the application of hybrid-electric narrow-body transport aircraft, a clean-sheet design of a narrow-body transport aircraft employing a fuel-battery parallel propulsion system was investigated by Pornet et al. [126]. Similar to the hybrid-electric propulsion system employed in Section 5.3, the electric motor powered by batteries is mounted in parallel on the low-pressure shaft of the gas-turbine. In the context of the concept investigated, the electric motor is mounted only in one of the gas-turbines. It was found in Section 5.3 that the simultaneous operation of the electric motor has negative consequence on the operational behaviour of the gas-turbine. A noticeable effect was the reduction of the gas-turbine efficiency forced to operate in part-load as shown in Figure 5.3. Modifying the operating line of the turbo-components, surge margins need to be also thoroughly considered during the design of the gas-turbine. In order not to change the design axioms of contemporary gas-turbine and to avoid impairing its efficiency through the utilization of the electric motor, the operational scheme of the hybrid-electric propulsion system was to switch-off the gas-turbine during cruise while the electric motor drives by itself the propulsor. As a result of the sizing and

operational strategy, the H_{Puse} is fixed at a value of 50% during cruise. The other segments are performed conventionally using the two gas-turbines.

5.4.1 Hybrid-Electric Propulsion System Model

The conventional powerplant system is equipped with a geared turbofan engine. The engine model was produced according to the methods described in Section 3.2.3.1. Four engines with design thrusts ranging from 15 kN to 35 kN were sized at TOC with maximum climb rating under the conditions *ISA*, FL 350 and M 0.78. The design deck implemented to capture the geometrical and weight sensitivity of the engines versus the design thrust and the design fan presssure ratio were represented in Figure 3.6 and Figure 3.7. The thrust characteristics of the geared turbofan were represented in Figure 3.8 for a design thrust of 21 kN and a design FPR of 1.41. The design yielded a $TSFC$ of 13.24 g/kN/s for the engine with the highest thrust and 13.30 g/kN/s for the engine with the lowest thrust. The $TSFC$ characteristics of the geared turbofan models were represented in Figure 3.9 for cruise condition at *ISA*+10°C, FL350 and M0.76 against the thrust setting for each design thrust.

5.4.2 Sizing and Integrated Performance Analysis

By sizing the aircraft for interval design ranges between 900 nm and 2100 nm, the sizing effects of integrating the fuel-battery propulsion system are investigated in terms of potential block fuel reduction and change in vehicular efficiency. The influence of the battery technological level is assessed by varying the e_{Bat} between 750 Wh/kg and 1500 Wh/kg. In each of the following figures, the relative change of the metrics is compared to an advanced conventional aircraft suitably projected to a YEIS 2035.
The relative change in block fuel is illustrated in Figure 5.12. The use of the electrical system improves the overall propulsion system efficiency of around 30% during cruise thanks to the highly efficient electrical components. In addition, as part of the energy is provided electrically during cruise, a significant reduction in fuel consumption can be achieved against the advanced conventional aircraft. When assuming e_{Bat} of 1500 Wh/kg, a block fuel reduction of 20% can be reached. However, it can be observed that these large potentials in block fuel reduction can be achieved at design ranges which reflect more of the regional market segment. Assuming a e_{Bat} of 1500 Wh/kg, a global minimum at 1100 nm gives rise to a design space between 800 nm and 1800 nm where the block fuel reduction is higher than 15%.
To understand this aspect, the Figure 5.13, which illustrates the change in MTOW, needs to be considered. It can be seen that the MTOW of the hybrid-electric aircraft is largely increased compared to the advanced gas-turbine only aircraft. It results from the utilization of batteries as an energy source, the additional system weight (according to the sizing of the electrical propulsion system components) and the sizing cascading effects. Even in the joint occurrence of reduction in fuel burn and increase in propulsion system efficiency, a large increase in MTOW compared to the advanced gas-turbine aircraft is observed. At a design range of 1100 nm, the MTOW of the hybrid-electric is 25% higher. The increase

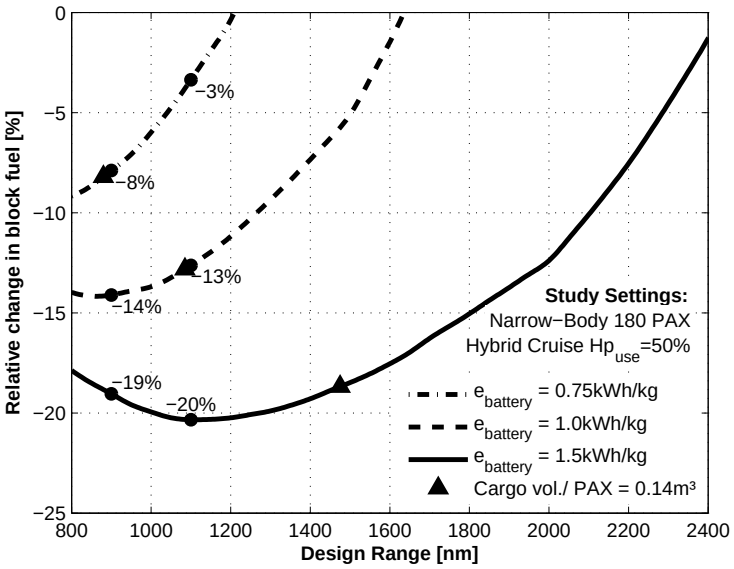

Figure 5.12: Relative change in block fuel versus relative change in block ESAR for a H_{Puse} of 50% during cruise [126]

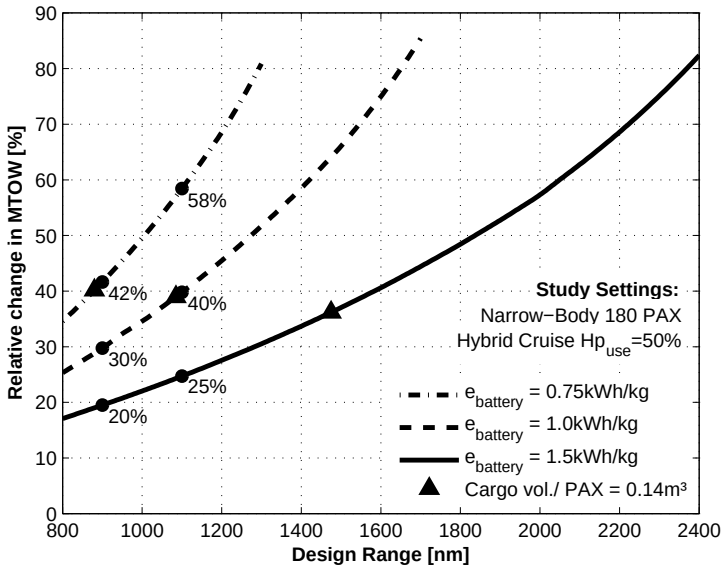

Figure 5.13: Relative change in MTOW for a H_{Puse} of 50% during cruise [126]

in MTOW is amplified with greater ranges due to higher demand in electrical energy during cruise. This is the main reason why the potential in block fuel reduction vanishes with greater range. The break-even range indicates the point where the degradation resulting from the increase in MTOW starts to overcome the fuel consumption benefit provided by the utilization of electrical energy and the increase in propulsion system efficiency. The benefit

of the hybrid-electric propulsion system is strongly counteracted by the increase in aircraft weight particularly for lower battery specific energy and for increasing design range. When assuming a e_{Bat} of 1000 Wh/kg, the fuel burn is reduced to -13% at 1100 nm and the MTOW is increased by 40% while with a e_{Bat} of 750 Wh/kg the relative changes are -3% and +58% respectively.

In summary, with the use of the electric energy as an additional source of energy and through the achievement of higher propulsion system efficiency, large fuel burn reduction can be achieved. However because of the additional weight of the batteries and of the electrical system components, the MTOW of the aircraft is largely increased. Consequently, the overall energy consumption of the aircraft, which means in this case the consumption of the fuel energy and of the electrical energy might be impaired compared to the advanced conventional aircraft.

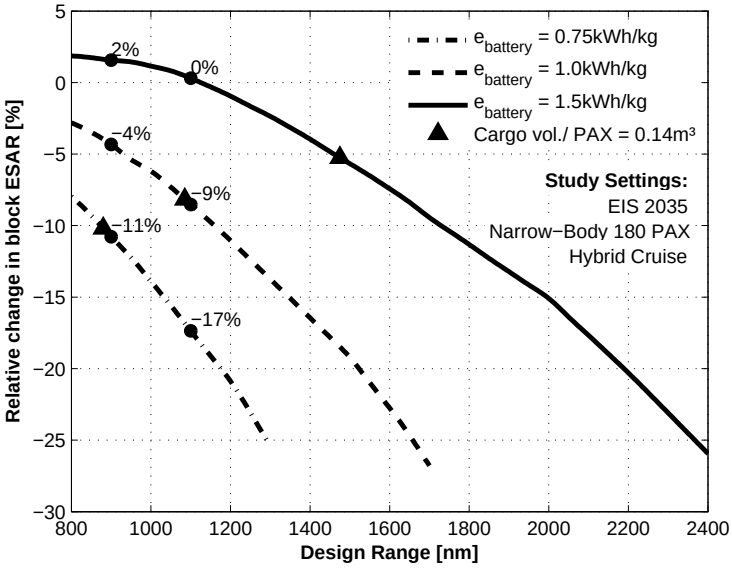

Figure 5.14: Relative change in ESAR for a H_{Puse} of 50% during cruise [126]

Figure 5.14 illustrates this important design implication where the relative change in block ESAR is represented on the vertical axis. For most ranges investigated the vehicular efficiency of the hybrid-electric aircraft is degraded compared to the advanced conventional aircraft. In other words, the hybrid-electric aircraft consumes more energy than the advanced gas-turbine aircraft for most of the stage lengths investigated. Only when assuming a e_{Bat} of 1500 Wh/kg, neutral energy outcomes can be achieved up to 1100 nm. At 1100 nm, the ESAR is 9% lower with a e_{Bat} of 1000 Wh/kg and 17% less with a e_{Bat} of 750 Wh/kg. The consideration of the overall energy consumption is important as the electrical energy might not be produced only through renewable energy sources and the production will have an impact on the carbon life cycle assessment. As the electric motor is used during cruise only, it is interesting to analyze in detail the block energy and the cruise energy consumed as illustrated in Table 5.5.
When focusing on the cruise energy consumed, even with the increase in aircraft gross-weight,

the cruise energy consumption is 10% less than the advanced gas-turbine aircraft at 1100 nm and 13% less at 900 nm, assuming a e_{Bat} of 1500 Wh/kg. However, because take-off and climb (as well as the reserves, including diversion and hold) are still performed using the advanced gas-turbine only, the larger MTOW produces inferior performance in these segments which leads to a neutral block energy consumption. Assuming a value of 1000 Wh/kg, the cruise energy is about neutral at 1100 nm and 8% less at 900 nm, whereas the hybrid concept consumes 9% and 5% more block energy respectively. At a e_{Bat} of 750 Wh/kg, the cruise energy is about neutral at 900 nm, but noticeably degraded at 1100 nm. At 1100 nm design range and assuming a e_{Bat} of 1500 Wh/kg, the H_E is 35% during cruise whereas it is 20% when considering the block mission. It is interesting to note that even if the H_{Puse} is 50%, the H_E cruise is less than 50% due to the lower efficiency chain of the conventional propulsion system compared to the electrical system.

Specific energy [Wh/kg]	750		1000		1500	
Design range [nm]	900	1100	900	1100	900	1100
Relative change in block Fuel [%]	-8	-3	-14	-13	-19	-20
Relative change in MTOW [%]	42	58	30	40	20	25
Relative change in block ESAR [%]	-11	-17	-4	-9	2	0
Relative change in block energy [%]	12	21	5	9	-2	0
Relative change in cruise energy [%]	-1	10	-8	-1	-13	-10

Table 5.5: Relative change in energy compared to the advanced conventional aircraft [126]

The analysis of potential block fuel reduction and change in vehicular efficiency indicate that the regional market segment turns out to be the most suited market for the application of fuel-battery hybrid-electric aircraft. As the regional-type market represents up to 38% (for year 2002) of the cumulative global commercial air transport fuel consumption [127], hybrid system technology could lead to reduction in in-flight emissions if the battery cell technology reaches at least a state of 1000 Wh/kg. When considering environmental impact, it is worth highlighting that by virtue of the fuel burn reduction achieved during cruise by utilizing the hybrid-electric concept, the harmful emissions at high altitudes are strongly reduced. However, these prospects would be more contrasted when analyzing the life-cycle CO_2 emissions because the electrical energy production and the life-cycle emissions resulting from the production and the recycling of the electrical components need to be considered.

The integration of hybrid-electric propulsion at aircraft level disrupts conventional aircraft design paradigm. First of all, fuel burn reduction can be achieved while the MTOW of the aircraft is increased and secondly a reduction in fuel burn does not mean automatically an improvement in vehicular efficiency.

The design points represented in Figure 5.12, Figure 5.13 and Figure 5.14 might be volumetrically constrained. As the fuselage geometry was kept fixed in this investigation, the cargo volume represents a constraint for the storage of the batteries and for the conventional cargo. The volumetric constraint is indicated for a typical regional cargo volume of 0.14 m^3/PAX. In view of improving the volume allocation for housing the batteries, evolution of the fuselage

geometry towards a double-bubble cross-section is conceivable with the lower lobe having a wider diameter.

The analysis of this hybrid-electric concept enables to highlight the design space for an H_{Puse} of 50% during cruise by gaining first insights into the sizing impact and the potential benefits of hybrid-electric propulsion system at aircraft level. In view of investigating the influence of H_{Puse} on the overall aircraft design and performance, a hybrid-electric clean sheet design featuring a partial parallel hybrid propulsion technology is proposed in Section 5.5.

5.4.3 Aircraft Characteristics and Benchmark

The aircraft characteristics of the hybrid-electric aircraft, assuming a battery gravimetric specific energy of 1.5 khW/kg at cell-level, are compared against the advanced conventional aircraft. Both aircraft are sized for the same ATLRS. The design mission is characterized by a 1100 nm range and a payload of 18360 kg. The aircraft main data and the mass breakdown are presented in the following.

Aircraft main data	Unit	Reference Aircraft	Hybrid Aircraft	Δ Ref.
MTOW	[kg]	59356	74023	25%
MLW	[kg]	56389	71802	27%
OEW/MTOW	[-]	0.601	0.571	-5%
Design payload/MTOW	[-]	0.309	0.248	-20%
Release fuel/MTOW	[-]	0.089	0.063	-30%
Total battery/MTOW	[-]	NA	0.118	NA
$T/MTOW_{\text{S.L,static}}$	[-]	0.325	0.312	-4%
$MTOW/S_{ref}$	[kg/m^2]	645	645	0%
S_{ref} (Airbus gross)	[m^2]	92	115	25%
Wing aspect ratio (Airbus gross)	[-]	12.5	12.5	0%
Wing Span	[m]	34.2	38.2	11%
Wing Leading Edge Sweep	[°]	26.4	26.4	0%
Geared Turbofan Design Thrust (*ISA*, FL350, M0.78)	[kN]	17.7	21.2	20%
TSFC (*ISA*, FL350, M0.78)	[g/kN/s]	13.29	13.28	0%
Electric Motor Maximal Power	[kW]	NA	5882	NA
L/D (initial cruise, *ISA*, FL350, M0.78, MTOW breakes release)	[-]	18.04	18.91	5%
TOFL (*ISA*, SL)	[m]	1866	1915	3%
Approach speed (*ISA*, SL, MLW)	[kts]	141	142	+1%

Table 5.6: Main aircraft data of the hybrid-electric aircraft sized at a design range of 1100 nm and a battery specific energy of 1.5 kWh/kg at cell-level [126]

5.4.3.0.1 Aircraft Main Data As highlighted in Table 5.6, the MTOW of the hybrid-electric aircraft is increased by 25%. Due to the wing sizing scheme at constant wing-loading, it results in a wing area increase of 25%. At design point, the design thrust of the geared turbofan is increased by 20%. The increase in design thrust is the result of a larger TOW at TOC, counteracted however by an improvement in aerodynamic efficiency. The wing being sized at a constant aspect ratio, the lift-induced drag coefficient remains unchanged for a given lift coefficient. However, besides the Reynolds number effects, the enhancement in lift-to-drag ratio of 5% at initial cruise altitude is explained by the increase in wing area while the fuselage geometry is kept constant. As a result, the contribution of the aerodynamic efficient wing component increases relatively compared to the fuselage which improves the lift-to-drag ratio. The improvement in lift-to-drag ratio for a wing sized at constant wing-loading and a fixed fuselage geometry was theoretically demonstrated by Isikveren et al. [13]. The sizing of the electric motor to drive by itself the propulsor during cruise results in a maximal installed power of 5882 kW. Due to the utilization of electrical energy during cruise, the variation of the aircraft mass is less pronounced during cruise which leads to a higher landing weight. The maximum landing weight (MLW) is consequently increased by 27% compared to the reference aircraft. The resulting higher wing-loading in landing phase results in a 1% increase in approach speed.

5.4.3.0.2 Aircraft Mass Breakdown As shown in Table 5.7, the structural weight of the hybrid-electric aircraft is increased by 17% due to the component sizing effects on the wing, the empennage and the landing gear. Because of the larger design thrust of 20%, the weight of the conventional powerplant is increased by 23%. The more than proportional increase in conventional powerplant weight is explained by the fact that weight and volume increase to a higher power than cross-sectional area for the increase in mass flow. The installed electric motor power of 5882 kW results in a weight of 740 kg. The electrical system weight increase of 41% results from the installation of the PMAD system. As the result the operating empty weight (OEW) is changed by 18%. According to the battery specific energy assumption of 1.5 kWh/kg at cell-level, 8765 kg of batteries are required to perform the design mission. The release fuel which includes the fuel reserves is reduced by 12% compared to the block fuel reduction of 20% stated previously.

Aircraft mass breakdown	Unit	Reference Aircraft	Hybrid Aircraft	Δ Ref.
Structure	[kg]	18097	21163	17%
Propulsion system	[kg]	4035	5709	41%
- Conventional powerplant	[kg]	4035	4951	23%
- Electric motor (incl. controller)	[kg]	NA	740	NA
Equipment	[kg]	9972	11791	18%
- Furnishing	[kg]	4435	4435	0%
- Hydraulic system (anti-icing)	[kg]	173	173	0%
- Electrical system	[kg]	4420	6239	41%
- - PMAD propulsion	[kg]	NA	1577	NA
- - Sub-systems	[kg]	4420	4662	5%
- Instruments	[kg]	944	944	0%
- Operational items	[kg]	3580	3580	0%
OEW	[kg]	35684	42243	18%
Payload	[kg]	18360	18360	0%
Release fuel (block and reserves)	[kg]	5312	4655	-12%
Total battery	[kg]	NA	8765	NA
MTOW	[kg]	59356	74023	25%

Table 5.7: Mass breakdown of the hybrid-electric aircraft sized at a design range of 1100 nm and a battery specific energy of 1.5 kWh/kg at cell-level [126]

5.5 Partial Parallel Hybrid Clean-Sheet Design

In the search of analysing the implications of increasing H_{Puse} on aircraft design, integrated performance as well as flight technique optimization, a partial parallel hybrid system was assessed by Pornet and Isikveren [14]. The hybrid-electric quad-fans concept illustrated in Figure 2.2 is investigated. The electrification concerns all operational phases of the mission except the taxi-in/out, descent, landing and hold, which are performed only with the turbofans.

The intrinsic thrust and power characteristics of the electric fan are key aspects to be well understood in order to size the propulsion system. They are detailed in Section 5.5.1 which focuses on the sizing strategy of the hybrid-electric propulsion. Based upon the sizing of the propulsion system, two different operational schemes of the hybrid-electric propulsion during cruise are investigated. During the cruise operation presented in Section 5.5.2, the turbofans are throttled back while the electric fans deliver the maximal available thrust. In Section 5.5.4, the second operational cruise strategy is assessed which consists of throttling the electric fans during cruise while the turbofans run close to their maximum efficiency [15].

5.5.1 Hybrid-Electric Propulsion System Sizing

The flow path sizing of the geared turbofans and the electric fans are performed at TOC conditions. With respect to the level of H_{Puse} and the thrust requirement at TOC, T_{TOC}, which includes a 300 fpm residual climb rate, the design thrust of the electric fan $T_{TOC_{EF}}$ and

of the geared turbofan, $T_{TOC_{GTF}}$, are determined according to Equation 3.31 and Equation 3.30 respectively. According to the design thrust, the geometric characteristics including fan diameter, nacelle reference diameter and length are determined according to the geared turbofan model and ducted fan model described respectively in Section 5.5.1.3 and Section 5.5.1.2.

5.5.1.1 Geared Turbofan Model

The conventional powerplant system is equipped with geared turbofans. The engine models implemented are described in Section 5.4.1. The engine models were produced according to the methods described in Section 3.2.3.1.

5.5.1.2 Ducted Fan Model and Electric Motor Sizing

The modelling of the thrust and power-demand characteristics of the electric fan model is based on the ducted fan model published by Steiner et al. [106]. The generic characteristics of this model were the focus of Section 3.2.3.2. The sizing of the electric fan which includes the sizing of the ducted fan and of the electric motor is essential in the design of the partial parallel hybrid propulsion system. The flow path sizing of the ducted fan is performed at TOC conditions (*ISA*, FL350, $M0.78$) according to Equation 3.31 and the design thrust $T_{TOC_{EF}}$. The sizing of the electric motor depends on the power characteristics of the ducted fan as highlighted in Section 3.2.6.2. The critical sizing case of the electric motor which depends on the level of H_{Puse} as well as the thrust and power lapse characteristics of the electric fan were reviewed in Section 3.2.3.2. In the context of the quad-fan concept investigated, the critical sizing scenarios of the electric motor are elaborated as function of H_{Puse}.

- For H_{Puse} values below 25%, the critical sizing condition of the electric motor is the shaft power requirement at TOC. By sizing the propulsion system at TOC according to Equation 3.30 and Equation 3.31, the TOFL (*ISA*, SL) without de-rating and the time-to-climb are below the constraint values declared in the ATLRS. This is explained by the fact that the thrust contribution of the electric fans during these segment remains low compared to the thrust delivered by the turbofans.

- For H_{Puse} values between 25% and 50%, the time-to-climb constraint becomes the sizing criteria. The electric motor power is sized in order not to exceed the time-to-climb of 25 min. As a consequence, the electric motor is slightly oversized for TOC condition.

- For H_{Puse} values above 50%, the electric motor power is sized to respect the TOFL (*ISA*, SL) limitation of 2200 m. Above an H_{Puse} of 50% the thrust provided by the electrical fans influences the low-speed performance. As the TOFL performance is the sizing criterion, the electric motor is oversized for time-to-climb and TOC criteria.

5.5.1.3 Electrical System Architecture

The layout of the electrical propulsion system and the component technological level assumed are described in Section 5.2.1. The all-electric subsystem power architecture equipping this aircraft concept is identical to all the aircraft concepts presented in this chapter and is detailed in Section 5.2.2.

5.5.2 Geared Turbofan Cruise Throttling

The operational strategy examined in this section is characterized by throttling the geared turbofans during cruise to adjust to the instantaneous thrust requirement while the electric fans provide their maximal available thrust. During the other segments of the mission where the electrical fans are employed, the maximal thrust available is delivered. The maximal thrust provided by the electric fans is a function of the sizing and thrust lapse characteristics of the ducted fan and of the maximum power of the electric motor installed. The difference in thrust requirement between TOC and cruise as well as the reduction in aircraft gross weight result in a necessity to throttle back the geared turbofans during cruise. The amount of thrust to be reduced is determined by the maximal thrust delivered by the electric fans, the sizing of the geared turbofans and the thrust required during cruise. Due to the throttling of the geared turbofans during cruise, the geared turbofan can be subjected to lower part load operating conditions. However, according to the sizing procedure of the geared turbofans and the electric fans at TOC as indicated in Section 3.2.6, the amount of thrust required by the geared turbofans during cruise remains mainly within the $TSFC$ bucket of the geared turbofan presented in Figure 3.9. This efficiency change of the geared turbofan is discussed in Section 5.5.2.3. According to the selected operation of the electric fans, the increase in H_{Puse} is limited in this model to a value that would result in a shut-down of the geared turbofans during cruise due to fact that the electric fans would deliver the required thrust. In this assessment, a maximal H_{Puse} value was set at 60% because above this H_{Puse} threshold the design thrust of the geared turbofan would violate the validity of the implemented models. Moreover, it was judged that the selected geared turbofan architecture would not be relevant anymore.

5.5.2.1 Integrated Performance Change Versus the Degree-of-Hybridization for Energy

The integrated performance change of the hybrid-electric aircraft concept according to a geared turbofan cruise throttling strategy was investigated by Pornet and Isikveren [31]. Sizing the aircraft for interval design ranges between 900 nm and 2100 nm and for increasing degree-of-hybridization for useful power H_{Puse}, the prospects were investigated in terms of potential fuel burn reduction (see Figure 5.15), change in vehicular efficiency (see Figure 5.16) and change in aircraft weight (see Figure 5.17). The relative change is measured against an under-wing podded twin-engine transport aircraft projected for YEIS 2035 sized for the respective design ranges. The design point selected for a benchmark analysis against the

reference aircraft in Section 5.5.2.6 is represented in the figures. The battery specific energy assumed at cell-level is 1500 Wh/kg. A sensitivity analysis with regards to the battery specific energy is provided in Figure 5.21 assuming 1000 Wh/kg at cell-level. As demonstrated in Figure 5.15, a large reduction in block fuel can be achieved by increasing H_{Puse} compared to an advanced conventional aircraft through greater utilization of the electrical energy and an increase in overall propulsion system efficiency resulting from the highly efficient electrical components. However, because of the large increase in system weight due notably to the utilization of batteries and the sizing of the electrical system, increasing H_{Puse} comes at the detriment of the vehicular efficiency as it can be observed in Figure 5.16. For design ranges below 1300 nm, block fuel reductions above 30% could be achieved for H_{Puse} higher than 45%.

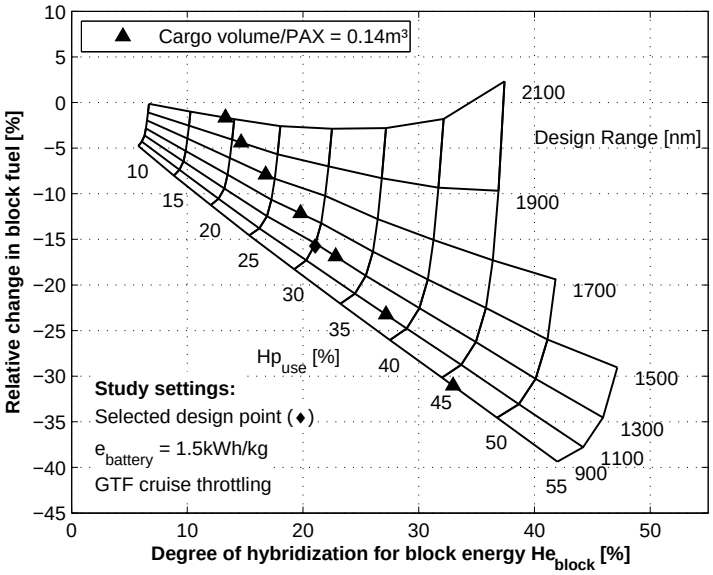

Figure 5.15: Relative change in block fuel versus H_{Eblock}. Geared-turbofan cruise throttling [15].

The increase in aircraft weight from 30% to 60% indicated in Figure 5.17 translates into block ESAR reduction between -5% and -20%. Between 1300 nm and 1700 nm, the reduction in block fuel achievable is between -15% and -30% for value of H_{Puse} larger than 45%.

The degradation in block ESAR becomes, however, significant with values between -20% and -30%. For design ranges above 1900 nm, no large potential in block fuel reduction could be reached. The decrease in potential block fuel burn reduction with increasing design ranges is the result of the higher demand in electrical energy and the resulting amplified sizing cascading effects as highlighted in Section 5.4. Interestingly, for this concept the region of short design range between 900 nm to 1300 nm and moderate level of H_{Puse} below 40% provides large potential block fuel savings of up to 25% combined with small to moderate reduction in vehicular efficiency.

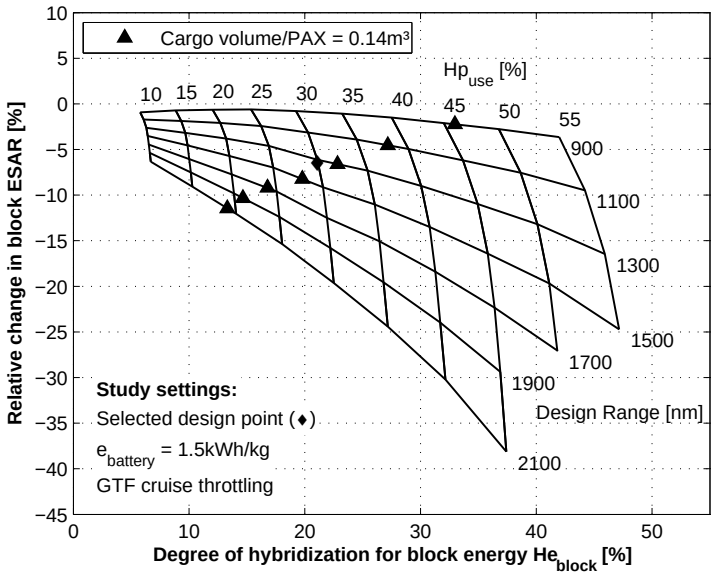

Figure 5.16: Relative change in block ESAR versus H_{Eblock}. Geared-turbofan cruise throttling [15].

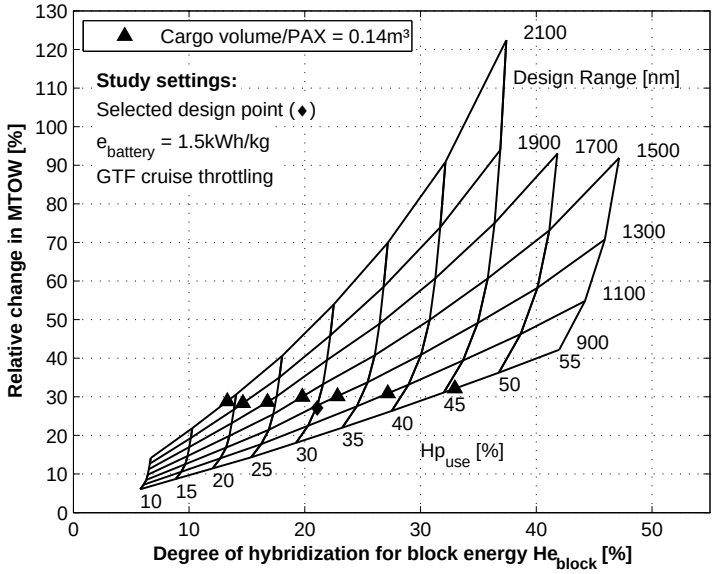

Figure 5.17: Relative change in MTOW versus H_{Eblock}. Geared-turbofan cruise throttling [15].

5.5.2.2 Point Performance Change Versus the Degree-of-Hybridization for Useful Power

The influence of increasing H_{Puse} on a cruise point performance in the context of the hybrid-electric quad-fan aircraft was examined in Pornet and Isikveren [31]. In order to gain more insights into the efficiency interplays at aircraft level with increasing H_{Puse}, a point perform-

ance calculation is evaluated in Figure 5.18 at the beginning of the cruise segment.

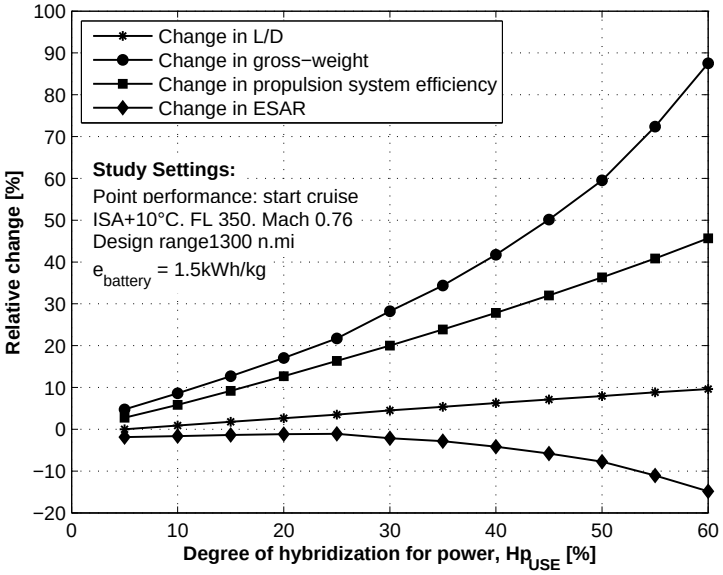

Figure 5.18: Point performance analysis at cruise start (*ISA*+10°C, FL 350, M 0.76) for a design range of 1300 nm. Geared-turbofan cruise throttling [31].

The change in propulsion system efficiency, in aerodynamic efficiency and in aircraft weight, which determine the change in vehicular efficiency are represented. The change in propulsion system efficiency with growing H_{Puse}, resulting from the increasing use of the highly efficient electrical system, produces a change above 30% for H_{Puse} larger than 40%. At very low H_{Puse}, the change in aerodynamic efficiency measured by the change in lift-to-drag ratio is about neutral compared to the twin-engine aircraft. The reduction in geared-turbofan size and the benefit resulting from Reynolds number effect due to the increasing size of the aircraft compensate the additional wetted area coming from the installation of the electrical fans. Sized for a constant wing-loading, as the wing area is increased for a given fuselage-wetted area, the hybrid-electric aircraft becomes aerodynamically more efficient [13]. This explains the aerodynamic improvement at larger H_{Puse}. These benefits resulting from the integration of the hybrid-electric propulsion system at aircraft level are however counteracted by the large increase in aircraft weight. The installation of the additional electrical system and the batteries result in change in aircraft weight above 40% for high value of H_{Puse}. As a consequence of this intermingling between the system, structural and aerodynamic efficiency, the cruise point ESAR remains about neutral up to an H_{Puse} of 25%. Above this value, the non-linearity in weight change negates the potential benefits of the hybrid-electric propulsion system, reaching degradation above 5% for H_{Puse} higher than 40%. It is worthwhile to note that ESAR represented in Figure 5.18 is the outcome of a point calculation in contrast to the block ESAR presented in Figure 5.16 which is an integrated value.

5.5.2.3 Efficiency Change of the Geared-Turbofan Versus the Degree-of-Hybridization for Useful Power

The change in geared-turbofan efficiency against increasing H_{Puse} is evaluated in this paragraph as published by Pornet and Isikveren [31]. To analyze the influence of the electric fans running at maximal available thrust during cruise on the efficiency of the geared-turbofans, the thrust lapse of the geared-turbofan between the thrust required at TOC and the thrust required at start cruise condition (ISA+10°C, FL350, M0.76) is illustrated in Figure 5.19.

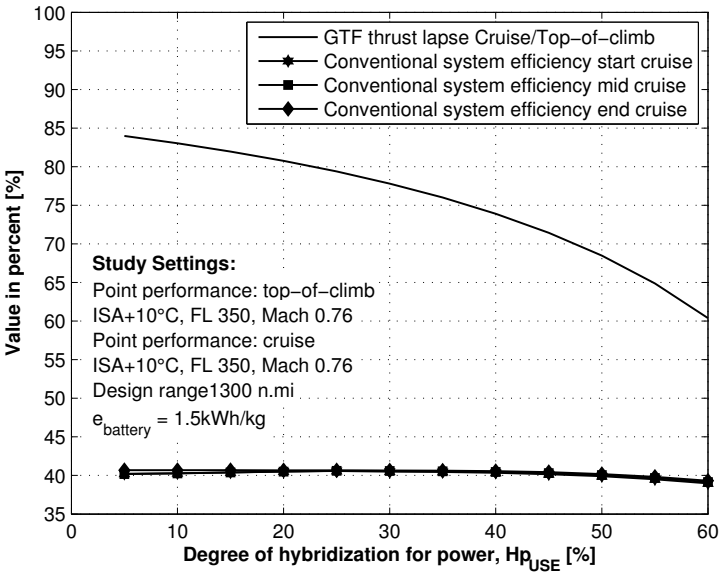

Figure 5.19: Analysis of the geared-turbofan efficiency variation during cruise (ISA+10°C, FL 350, M 0.76) for a design range of 1300 nm. Geared-turbofan cruise throttling [31].

The efficiency of the conventional propulsion system is represented at start, mid-cruise and end-cruise conditions with respect to H_{Puse}. Recalling the $TSFC$ bucket of the geared-turbofans spans between 70% to 100% of the maximum thrust (see Figure 3.9), it can be concluded that for H_{Puse} values up to 45%, the geared-turbofan still operates well within the $TSFC$ bucket. As a result the efficiency of the geared-turbofan even at mid-cruise and end-cruise remains almost unchanged. However, for H_{Puse} values above 45%, the thrust lapse increases as the thrust delivered by the electric fans during cruise increases. Consequently, the efficiency of the geared-turbofan is slightly impaired. In Figure 3.9, the $TSFC$ of the geared-turbofan is reduced by roughly 4% at a thrust setting of 60% of maximum thrust. When computing the change in efficiency of the combustion-based system between, for instance, H_{Puse} of 30% and 60%, a similar value of about -4% is obtained. Moreover, due to the fuel consumed during cruise and the resulting decrease in aircraft mass, the required thrust reduces from the start to the end of the cruise phase. As the result, the thrust lapse incrementally increases at mid-cruise and end-cruise leading to a more pronounced part-load operating geared-turbofan. However, this effect is counter-balanced by a corresponding re-

duction in fuel flow with increasing H_{Puse}, thus the change in aircraft mass becomes less pronounced during cruise.

5.5.2.4 Take-Off Performance Change Versus the Degree-of-Hybridization for Useful Power

The evolution of the take-off performance according to increasing H_{Puse} was assessed in Pornet and Isikveren [31]. Take-off performance was analysed according to the assumption that the one engine inoperative (OEI) case results from a failure of the critical geared-turbofan only, whereas the electric fans are still operating according to the electric motor power available and the off-design characteristics of the ducted fan. As the electrical fans produce a smaller thrust contribution during takeoff, a failure of the geared turbofan is the critical case. Moreover, this assumption can be legitimized by the knowledge that electrical components would exhibit a greater level of reliability.

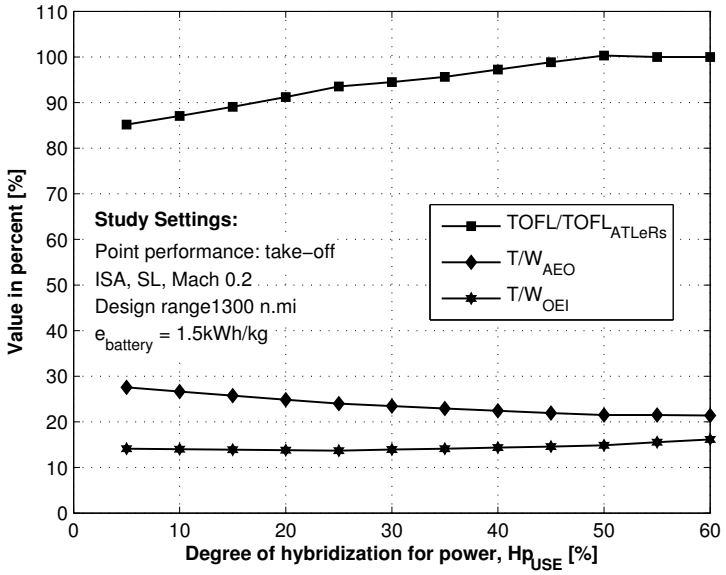

Figure 5.20: Takeoff field length, thrust-to-weight ratios of all-engine operational and one engine inoperative conditions against degree-of-hybridization for useful power for a design range of 1300 nm. Geared-turbofan cruise throttling [31].

Increasing the thrust contribution of the electric fans during take-off compared to the geared-turbofans enhances the OEI take-off performance. This is visualized by plotting in Figure 5.20 the evolution of the OEI thrust-to-weight ratio $T/MTOW_{OEI}$ against H_{Puse} at a given take-off condition (*ISA*, SL, M0.20). The variation of the ratio between the TOFL and the TOFL limitation of 2200 m stipulated by the ATLRS in Section 5.1 reflects the scenario employed for the sizing of the electric motors as discussed in Section 5.5.1.2. As the TOFL is not a critical sizing criterion up to an H_{Puse} of 50%, it is an outcome of the overall sizing process. According to the other active sizing criteria, the TOFL increases up until the TOFL requirement defined in the ATLRS is reached. Consequently, the all engine operative

(AEO) thrust-to-weight ratio $T/MTOW_{AEO}$ decreases with increasing H_{Puse} up to 50%. At an H_{Puse} value of around 50%, the TOFL becomes the critical sizing criterion. However, it can be observed that instead of remaining constant, $T/MTOW_{AEO}$ still decreases slightly. Besides the change in aerodynamic efficiency due to sizing effects with increasing H_{Puse}, it is also a result of increases in $T/MTOW_{OEI}$ with higher H_{Puse}. In other words, by increasing H_{Puse} more thrust per weight is available during the OEI case.

5.5.2.5 Sensitivity Study According to Battery Gravimetric Specific Energy

The influence of lower battery specific energy on aircraft sizing and performance was assessed in Section 5.4. The sensitivity of the quad-fan model against the technological level of the battery was investigated by Pornet and Isikveren [31]. Figure 5.21 represents the relative change in block fuel versus the change in block ESAR for a e_{Bat} of 1000 Wh/kg. The reduction of the potential block fuel benefits as well as the increased degradation of the vehicular efficiency are observable. A notable effect is the reduction in the design range for potential fuel burn reduction achievement. Assuming 1000 Wh/kg, no significant potential block fuel reduction is to be expected for design range above 1200 nm. In comparison, for a e_{Bat} of 1500 Wh/kg, potential block fuel reduction could not be achieved above a design range of 1900 nm. The level of potential savings in block fuel reduces also considerably. For design ranges of 900 nm and 1100 nm, block fuel reduction of 23% and 16% are reached for H_{Puse} of 50%. It is about half of the potential achieved assuming a e_{Bat} of 1500 Wh/kg. The amplified sizing cascading effects of the battery weight is clearly perceived through the significant degradation in vehicular efficiency. At a design range of 1100 nm and an H_{Puse} of 50% the block ESAR is reduced by more than 25% compared to the conventional twin-engine aircraft.

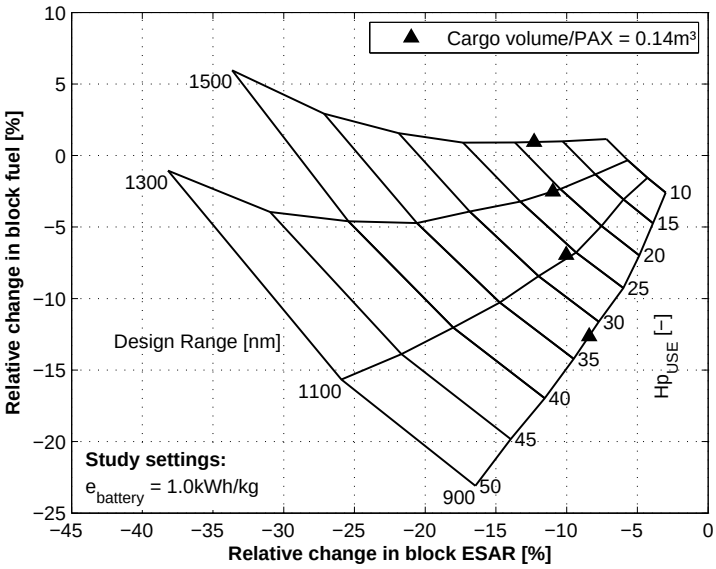

Figure 5.21: Relative change in block fuel versus relative change in block ESAR. Geared-turbofan cruise throttling [31].

5.5.2.6 Aircraft Characteristics and Benchmark

In order to gain detailed insights in the design implications of hybrid-electric propulsion integration, the hybrid-electric quad-fan concept is benchmarked against the advanced conventional reference aircraft. The analysis of this benchmark was published by Pornet and Isikveren [31]. The design range to provide the benchmark was selected at 1300 nm. This selection is justified by projected market analysis for YEIS 2035, which indicates that this design range will cover 90% of the projected cumulative stage lengths for the narrow-body class of aircraft [128, 129]. Recalling for instance Figure 5.15, since the housing of batteries is volumetrically constrained at an H_{Puse} above 33% a design point with an H_{Puse} of 30% was selected for the sizing of the hybrid-electric aircraft. The selected design point is represented in the previous design charts. With respect to the previously quoted design range and H_{Puse}, the level of H_{Eblock} achieved is 21% as indicated in Figure 5.15. In view of highlighting the influence of H_{Puse} on aircraft size, the changes in aircraft geometry according to an H_{Puse} of 10%, 30% and 50% are overlayed in Figure 5.22.

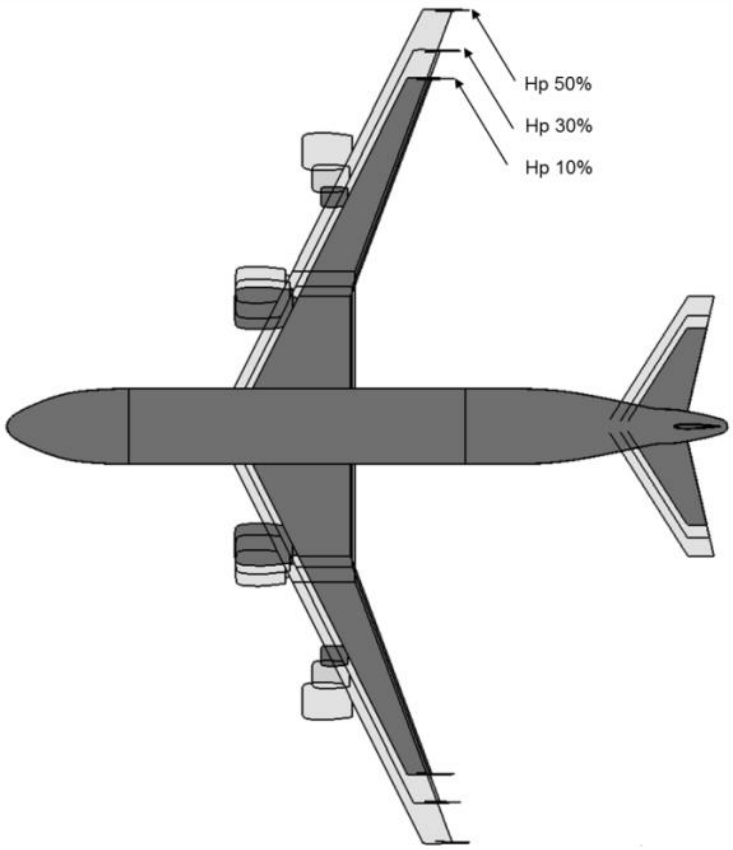

Figure 5.22: Aircraft sizing according to H_{Puse} [31]

5.5.2.6.1 Aircraft Main Data Comparison of the hybrid-electric concept with the reference aircraft in Table 5.8 indicates that through the implementation of the fuel-battery hybrid-electric propulsion system, the MTOW is increased by 28%. This large change in MTOW was discussed in Section 5.5.2.1 and illustrated in Figure 5.17. As a result of the sizing of the wing with constant aspect ratio and constant wing-loading, the wing area is increased by 28% and the wing span by 13%. As a consequence, with a 39.1 m wing span the ICAO Code C airport compatibility is violated and needs to be reclassified as Code D. As a result of the sizing effect, the aerodynamic efficiency is increased by 5%. According to the downsizing of geared turbofans with the introduction of electric fans, design thrust has been reduced by 14%. It results in a modest increase in $TSFC$ by +2% at design point. At the selected H_{Puse} of 30%, the sizing criterion of the electric motors is the time-to-climb requirement as highlighted in Section 5.5.1.2. The resulting installed power of a single electric motor is 2220 kW. As illustrated in Figure 5.20, TOFL is increased by 13% compared to the non-rated TOFL performance of the reference aircraft.

Aircraft main data	Unit	Reference Aircraft	Hybrid Aircraft	Δ Ref.
MTOW	[kg]	60840	77730	28%
MLW	[kg]	59010	76170	29%
OEW/MTOW	[-]	0.594	0.538	-9%
Design payload/MTOW	[-]	0.302	0.236	-22%
Release fuel/MTOW	[-]	0.104	0.075	-28%
Total battery/MTOW	[-]	NA	0.150	NA
$T/MTOW_{\text{S.L,static}}$	[-]	0.320	0.290	-12%
$MTOW/S_{ref}$	[kg/m^2]	645	645	0%
S_{ref} (Airbus gross)	[m^2]	94.3	120.4	28%
Wing aspect ratio (Airbus gross)	[-]	12.5	12.5	0%
Wing Span	[m]	34.6	39.1	13%
Wing Leading Edge Sweep	[°]	26.4	26.4	0%
Geared Turbofan Design Thrust (*ISA*, FL350, M0.78)	[kN]	18.1	15.6	-14%
Electric fan Design Thrust (*ISA*, FL350, M0.78)	[kN]	NA	6.8	NA
TSFC (*ISA*, FL350, M0.78)	[g/kN/s]	13.29	13.50	2%
Electric Motor Maximal Power	[kW]	NA	2220	NA
L/D (initial cruise, *ISA*, FL350, M0.78, MTOW breakes release)	[-]	18.1	19.0	5%
TOFL (*ISA*, SL)	[m]	1850	2080	13%
Approach speed (*ISA*, SL, MLW)	[kts]	143	143	+0%

Table 5.8: Main aircraft data of the reference and hybrid-electric aircraft sized at a design range of 1300 nm and a H_{Puse} of 30% [31]

5.5.2.6.2 Aircraft Mass Breakdown As shown in Table 5.9, the sizing effects have produced an outcome where the structural weight of the hybrid-electric aircraft is increased by 17% compared to the advanced conventional aircraft. Focusing on the propulsion system, the 14% down-size in design thrust of the geared turbofan leads to a decrease of 14% in the combustion-based power plant weight. However, due to the installation of the electric fans, which includes the weight of the ducted fans and of the electric motors, the combined propulsion system weight is increased by 24%. The installation of the PMAD with 1348 kg results in a 37% increase in electrical system weight. Consequently, the OEW of the hybrid-electric aircraft is 16% higher. The release fuel (including block and reserves/contingency) is reduced by 8%. The block fuel reduction was found to be around 15%. The total battery mass installed is 11740 kg.

Aircraft mass breakdown	Unit	Reference Aircraft	Hybrid Aircraft	Δ Ref.
Structure	[kg]	18440	21487	17%
Propulsion system	[kg]	4132	5117	24%
- Conventional powerplant	[kg]	3861	3553	-14%
- Electric motors	[kg]	NA	444	NA
- Ducted fans	[kg]	NA	1119	NA
Equipment	[kg]	10012	11640	16%
- Furnishing	[kg]	4435	4435	0%
- Hydraulic system (anti-icing)	[kg]	173	173	0%
- Electrical system	[kg]	4460	6088	37%
- - PMAD propulsion	[kg]	NA	1348	NA
- - Sub-systems	[kg]	4460	4740	6%
- Instruments	[kg]	944	944	0%
- Operational items	[kg]	3580	3580	0%
OEW	[kg]	36159	41818	16%
Payload	[kg]	18360	18360	0%
Release fuel (block and reserves)	[kg]	6317	5806	-8%
Total battery	[kg]	NA	11740	NA
MTOW	[kg]	60840	77730	28%

Table 5.9: Mass breakdown of the reference and hybrid-electric aircraft sized at a design range of 1300 nm and a H_{Puse} of 30% [31]

5.5.3 Electric Fan Cruise Throttling

The strategy of throttling back the geared-turbofan was assessed to be suitable up to a H_{Puse} of around 45% as for higher values of H_{Puse} the efficiency of the geared-turbofan degrades due to stronger off-design part load operations. Consequently, a novel operational strategy consisting of throttling back the electric fans during cruise while the geared turbofans operate close to their efficiency peak is investigated in this section and the results are compared to the cruise strategy previously investigated in Section 5.5.2. The analysis of this strategy was published by Pornet [15].

The relative change in block fuel versus H_{Eblock} is illustrated in Figure 5.23. Similar trends in terms of change in block fuel with respect to increasing H_{Puse} and growing design ranges are noticeable compared to the evolutions indicated in Section 5.5.2. For a given H_{Eblock}, it can be observed that the achievement in block fuel reduction are about identical when comparing Figure 5.15 against Figure 5.23. However in the case of throttling the electric fans during cruise, the level of H_{Puse} reached is higher for an identical H_{Eblock}. In other words in order to achieve the same potential in block fuel reduction, a higher useful electric power relative to the total useful power is realized. Basically it means that for achieving the same block energy split, a larger electric motor power needs to be installed. This trend is elucidated by the fact that for an identical H_{Puse} the throttling of the electric fans during cruise results in a lower electrical energy consumption compared to the first energy management strategy highlighted in Section 5.5.2. For the same variation of H_{Puse}, the reduction in electrical energy utilized

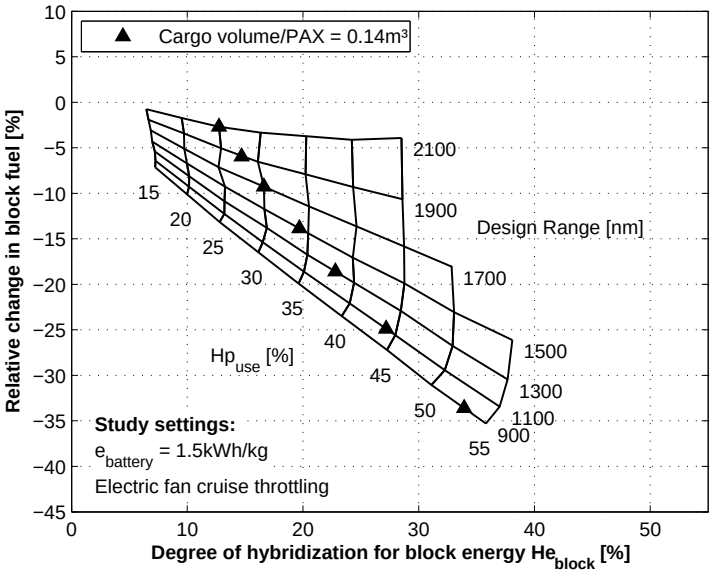

Figure 5.23: Relative change in block fuel versus H_{Eblock}. Electric fan cruise throttling [15].

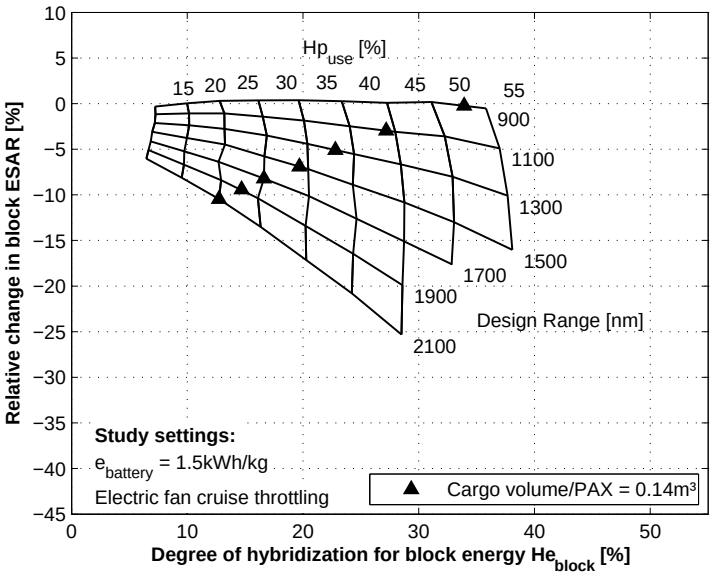

Figure 5.24: Relative change in block ESAR versus H_{Eblock}. Electric fan cruise throttling [15].

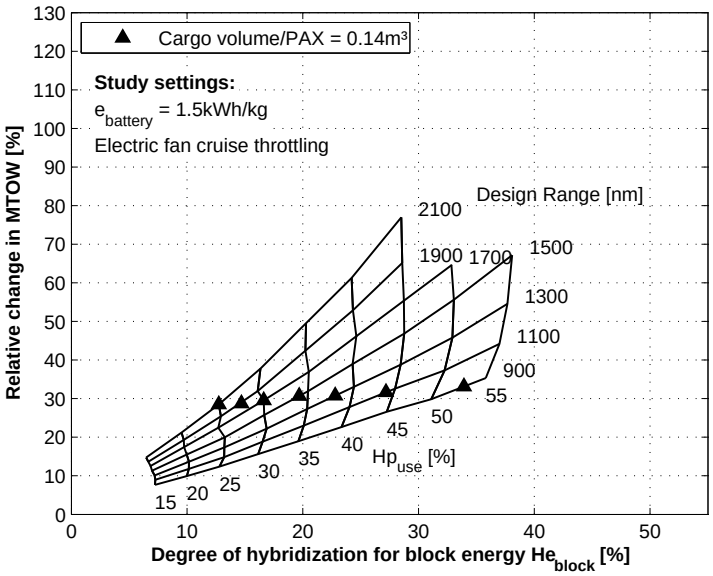

Figure 5.25: Relative change in MTOW versus H_{Eblock}. Electric fan cruise throttling [15].

during cruise results in lower value of H_{Eblock}. It explains the more "compact" form of the carpet plots as observed in Figure 5.24 and in Figure 5.25. The block fuel reduction outcomes are benchmarked against the hybrid-electric aircraft concept presented in Section 5.5.2.6 and sized for a design range of 1300 nm and a H_{Puse} of 30%. Utilizing the electric fans cruise throttling strategy at an H_{Puse} of 30% results in a block fuel reduction of -13% for an H_{Eblock} of 16%. This is to be compared against the -16% fuel burn reduction achieved at a H_{Eblock} of 21% in the case of the geared turbofan cruise throttling operation. These values illustrate that for the same level of H_{Puse}, a lower level of H_{Eblock} is obtained. In order to attain the same level of H_{Eblock}, an H_{Puse} level of 35% would need to be reached. At this level of H_{Puse}, around the same level of block fuel reduction would be achieved.

The change in energy resulting from the different system management strategies are revealed in Figure 5.24 which illustrates the change in block ESAR against H_{Eblock}. Throttling back the electrical fans while the geared turbofans run close to their maximum efficiency during cruise leads to a slight increase of block ESAR with H_{Puse} as the overall propulsion system efficiency is improved through the use of the efficient electrical system. It can be noticed that block ESAR remains almost independent of H_{Puse} for short design ranges. The decrease in block ESAR at higher design ranges with increasing level of H_{Puse} is attributable to sizing cascade effects resulting from the higher electric energy requirement which leads to large increase in aircraft mass as illustrated in Figure 5.17. However, the difference in delta block ESAR remains small between the different strategies for a given H_{Eblock}. Following the electric fans cruise throttling strategy, a degradation of -3% in ESAR is observed at H_{Puse} of 30% and a design range of 1300 nm compared to the -7% for the benchmarked hybrid-electric aircraft in Section 5.5.2.6. For the same level of H_{Eblock} of 21% achieved with an H_{Puse} of 35%, the ESAR is reduced by a similar value of around -6%.

Figure 5.25 illustrates the change in MTOW versus the change in H_{Eblock} for the electric fans cruise throttling strategy. The increasing change in MTOW with growing design ranges and raising level of H_{Puse} is clearly noticeable. For identical H_{Eblock}, similar values in MTOW change are observable when comparing the different energy management strategies. At an H_{Puse} of 30% and a design range of 1300 nm, a 24% MTOW change is observed compared to the 28% quoted for the hybrid-electric aircraft benchmarked in Section 5.5.2.6. For the same level of H_{Eblock} of 21% reached with an H_{Puse} of 35%, an identical change in MTOW is observed.

In view of the outcomes, the operational strategy of throttling the electric fans during cruise is interesting when designing hybrid-electric aircraft concepts for large values of H_{Puse}. The geared turbofan throttling strategy remains suitable for low-to-moderate values of H_{Puse} as the shape of the $TSFC$ bucket enables variation in thrust while the efficiency of the geared turbofan remains close to optimum.

5.5.4 Optimum Flight Technique

The influence of H_{Puse} on flight technique optimality together with the implications to operational procedures are investigated in the context of the hybrid-electric quad-fan concept according to the geared turbofan cruise throttling strategy. The assessment of the optimum flight techniques of the hybrid-electric quad-fan aircraft concept was published in [31]. The ESAR change is analysed versus the altitude-speed sensitivity for an aircraft sized at a design range of 1300 nm, a typical TOC gross-weight scenario of 98% MTOW. The ESAR sensitivity of the hybrid-electric quad-fan aircraft is evaluated against increasing value of H_{Puse}. The altitude-speed sensitivity of the reference aircraft is illustrated in Figure 5.26. As the reference aircraft is kerosene based only, using SAR or COSAR would lead to the identification of the same flight techniques optimum as when utilizing ESAR. The sensitivity in terms of ESAR for the hybrid-electric aircraft is illustrated in Figure 5.27, Figure 5.28 and Figure 5.29 for a H_{Puse} of 25%, 30% and 40% respectively. The analysis of the speed and altitude evolution for maximum ESAR indicates that the optimum flight technique tends towards lower speed and lower altitude with increasing H_{Puse} compared to the reference aircraft. At an H_{Puse} of 25%, the maximum ESAR is found to be $M0.70$/FL345. At an H_{Puse} of 30% the optimum is at $M0.69$/FL335. At an H_{Puse} of 40% the ESAR optimum occurs at $M0.67$/FL310. A similar trend was already identified when comparing the flight technique optimality of an universally-electric aircraft concept [10] against a projected gas-turbine only aircraft [104]. The change in altitude-speed optimality depends on the evolution of the overall propulsion system efficiency and of the aerodynamic efficiency characteristics with speed and altitude. For increasing H_{Puse}, the flight technique optimality of the hybrid-electric aircraft is driven more importantly by the characteristics of the electric fans as they produce a larger proportion of the thrust. The change in electrical propulsion system efficiency depends only on the change of the propulsor efficiency of the ducted-fans with altitude-speed variation. The electrical components are assumed to be suitably thermally managed resulting in a constant efficiency with altitude and speed. Except for the battery, the additional assumption was made that the efficiency of the components remains independent of the operating condition.

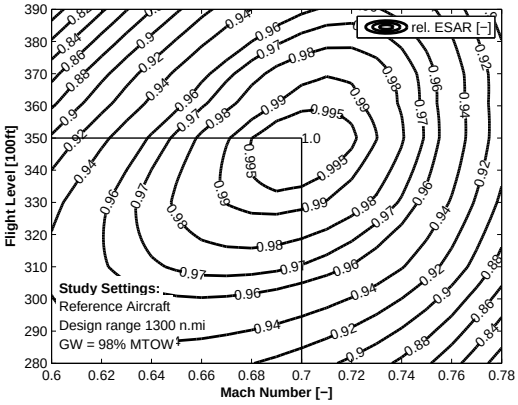

Figure 5.26: ESAR altitude-speed sensitivity of the reference aircraft for a design range of 1300 nm and at 98% of MTOW [31]

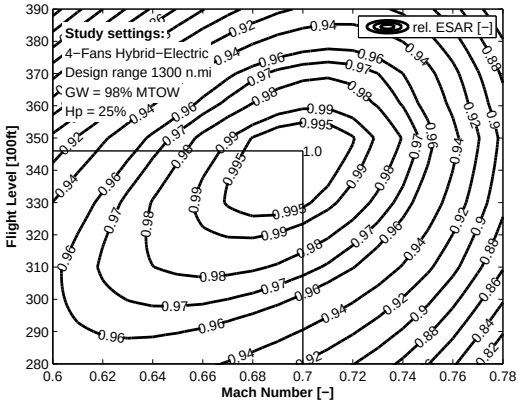

Figure 5.27: ESAR altitude-speed sensitivity for a H_{Puse} of 25% at a design range of 1300 nm and at 98% of MTOW [31]

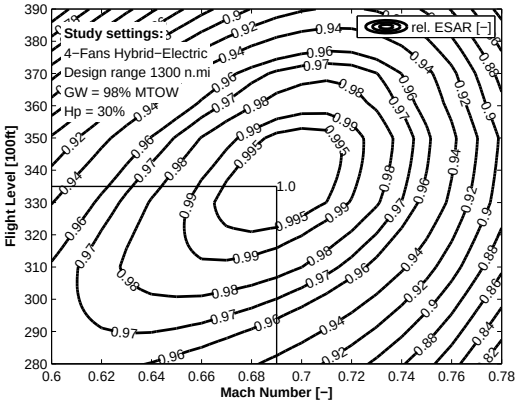

Figure 5.28: ESAR altitude-speed sensitivity for a H_{Puse} of 30% at a design range of 1300 nm and at 98% of MTOW [31]

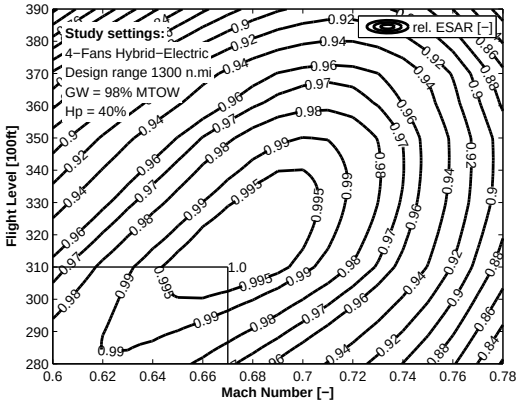

Figure 5.29: ESAR altitude-speed sensitivity for a H_{Puse} of 40% at a design range of 1300 nm and at 98% of MTOW [31]

As the study is conducted on a point performance analysis, the efficiency of the battery is assumed constant at the point calculation. As a result, the change in overall propulsion system efficiency with speed-altitude becomes less pronounced when H_{Puse} increases. Consequently, ESAR optimality is mainly driven by the sensitivity of the aerodynamic polar characteristics of the aircraft governed by speed and altitude. These characteristics tend notably to slow the optimum speed of the aircraft and to lower the flight altitude as detailed in [31]. However, when considering the long-range cruise flight technique determined by the 99% ESAR condition, only a slight reduction in terms of optimum speed is observed while the optimum altitude is not changed compared to the reference aircraft. Moreover, it can be observed that the Mach margin between maximum ESAR and 99% ESAR becomes greater with increasing H_{Puse}. The LERC altitude-speed technique of the hybrid-electric aircraft results in M0.72/FL350 for H_{Puse} of 25%, M0.72/FL350 for H_{Puse} of 30%, and, M0.71/FL350 for H_{Puse} of 40% compared to the LERC at M0.73/FL350 for the reference aircraft. In conclusion the flight technique optimization of hybrid-electric aircraft will not be strongly affected by the level of H_{Puse}. Commercial transport network routes will not be disrupted by the integration of hybrid-electric aircraft within current turbofan airliners fleet.

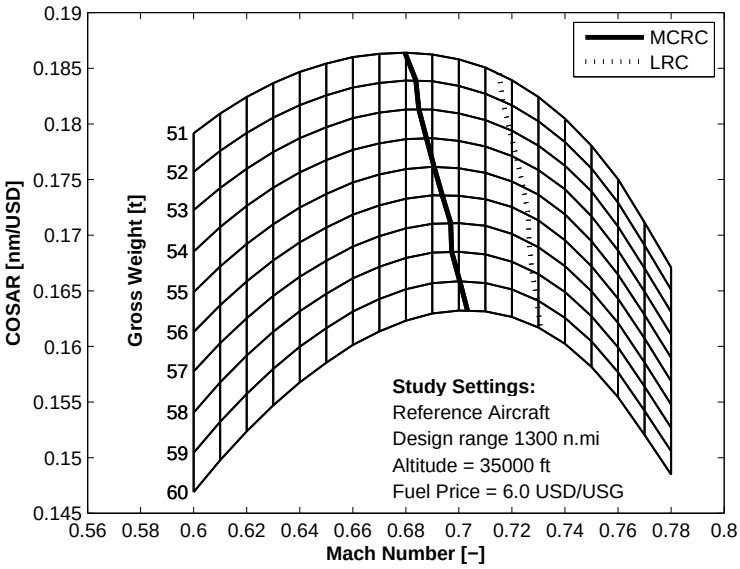

Figure 5.30: COSAR speed sensitivity of the reference aircraft versus gross-weight variation at 1300 nm, FL 350 and a specific fuel price of 6.00 USD/USG [31]

To gain more insights into the implications of the hybrid-electric propulsion system on flight technique optimization, the speed sensitivities based on the COSAR metric are represented at FL350 versus a variation in gross-weight and in Mach number. Like in Section 5.3.4 the fuel price is set at a constant 6.00 USD/USG, whereas the electricity price is varied assuming 0.07 USD/kWh and 0.16 USD/kWh. In Figure 5.30, the variation of the optimum speeds MCRC and LRC of the reference aircraft are represented against variation in gross-weight and Mach number. The optimum speeds MRC, MCRC, MERC and LRC are indicated in Figure 5.31 for the assessment of the optimum flight techniques of the hybrid-electric air-

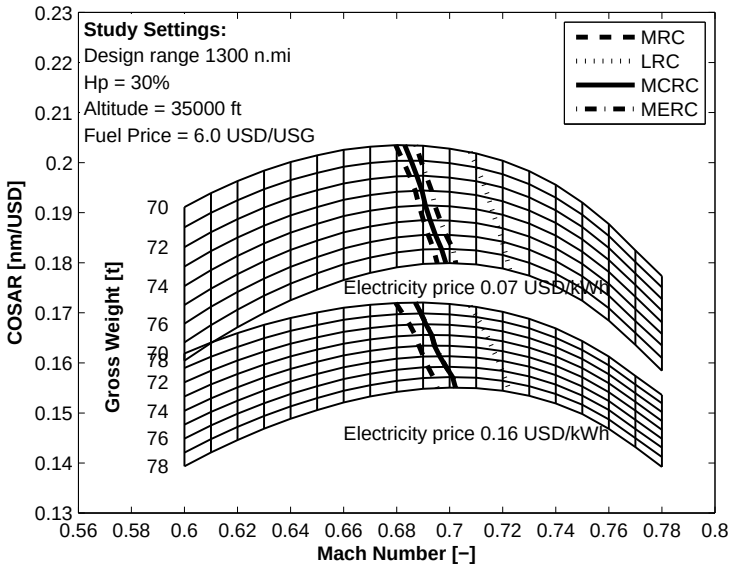

Figure 5.31: COSAR speed sensitivity versus gross weight variation at 1300 nm, H_{Puse} 30%, FL 350, a specific fuel price of 6.00 USD/USG and for variation in specific electricity price [31]

craft. The energy management strategy investigated in these plots is the throttling of the geared-turbofan during cruise, the electric fans run at their maximum thrust during cruise. Consequently, the electrical energy consumed is mainly a function of flight time. This parameter depends directly on the flight speed. By flying faster, the cruise time is decreased for a given stage length, reducing the electrical energy required during cruise. This operating characteristic of the propulsion system leads to a MERC optimum speed higher than the MRC reflecting the fact that the condition for minimum energy occurs at higher speed than for minimum fuel consumption. The increase in MERC is however counteracted by the larger in fuel consumption occurring at higher speed. The change in optimum speed between MRC and MERC is found to be rather small. The MCRC tends to an optimum speed slower than that of the MERC optimum, but still slightly faster than that of the MRC optimum speed when the specific electricity price is 0.07 USD/kWh. This is explained by the fact that under this market price condition, the fuel energy cost has a higher contribution to the COSAR metric. The MCRC and MERC coincides for a specific electricity price is 0.16 USD/kWh as the fuel price and the electricity price are equally weighted in the COSAR metric. The change in optimum speed sensitivity using either MERC or MCRC speeds remain small compared to the reference aircraft.

Chapter 6

Conclusion and Outlook

A comprehensive development of conceptual design methods was proposed in this thesis in order to resolve the shortcomings of traditional methods for the sizing and performance analysis of hybrid-electric transport aircraft. Concerned by the utilization of legacy programs in industry, the methods were developed with the constraints of being implemented in traditional sizing and performance programs. In particular, the consideration of the electricity as an additional energy source to the fuel energy within the sizing and performance environment was dealt within the methods. In traditional sizing and performance environment, the propulsion system is commonly interfaced via thrust and fuel flow tables. By conserving the format of these tables and adding the electric power required at the electric energy and power device as an additional output in the fuel flow table, the electric energy could be mapped out in the sizing and performance environment while ensuring the compatibility of the methods with traditional programs. The engineering components constituting the hybrid-electric system including the electric energy and power devices as well as their interfaces within the propulsion and power system were established by the methods. The integration of the propulsion system enabled to compute the electric energy consumed and the maximum thrust available as a function of the operational utilization, intrinsic efficiency and power characteristics of the hybrid-electric propulsion system. Finally, the methods established the overall aircraft sizing process to determine the sizing and integrated performance analysis of hybrid-electric transport aircraft.

The design of hybrid-electric transport aircraft required the formulation of metrics for the evaluation of optimum flight techniques. Methods for optimum flight techniques identification of hybrid-electric transport aircraft were consequently proposed. Considering the different market prices of the energy sources, the cost specific air range (COSAR) metric was developed to enable the flight profile optimization of hybrid-electric transport aircraft according to minimum energy cost. Moreover, cost index (CI) metrics definition for hybrid-electric aircraft were developed to determine the economical flight profile of hybrid-electric aircraft by taking into consideration the cost of time in addition to the cost of energy.

The methods were employed for the design of fuel-battery narrow-body transport aircraft accommodating 180 passengers (PAX) in order to investigate the integration implications of hybrid-electric propulsion system at aircraft level and to establish design heuristics and

sizing axioms. Starting with the retrofit of a narrow-body aircraft, the topological approach consisted of installing an electric motor powered by batteries on the shaft of the gas-turbine to support its operation during cruise and climb. By installing an electric propulsion system in parallel to the conventional gas-turbine, the role of new design parameters such as the degree-of-hybridization for power (H_P) and the introduction of new constraint in the sizing process of hybrid-electric aircraft due to the characteristics of the battery as energy and power device in the sizing of hybrid-electric transport aircraft were highlighted. Due to the intrinsic nature of a retrofit, the installation of the additional electrical system was constrained by the certified maximum take-off weight (MTOW) of the aircraft. Aiming to achieve minimum fuel at maximum utilization stage length of the aircraft, the hybrid-electric system was sized for a 900 nautical miles (nm) mission. The sizing of the propulsion system was found to be an interplay between maximum power of the electric motor installed, which mainly determined the mass of the associated electrical system, total battery mass and the potential block fuel reduction under the constraint of the MTOW and the state-of-charge of the battery. By supporting the gas-turbine utilizing the electric motor during cruise, a block fuel reduction of -13% could be achieved compared to the reference conventional aircraft when assuming a gravimetric specific energy of 1500 Wh/kg at cell-level. When utilizing the electric motor during climb and cruise, block fuel reduction was increased to -16%. In view of taking the overall aircraft sizing effects into consideration and to determine the market range application of hybrid-electric transport aircraft, clean-sheet designs of narrow-body aircraft were investigated.

In this regards, the design of a hybrid-electric narrow-body aircraft was investigated by installing an electric motor in parallel to the shaft of one gas-turbine of the twin-engine aircraft. Running an electric motor in parallel to a gas-turbine impacts the operational characteristics of the gas-turbine. Forced to operate into part-load, it leads notably to a reduction of its efficiency. In order not to impact the design axiom of the gas-turbine and perturb its operation, the operational strategy selected in this investigation was to drive the ducted-fan by the electric motor itself during cruise while the gas-turbine is shut down. The other segments of the mission were performed conventionally using the two gas-turbines. As a result, the degree-of-hybridization for useful power (H_{Puse}) was fixed to 50% during cruise. In order to analyze the best suited design range for the application of this concept, the aircraft was sized for interval design ranges between 900 nm to 2100 nm. Moreover the influence of battery technology on the aircraft sizing and performance was assessed by varying the battery specific energy between 750 Wh/kg and 1500 Wh/kg. Comparing the performance of the hybrid-electric aircraft, to a suitably projected reference aircraft for year entry-into-service 2035, it was found that the greatest block fuel reduction potential was achieved for design ranges reflecting the regional market segment. Assuming a battery specific energy at cell-level of 1500 Wh/kg, 1000 Wh/kg and 750 Wh/kg, block fuel reduction of -20%, -12% and -2% could be achieved respectively at 1100 nm. Besides the potential benefit in terms of emissions reduction, the total energy consumption was examined based on energy specific air range (ESAR), the vehicular efficiency metric. The results shown that the vehicular efficiency of the hybrid-electric aircraft was for most design ranges investigated degraded compared to the advanced reference aircraft. This trend was to be explained by the significant change in

aircraft mass due to the additional electrical system and the utilization of batteries. Only at a design range of 1100 nm and assuming a battery technology of 1500 Wh/kg, a neutral energy outcome was reached. For higher design ranges or lower battery technology state, the vehicular efficiency was impaired due to the amplified sizing effects. Moreover, the volumetric constraint of the fuselage for the installation of the batteries was found to be a limitation in order to provide similar baggage volume standard in the cargo compartment to contemporary regional aircraft.

Motivated by the analysis of the influence of increasing H_{Puse} on overall aircraft design, the integrated performance of a partial parallel hybrid-electric system was assessed. Benefiting from the capability offered by aircraft vehicle to distribute the thrust, a quad-fan arrangement composed of two geared-turbofans and two electric fans was investigated on a narrow-body transport aircraft. Because the electric propulsion system is completely decoupled from the conventional propulsion system, it allows for free variation of the degree-of-hybridization for power. A first operational strategy selected was to run the electric fan at its maximum thrust available during the mission while the geared-turbofan is throttle back during cruise. This strategy was found to be pertinent up to a degree-of-hybridization for power of around 45%. Above this value, the efficiency of the gas-turbine starts to be impaired because of stronger part-load operations. The performance assessment indicated that for increasing degree-of-hybridization for power, the block reduction potential increases however at the detriment of the vehicular efficiency. This is the result of the mass impact of the battery and the electrical system. The potential in block reduction decreases however for higher design ranges and lower battery technological state. Assuming a gravimetric specific energy of 1500 Wh/kg at cell-level and for design ranges below 1300 nm, block fuel reductions beyond 30% could be achieved at degree-of-hybridization for power of 50% while the block ESAR reduces to values between -5% and -15%. Between 1300 nm and 1700 nm, the reduction in block fuel achievable is between -20% and -30%. The degradation in block ESAR becomes, however, significant with values between -20% and -30%. For design ranges above 2100 nm, no potential block fuel reduction could be reached.

In the context of this hybrid-electric quad-fans concept, a second operational scheme was analysed by throttling the electric motors during cruise while the geared-turbofans run close to their peak efficiency. The main implication of this different operational strategy is on the sizing of the electrical system. As a result of the throttling of the electric motors during cruise less electrical energy is utilized. Consequently in order to reach an identical degree-of-hybridization for energy (H_E) as with the previous strategy, an higher H_P needs to be achieved. This translates basically into the installation of a higher electrical motor power. At the same level of H_E, however, similar changes in terms of block fuel reduction, vehicular efficiency and MTOW were evaluated. The operational strategy of throttling the electric fans during cruise is interesting when designing hybrid-electric aircraft concepts for large values of H_{Puse} as it avoids the efficiency degradation of the geared-turbofans.

Beyond the sizing and integrated performance analysis, the flight techniques of the hybrid-electric quad-fans concept were analysed considering the geared-turbofan throttling strategy during cruise. Increasing H_{Puse} was found to have a tendency to reduce the optimum speed.

However, if the strategy of the long range cruise (LRC) speed is followed, it does not affect the contemporary altitude-speed flight technique of conventional aircraft.

These integrated aircraft performance analyses indicate that the application of fuel-battery hybrid-electric propulsion to transport aircraft seems limited to the high-density PAX regional market segment and for low-to-moderate values of H_P. However, the investigation of higher synergistic integration of the hybrid-electric propulsion system needs to be further pursued particularly in combination with technologies such as distributed propulsion. Moreover, in view of notably reducing the technological requirements imposed to the batteries, partial turboelectric systems need to be assessed in future work.
For achieving optimum energy management strategies, the methods will need to be further developed to introduce optimum power allocation schedule and control into the sizing scheme. The synergistic integration of the propulsion system at aircraft level through tightly interlaced coupling with the airframe and the other systems on-board the aircraft as well as the establishment of optimum control strategies will enable to reveal the full potential of the application of hybrid-electric propulsion system to transport aircraft. Although optimisation studies were not constructed in the thesis, the presented methods offer the methodological components to facilitate hyper-dimensional, multi-objective and multi-constraint optimization.
In the context of the hybrid-electric aircraft concepts investigated, the analyse of aircraft performance were focused on the design mission. Off-design mission performance and in particular the trade between the payload and the range determined by the combined use of fuel and batteries as energy source need to be established to compare the operational transport capability of hybrid-electric aircraft against conventional fuel-only aircraft.
While the introduction of the COSAR metric bridged technical evaluation to economics analysis, the inclusion in design charts of constraint lines related to economics in order to select “best and balanced” aircraft concepts requires rigorous assessment of the economics implications resulting from the integration and operation of hybrid-electric propulsion system. Moreover, economics analysis need to be included in further work as they can drive the aircraft morphological selection. The economics analysis must be further expanded to cover the overall life cycle assessment of hybrid-electric aircraft to provide wells-to-wheels comparison to kerosene-based aircraft.

Bibliography

[1] Advisory Council for Aviation Research and Innovation in Europe (ACARE). Strategic Research and Innovation Agenda (SRIA) - Volume 1. Technical report, Brussels, 2012.

[2] NASA Environmentally Responsible Aviation. N+2 Advanced Vehicle Concepts NRA Draft Solicitation Synopsis. Technical report, 2012. URL `http://www.aeronautics.nasa.gov/calendar/era_preconference_synopsis.html`.

[3] Sam Bruner, Scott Baber, Chris Harris, Nicholas Caldwell, Peter Keding, Kyle Rahrig, Luck Pho, and Richard Wlezian. NASA N+3 Subsonic Fixed Wing Silent Efficient Low-Emissions Commercial Transport (SELECT) Vehicle Study. Technical Report November, El Segundo, California, 2010.

[4] Askin T. Isikveren and Michael Schmidt. Future Transport Aircraft Ultra-Low Emissions Technology Options. In *GARS Workshop Air Transport and Climate Change*, Worms, Germany, 2014.

[5] K. Sivasubramaniam, T. Zhang, M. Lokhandwalla, E. T. Laskaris, J. W. Bray, B. Gerstler, M. R. Shah, and J P Alexander. Development of a High Speed HTS Generator for Airborne Applications. *IEEE Transactions on applied superconductivity*, 19(3):1656–1661, 2009. doi:10.1109/TASC.2009.2017758.

[6] Gerald V Brown. Weights and Efficiencies of Electric Components of a Turboelectric Aircraft Propulsion System. In *49th AIAA Aerospace Sciences Meeting including the New Horizons Forum and Aerospace Exposition*, Orlando, Florida, 2011. doi:2011-225.

[7] Philippe J Masson and Cesar A Luongo. HTS Machines for Applications in All-Electric Aircraft. In *Proceedings of the PES Meeting*, Tampa, Florida, 2007. ISBN 1424412986. doi:1-4244-1298-6/07.

[8] Cesar A Luongo, Philippe J Masson, Taewoo Nam, Dimitri Mavris, Hyun D Kim, Gerald V Brown, Mark Waters, and David Hall. Next Generation More-Electric Aircraft: A Potential Application for HTS Superconductors. *IEEE Transactions on applied superconductivity*, 19(3):1055–1068, 2009.

[9] Stefan Stückl, Jan van Toor, and Hans Lobentanzer. VOLTAIR - The All Electric Propulsion Concept Platform - A Vision For Atmospheric Friendly Flight. In *28th International Congress Of The Aeronautical Sciences, ICAS*, Brisbane, 2012.

[10] Askin T. Isikveren, Arne Seitz, Patrick C Vratny, Clément Pornet, Kay O Plötner, and Mirko Hornung. Conceptual Studies of Universally-Electric Systems Architectures Suitable for Transport Aircraft. In *Deutscher Luft- und Raumfahrt Kongress, DLRK*, Berlin, 2012. Bauhaus Luftfahrt.

[11] Arun K Sehra and Jaiwon Shin. Revolutionary Propulsion Systems for 21st Century Aviation. Technical Report October, NASA, 2003.

[12] Christopher Perullo and Dimitri Mavris. A review of hybrid-electric energy management and its inclusion in vehicle sizing. *Aircraft Engineering and Aerospace Technology*, 86 (6):550–557, September 2014. ISSN 0002-2667. doi:10.1108/AEAT-04-2014-0041.

[13] Askin T. Isikveren, Sascha Kaiser, Clément Pornet, and Patrick C. Vratny. Pre-design Strategies and Sizing Techniques for Dual-Energy Aircraft. *DOI: 10.1108/AEAT-08-2014-0122, Aircraft Engineering and Aerospace Technology Journal, Vol. 86, Iss. 6, pp. 525-542*, 2014. doi:10.1108/AEAT-08-2014-0122.

[14] Clément Pornet. Hybrid and Universally-Electric Aircraft Concepts. *AccessScience, McGraw-Hill Yearbook of Sciences and Technology (McGraw-Hill Education, 2014), http://dx.doi.org/10.1036/1097-8542.YB150553.*

[15] Clément Pornet. Electric drives for propulsion system of transport aircraft. In Miroslav Chomat, editor, *New Applications of Electric Drives*. InTech, 2015. ISBN 9789535146032.

[16] Holger Kuhn, Arne Seitz, Larissa Lorenz, Askin T. Isikveren, and Andreas Sizmann. Progress and Perspectives of Electric Air Transport. In *28th International Congress Of The Aeronautical Sciences, ICAS*, Brisbane, 2012.

[17] Timothy P Dever, Kirsten P Duffy, Andrew J Provenza, Patricia L Loyselle, Benjamin B Choi, Carlos R Morrison, and Angela M Lowe. Assessment of Technologies for Noncryogenic Hybrid Electric Propulsion. Technical Report January, NASA/Technical Report 2015-216588, Cleveland, Ohio, 2015.

[18] Jeffrey Freeman, Philip Osterkamp, Michael Green, Andrew Gibson, and Benjamin Schiltgen. Challenges and opportunities for electric aircraft thermal management. *Aircraft Engineering and Aerospace Technology*, 86(6):519–524, September 2014. ISSN 0002-2667. doi:10.1108/AEAT-04-2014-0042.

[19] Susan Liscouët-Hanke. *A Model-Based Methodology for Integrated Preliminary Sizing and Analysis of Aircraft Power System Architectures*. PhD thesis, Institut National des Sciences Appliquée - Université Paul Sabatier, 2008.

[20] National Academies of Sciences, Engineering, and Medicine. Commercial Aircraft Propulsion and Energy Systems Research: Reducing Global Carbon Emissions. Technical report, Washington, DC: The National Academies Press, 2016.

[21] James Felder, Hyun Kim, and Gerald Brown. Turboelectric Distributed Propulsion Engine Cycle Analysis for Hybrid-Wing-Body Aircraft. In *47th AIAA Aerospace Sciences Meeting including The New Horizons Forum and Aerospace Exposition*, pages 1–25, Orlando, Florida, January 2009. American Institute of Aeronautics and Astronautics. ISBN 978-1-60086-973-0. doi:10.2514/6.2009-1132.

[22] Andrew R Gibson, David Hall, Mark Waters, Benjamin Schiltgen, Trevor Foster, Jonathan Keith, and Philippe J Masson. The Potential and Challenge of TurboElectric Propulsion for Subsonic Transport Aircraft. In *48th AIAA Aerospace Sciences Meeting Including the New Horizons Forum and Aerospace Exposition*, number January, Orlando, Florida, 2010.

[23] Hyun Dae Kim, James L. Felder, Michael T. Tong, Jeffrey J. Berton, and William J. Haller. Turboelectric distributed propulsion benefits on the N3-X vehicle. *Aircraft Engineering and Aerospace Technology*, 86(6):558–561, September 2014. ISSN 0002-2667. doi:10.1108/AEAT-04-2014-0037.

[24] Devaiah Nalianda and Riti Singh. Turbo-electric distributed propulsion: opportunities, benefits and challenges. *Aircraft Engineering and Aerospace Technology*, 86(6):543–549, September 2014. ISSN 0002-2667. doi:10.1108/AEAT-03-2014-0035.

[25] Marty K. Bradley and Christopher K Droney. Subsonic Ultra Green Aircraft Research : Phase I Final Report. Technical Report April, Huntington Beach, California, 2011.

[26] Marty K. Bradley and Christopher K. Droney. Subsonic Ultra Green Aircraft Research Phase II : N + 4 Advanced Concept Development. Technical report, NASA, Huntington Beach, California, 2012.

[27] Clément Pornet, Corin Gologan, Patrick C. Vratny, Arne Seitz, Oliver Schmitz, Askin T Isikveren, and Mirko Hornung. Methodology for Sizing and Performance Assessment of Hybrid Energy Aircraft. *Journal of Aircraft, Vol. 52, No. 1 (2015), pp. 341-352. doi: 10.2514/1.C032716*, pages 1–12, 2014. doi:10.2514/1.C032716.

[28] Oliver Schmitz and Mirko Hornung. Methods for Simulation and Analysis of Hybrid Energy Propulsion Systems. In *Proceedings of the 62nd Deutscher Luft- und Raumfahrt Kongress (DLRK)*, Stuttgart, 2013.

[29] Oliver Schmitz. Fahrzeugtriebwerk, Fahrzeug mit diesem Fahzeugtriebwerk und Verfahren zum Betrieb dieses Fahrzeugtriebwerkes, 2012.

[30] Oliver Schmitz and Mirko Hornung. Unified Applicable Propulsion System Performance Metrics. *J. Eng. Gas Turbines Power*, 135(11):1–9, 2013. doi:10.1115/1.4025066.

[31] Clément Pornet and Askin T. Isikveren. Conceptual Design of Hybrid-Electric Transport Aircraft. *Journal of Progress in Aerospace Sciences, DOI: 10.106/j.paerosci.2015.09.002*, 2015.

[32] R. W. Schurhoff. *The Development and Evaluation of an Optimal Powertrain Control Strategy for a Hybrid Electric Vehicle*. PhD thesis, University of California - Davis, CA, 2002.

[33] Frederick G. Harmon, Andrew A. Frank, and Jean-Jacques Chattot. Conceptual Design and Simulation of a Small Hybrid-Electric Unmanned Aerial Vehicle. *Journal of Aircraft*, 43(5):1490–1498, September 2006. ISSN 0021-8669. doi:10.2514/1.15816.

[34] Florian Martini. Siemens entwickelt Weltrekord-Elektromotor für Luftfahrzeuge, 2015.

[35] Prof H K Patel, Raj Nagarsheth, and Sharang Parnerkar. Performance Comparison of Permanent Magnet Synchronous Motor and Induction Motor for Cooling Tower Application. *International Journal of Emerging Technology and Advanced Engineering*, 2(8):167–171, 2012. doi:2250-2459.

[36] Philippe J Masson. Wind Turbine Generators: Beyond the 10MW Frontier. In *Symposium on Superconducting Devices for Wind Energy Systems*, Barcelona, Spain, 2011.

[37] Hans-Jörg Steiner, Arne Seitz, Kerstin Wieczorek, Kay Plötner, Askin T Isikveren, and Mirko Hornung. Multi-Disciplinary Design And Feasibility Study of Distributed Propulsion Systems. In *28th International Congress Of The Aeronautical Sciences, ICAS*, Brisbane, 2012.

[38] Patrick C Vratny, Philipp Forsbach, Arne Seitz, and Mirko Hornung. Investigation of Universally Electric Propulsion Systems for Transport Aircraft. In *29th Congress of the International Council of the Aeronautical Sciences*, St. Petersburg, Russia, 2014.

[39] H. K Xi, W. Z. Gong, Y. Zhang, Y. F. Bi, H. K. Ding, H. Wen, B. Hou, and Y. Xin. China's 33.5 m, 35kV/2kA HTS AC power cable's operation in power grid. *Physica*, C 445-448:1054–1057, 2006.

[40] F. Paschen. Ueber die zum Funkenuebergang in Luft, Wasserstoff und Kohlensaeure bei verschiedenen Drucken erforderliche Potentialdifferenz. *Annalen der Physik. 273 (5): 69-75.*, 1889.

[41] Behkle Electronic GmbH. Fast High Voltage Transistor Switches, Technical data. Technical report, Behlke Power Electronics GmbH, 2011.

[42] Patrick Christoph Vratny. *A Battery Powered Transport Aircraft*. AV Akademikerverlag, Saarbrücken, 2012. ISBN 978-3-639-38521-2.

[43] EE Tech Team. Advanced Power Electronics and Electric Machines. Technical report, National Renewable Energy Laboratory, 2004.

[44] K.C. Divya and Jacob Ostergaard. Battery energy storage technology for power systems: an overview. *Electric Power Systems Research*, 79:511–520, April 2009. ISSN 03787796. doi:10.1016/j.epsr.2008.09.017.

[45] Bruno Scrosati and Jürgen Garche. Lithium batteries: Status, prospects and future. *Journal of Power Sources*, 195:2419–2430, May 2010. ISSN 03787753. doi:10.1016/j.jpowsour.2009.11.048.

[46] B. Ketterer, U. Karl, D. Möst, and S. Ulrich. Lithium-Ion Batteries: State of the Art and Application Potential in Hybrid-, Plug-In Hybrid- and Electric Vehicles. Technical report, Forschungszentrum Karlsruhe in der Helmholtz-Gemeinschaft, Institut für Materialforschung I, 2009.

[47] William H. Woodford, R. Alan Ransil, and Yet-Ming Chiang. Advanced Batteries: Beyond Li-ion. Technical report, NPC Future Transportation Fuels Study, 2012.

[48] Jake Christensen, Paul Albertus, Roel S. Sanchez-Carrera, Timm Lohmann, Boris Kozinsky, Ralf Liedtke, Jasim Ahmed, and Aleksandar Kojic. A Critical Review of Li-Air Batteries. *Journal of The Electrochemical Society*, 159, 2012. ISSN 00134651. doi:10.1149/2.086202jes.

[49] H Kuhn and A Sizmann. Fundamental Prerequisites for Electric Flying. In *Deutscher Luft- und Raumfahrt Kongress, DLRK*, Berlin, Germany, 2012. Bauhaus-Luftfahrt.

[50] Alexander Kraytsberg and Yair Ein-Eli. Review on Lithium air batteries: Opportunities, limitations and perspective. *Journal of Power Sources*, 196:886–893, February 2011. ISSN 03787753. doi:10.1016/j.jpowsour.2010.09.031.

[51] S Visco, E Nimon, B Katz, M Chu, and L De Jonghe. High Energy Density Lithium-Air Batteries with No Self Discharge. In *in Proceedings of the 42nd Power Sources Conference*, pages 201–203, 2006.

[52] Axel Thielmann. Technologie-Roadmap Lithium-Ionen-Batterien 2030. Technical report, Fraunhofer-Institut für System- und Innovationsforschung ISI„ Karlsruhe, 2010.

[53] Holger Kuhn, Christoph Falter, and Andreas Sizmann. Renewable Energy Perspectives for Aviation. In *Proceedings of the 3rd CEAS Air&Space Conference and 21st AIDAA Congress*, volume 1259, pages 1249–1259, Venice, Italy, 2011.

[54] Óscar González-Espasandín, Teresa J Leo, and Emilio Navarro-Arévalo. Fuel Cells: A Real Option for Unmanned Aerial Vehicles Propulsion. *The Scientific World Journal*, 2014. doi:10.1155/2014/497642.

[55] Gerald Gradwohl. *Conceptual Design of a Fuel Cell Powered All Electric Regional Aircraft*. PhD thesis, FH Joanneum, 2011.

[56] Mike Krok, Juan Bedout, and Orges Gjini. Exploring the Role of Fuel Cell Electric Power Systems for Commercial Aviation Applications. In *45th AIAA Aerospace Sciences Meeting and Exhibit*, Reno, Nevada, 2007. American Institute of Aeronautics and Astronautics.

[57] Michael Dudley. Promising Electric Aircraft Drive Systems. In *EAA Electric Aircraft World Symposium*, 2010.

[58] Christopher A Snyder, Jeffrey J Berton, Gerald V Brown, James L Dolce, Narayan V Dravid, Dennis J Eichenberg, Joshua E Freeh, Christopher A Gallo, Scott M Jones, Krishna P Kundu, Cecil J Marek, Marc G Millis, Pappu L Murthy, Timothy M Roach, Timothy D Smith, George L Stefko, Roy M Sullivan, Robert T Tornabene, Karl A Geiselhart, and Albert Kascak. Propulsion Investigation for Zero and Near-Zero Emissions Aircraft. Technical Report May, NASA/TM-2009-215487, National Aeronautics and Space Administration, Cleaveland, Ohio, 2009.

[59] Philippe J Masson, Gerald V Brown, Danielle S Soban, and Cesar A Luongo. HTS machines as enabling technology for all-electric airborne vehicles. *Superconductor Science and Technology*, 20(8):748–756, August 2007. ISSN 0953-2048. doi:10.1088/0953-2048/20/8/005.

[60] Jacek F Gieras. Superconducting Electrical Machines - State of the Art. *Przeglad Elektrotechniczny (Electrical Review), Bd. 85, Nr. 1*, pages 1–21, 2009.

[61] Peter Malkin and Meletios Pagonis. Superconducting electric power systems for hybrid electric aircraft. *Aircraft Engineering and Aerospace Technology*, 86(6):515–518, September 2014. ISSN 0002-2667. doi:10.1108/AEAT-05-2014-0065.

[62] Paul N. Barnes, Michael D. Sumption, and Gregory L. Rhoads. Review of high power density superconducting generators: Present state and prospects for incorporating YBCO windings. *Elsevier, Cryogenics*, 45(10-11):670–686, October 2005. ISSN 00112275. doi:10.1016/j.cryogenics.2005.09.001.

[63] Paul M. Ordin. Safety Standard for Hydrogen and Hydrogen Systems. Technical report, NASA NSS1740.16, National Aeronautics and Space Administration, 2005.

[64] A Westenberger. Liquid Hydrogen Fuelled Aircraft - System Analysis. Technical Report May 2002, Final Technical Report, Cryoplane Project, 2003.

[65] The Boeing Commercial Airplane Company. An exploratory study to determine the integrated technological air transportation system gound requirements of liquid-hydrogen-fueled subsonic, long-haul civil air transports. Technical Report September 1976, NASA Contractor Report, 1976.

[66] Lockheed Company. LH2 Airport Requirements study. Technical report, NASA Contractor Report, 1976.

[67] Panagiotis Laskaridis. *Performance investigations and systems architectures for the More Electric Aircraft.* PhD thesis, Crandfield University, 2004.

[68] V. Mantic-Lugo, G. Doulgeris, and R. Singh. Computational Analysis of the Effects of a Boundary Layer Ingesting Propulsion System in Transonic Flow. In *Proceedings of the Institution of Mechanical Engineers, Part G: Journal of Aerospace Engineering*, 2012.

[69] Mark D Moore and Bill Fredericks. Misconceptions of Electric Propulsion Aircraft and their Emergent Aviation Markets. In *AIAA doi/0.2514/6.2014-0535, SciTEch*, 2014.

[70] William J Fredericks, Mark D Moore, and Ronald C Busan. Benefits of Hybrid-Electric Propulsion to Achieve 4x Increase in Cruise Efficiency for a VTOL Aircraft. In *AIAA Aviation Technology, Integration, and Operations (ATIO) Conference*, Los Angeles, California, 2013.

[71] William J Fredericks. Impact of Distributed Electric Propulsion (DEP) on Aircraft Design. In *Special Conference on Disruptive Green Propulsion Technologies: Beyond the Competitive Horizon*, number November, London, United Kingdom, 2014.

[72] Alex M Stoll, Joeben Bevirt, Mark D Moore, William J Fredericks, and Nicholas K Borer. Drag Reduction Through Distributed Electric Propulsion. In *Aviation Technology, Integration and Operations Conference*, number June, Atlanta, Georgia, 2014.

[73] Amir S. Gohardani, Georgios Doulgeris, and Riti Singh. Challenges of future aircraft propulsion: A review of distributed propulsion technology and its potential application for the all electric commercial aircraft. *Progress in Aerospace Sciences*, 47(5):369–391, July 2011. ISSN 03760421. doi:10.1016/j.paerosci.2010.09.001.

[74] Amir S. Gohardani. A synergistic glance at the prospects of distributed propulsion technology and the electric aircraft concept for future unmanned air vehicles and commercial or military aviation. *Progress in Aerospace Sciences*, 57:25–70, 2013.

[75] R.; Kirner, L.; Raffaelli, A.; Rolt, P.; Laskaridis, and R. Singh. Analysis of Distributed Propulsion on Advanced Vision 2020 Aircraft Concepts. In *International Society for Air Breathing Engines*, Busan, Korea, 2013.

[76] Amir S. (Editor) Gohardani. *Distributed Propulsion Technology, ISBN: 978-1-62948-588-1.* Nova Science Publishers, 2014. ISBN 978-1-62948-588-1.

[77] Howard Smith. Airframe integration for an LH2 hybrid-electric propulsion system. *Aircraft Engineering and Aerospace Technology*, 86(6):562–567, September 2014. ISSN 0002-2667. doi:10.1108/AEAT-04-2014-0045.

[78] Askin T Isikveren, Arne Seitz, Julian Bijewitz, Mirko Hornung, Artur Mirzoyan, Alik Isyanov, Jean-luc Godard, Stefan Stückl, and Jan Van Toor. Recent Advances in Airframe-Propulsion Concepts with Distributed Propulsion. In *29th Congress of the International Council of the Aeronautical Sciences*, St. Petersburg, Russia, 2014.

[79] Arne Seitz, Julian Bijewitz, Sascha Kaiser, and Guido Wortmann. Conceptual investigation of a propulsive fuselage aircraft layout. *Aircraft Engineering and Aerospace Technology*, 86(6):464–472, September 2014. ISSN 0002-2667. doi:10.1108/AEAT-06-2014-0079.

[80] Julian Bijewitz, Arne Seitz, and Mirko Hornung. Multi-disciplinary Design Investigation of Propulsive Fuselage Aircraft Concepts. In *4th EASN Association International Workshop on Flight Physics and Aircraft Design*, Aachen , Germany, 2014.

[81] Askin T Isikveren, Arne Seitz, Julian Bijewitz, Arthur Mirzoyan, Alik Isyanov, Richard Grenon, Olivier Atinault, Jean-luc Godard, and Stefan Stückl. Distributed Propulsion and Ultra-High By-Pass Rotor Study at Aircraft Level. *The Aeronautical Journal (accepted)*, 2015.

[82] Airbus Group. The future of e-aircraft, accessed april 2015, http://www.airbusgroup.com. URL `http://www.airbusgroup.com/int/en/story-overview/future-of-e-aircraft.html`.

[83] J. Paulson T. Banning, G. Bristow, C. Level, L. Sollmann, J. Calderon-Fernandez, D. Wells, M. Olson, N. Davis, C, Du, S. Ambadpudi. 2012-2013 FAA Design Competition for Universities Electric / Hybrid-Electric Aircraft Technology Design Category - NXG-50 - Georgia Tech. Technical report, 2013.

[84] Jan Roskam. *Airplane Design I - VII*. 1985.

[85] L. K Loftin. *Subsonic Aircraft: Evolution and the Matching of Size to Performance*. NASA, Hampton, Virginia, 1980.

[86] E. Torenbeek. *Synthesis of Subsonic Airplane Design*. Delft University Press, Delft, The Netherlands, 1982.

[87] Daniel P. Raymer. *Aircraft Design: A Conceptual Approach*. AIAA Education Series, 1992.

[88] J. D. Anderson. *Aircraft Performance and Design*. McGraw-Hill, 1999.

[89] D. Stinton. *The Design of the Airplane*. Reston, VA, 2nd ed. edition, 2001.

[90] Jack D Mattingly, William H. Heiser, and David T Pratt. *Aircraft Engine Design*. AIAA Education Series, second edi edition, 2002. ISBN 1563475383.

[91] T. C. Corke. *Design of Aircraft*. PrenticeâĂŞHall, Upper Saddle River, NJ, H. A. Stokely„ Virginia Beach, VA, 2003.

[92] Taewoo Nam. *A Generalized Sizing Method for Revolutionary Concepts under Probabilistic Design Constraints*. PhD thesis, Georgia Institute of Technology, 2007.

[93] Ohad Gur, William H Mason, and Joseph A Schetz. Full Configuration Drag Estimation. In *27th AIAA Applied Aerodynamics Conference*, number June, San Antonio, Texas, 2009.

[94] R. W. Claus, A. L. Evans, J. K. Lylte, and L. D. Nichols. Numerical Propulsion System Simulation. Computing Systems in Engineering, 2(4):357 364, 1991.

[95] Joachim Kurzke. GasTurb11, compiled with delphi 2007 on 27 january, 2010., 2010.

[96] A. Bala, P. Pilidis, V. Pachidis, E. L. Gatto, and V. Sethi. PROOSIS - A Collaborative Venture for Gas Turbine Performance Simulation Using an Object Oriented Programming Schema. In Proceedings of the 18th International Society for Air Breathing Engines, 2007.

[97] Mihaela Florentina Nita. *Aircraft Design Studies Based on the ATR 72.* Master thesis, Hamburg University of Applied Sciences, 2008.

[98] Luftfahrttechnisches Handbuch, 2006. URL `www.lth-online.de`.

[99] L.A. McCullers. Flight Optimization System Release 8.23 User Guide. Technical report, NASA Langley Research Center, Hampton, VA, 2011.

[100] ALR Aerospace, DARcorporation, and RUAG. Aircraft Performance Program, APP 5.10, Technical Reference. Technical report, Zürich, Switzerland, 2011.

[101] D. Simos. Piano Online User Guide. Copyright Lissys Limited / D. Simos, http://www.piano.aero, 2009, 2009. URL `http://www.piano.aero`.

[102] PACE Aerospace Engineering and Information Technology GmbH. Pacelab APD 3.0.0. Release Note, 2012.

[103] Larissa Lorenz, Arne Seitz, Holger Kuhn, and Andreas Sizmann. Hybrid Power Trains for Future Mobility. In *Paper 1316, Deutscher Luft- und Raumfahrtkongress*, pages 1–17, Stuttgart, Germany, 2013.

[104] Arne Seitz, Oliver Schmitz, Askin T Isikveren, and Mirko Hornung. Electrically Powered Propulsion: Comparison and Contrast to Gas Turbines. In *Deutscher Luft- und Raumfahrt Kongress, DLRK*, Berlin, 2012. Bauhaus Luftfahrt. doi:281358.

[105] Hubert Grieb. *Projektierung von Turboflugtriebwerken.* Birkhäuser Verlag, Basel-Boston-Berlin, 2004.

[106] Hans-Jörg Steiner, Patrick C Vratny, Corin Gologan, Kerstin Wieczorek, Askin T Isikveren, and Mirko Hornung. Optimum number of engines for transport aircraft employing electrically powered distributed propulsion. *CEAS Aeronautical Journal*, Volume 5 (Issue 2):157–170, 2014. doi:10.1007/s13272-013-0096-6.

[107] Mark H. Waters and Edward T. Schairer. Analysis of Turbofan Propulsion System Weight and Dimensions. Technical report, NASA Technical Report, 1977.

[108] E Onat and G. W. Klees. A Method to Estimate Weight and Dimensions of Large and Small Gas Turbine Engines. Technical report, NASA, 1979.

[109] D. Sagerser, S. Lieblein, and R. Krebs. Empirical expressions for estimating length and weight of axial-flow components of VTOL powerplants. Technical report, NASA Technical Memorandum, 1971.

[110] Arne Seitz. *Advanced Methods for Propulsion System Integration in Aircraft Conceptual Design.* Phd dissertation, PhD Dissertation, Technische Universität München, 2012.

[111] Patrick Christoph Vratny, Corin Gologan, Clément Pornet, Askin T. Isikveren, and Mirko Hornung. Battery Pack Modeling Methods for Universally-Electric Aircraft. In *4th CEAS Air & Space Conference*, pages 525–535, Linköping, Sweden, 2013. Linköping University Electronic Press. doi:978-91-7519-519-3.

[112] Shaker Haji. Analytical modeling of PEM fuel cell i-V curve. *Renewable Energy*, 36: 451–458, 2011. doi:10.1016/j.renene.2010.07.007.

[113] J.G. Coffin. A Study of Airplane Ranges And Useful Loads. Technical report, NACA Report No.69, 1920.

[114] The Boeing Commercial Airplane Company. Cost Index. Technical report, Boeing Flight Operations Engineering, 1990.

[115] Clément Pornet, Sascha Kaiser, and Corin Gologan. Cost-Based Flight Technique Optimization for Hybrid Energy Aircraft. *DOI 10.1108/ AEAT-05-2014-0075, Aircraft Engineering and Aerospace Technology Journal*, 86(6), 2014. doi:10.1108/ AEAT-05-2014-0075.

[116] Lester Faleiro. Beyond the More Electric Aircraft. *Aerospace America*, (September 2005):35–40, 2005.

[117] A A Abdelhafez and A J Forsyth. A Review of More-Electric Aircraft. In *13th International Conference on Aerospace Science & Aviation Technology - Paper: ASAT-13-EP-01*, Cairo, Egypt, 2009.

[118] Larry Chick. Assessment of Solid Oxide Fuel Cell Power System for Greener Commercial Aircraft Introduction, Annual Progress Report,. Technical report, Pacific Northwest National Laboratory (PNNL), Richland, WA 99352, 2011.

[119] Lester Faleiro, Jacques Herzog, Bernd Schievelbusch, and Taehun Seung. Integrated Equipment Systems for a More Electric Aircraft - Hydraulics and Pneumatics. In *24th International Congress of the Aeronautical Sciences, ICAS - Paper ICAS 2004-7.4.2*, 2004.

[120] Roland Slingerland, Sijmen Zandstra, Dieter Scholz, and Kolja Seeckt. Green Freighter Systems. Technical report, 2007.

[121] S.C. Jensen, G.D. Jenney, and D. Dawson. Flight test experience with an electromechanical actuator on the F-18 Systems Research Aircraft. In *19th DASC. 19th Digital Avionics Systems Conference, IEEE*, pages 1–11, 2000. ISBN 0-7803-6395-7. doi:10.1109/DASC.2000.886914.

[122] Norio Takahashi, Taku Kondo, Masayuki Takada, Kazuhiro Masutani, Shingo Okano, Mitsuhiro Tsujita, Aerospace Sumitomo, and Precision Products. Development of Prototype Electro-Hydrostatic Actuator for Landing Gear Extension and Retraction System. In *Proceedings of the 7th JFPS International Symposium on Fluid Power*, pages 165–168, Toyama, 2008.

[123] O Meier and D Scholz. A Handbook Method for the Estimation of Power Requirements for Electrical De-Icing Systems. In *DLRK*, Hamburg, 2010. DLRK.

[124] Xiuxian Xia. *Dynamic Power Distribution Management for All Electric Aircraft.* PhD thesis, Cranfield University, 2011.

[125] Mirko Hornung, Askin T Isikveren, Mara Cole, and Andreas Sizmann. Ce-Liner âĂŞ Case Study for eMobility in Air Transportation. In *AIAA Aviation 2013*, Los Angeles, California, 2013. Bauhaus Luftfahrt.

[126] Clément Pornet, Sascha Kaiser, Askin T. Isikveren, and Mirko Hornung. Integrated Fuel-Battery Hybrid for a Narrow-Body Sized Transport Aircraft. *DOI 10.1108/AEAT-05-2014-0062, Aircraft Engineering and Aerospace Technology, Vol. 86, Iss. 6, pp. 568-574*, 86(6), 2014. doi:10.1108/AEAT-05-2014-0062.

[127] AERO2k. Global Aviation Emissions Inventories for 2002 and 2025, 2013. URL `http://aero-net.info/fileadmin/aeronet_files/links/documents/AERO2K_Global_Aviation_Emissions_Inventories_for_2002_and_2025.pdf`.

[128] Aviation OAG. Official Airline Guide Database. Technical report, 2010.

[129] Airports Council International. ACI Global Traffic Forecast Report 2008-2027. Technical report, 2008.

Appendix A

Appendix

The aircraft synthesis procedure presented in Figure 3.2 is applicable for any hybrid-electric topologies discussed in Section 2.1. However, in the case of partial parallel hybrid systems, a more practical sizing procedure can be deployed as represented in Figure A.1. This procedure was followed for the integrated performance assessment of a partial parallel hybrid system presented in Section 5.5.

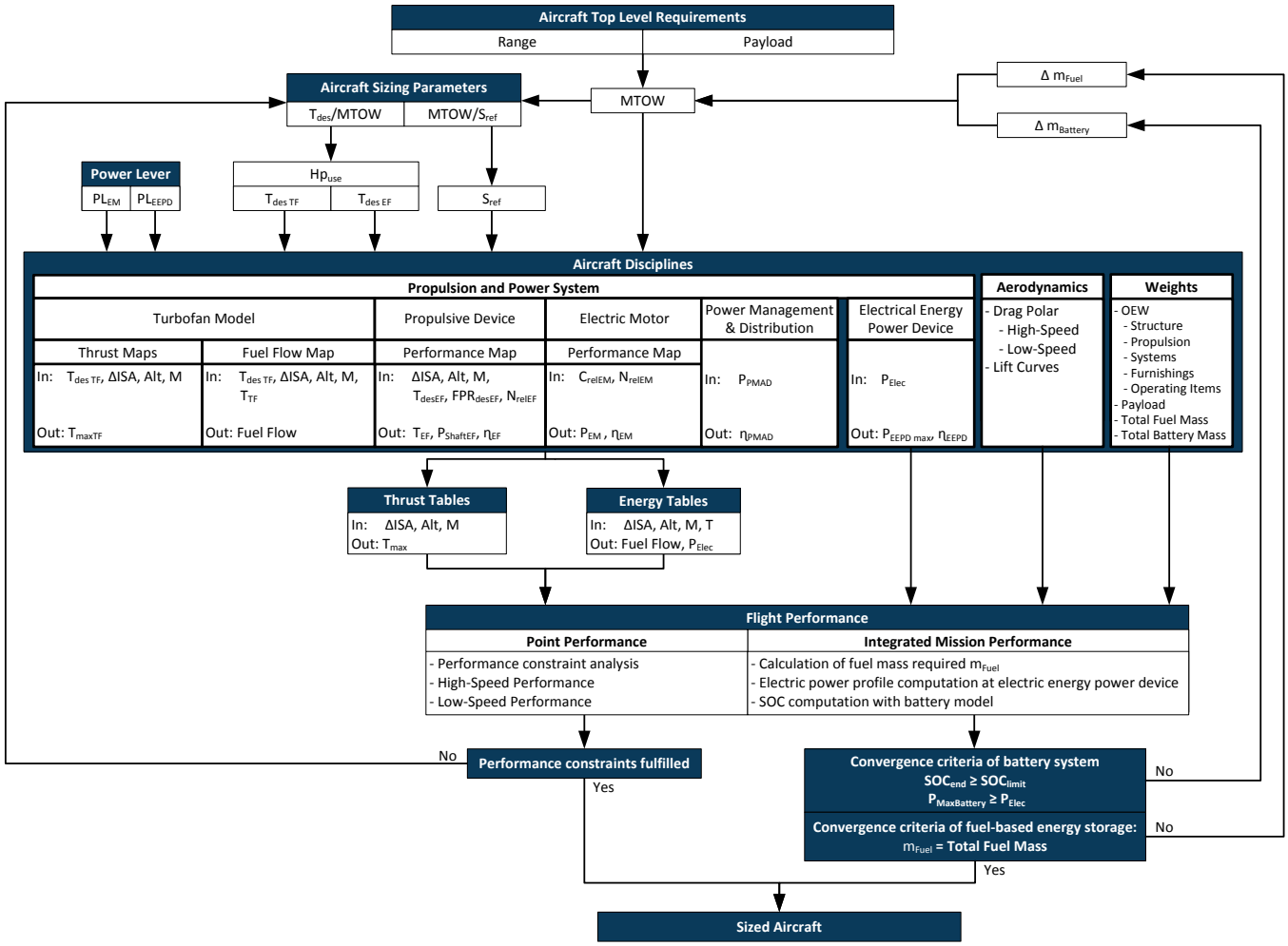

Figure A.1: Aircraft synthesis procedure for partial hybrid parallel system

The most common conventional powerplant system for a commercial transport aircraft is a turbofan. The thrust and fuel flow tables of a turbofan model can be generated using gas-turbine performance software as discussed in Section 3.1.3. Instead of decoupling the thrust production from the energy generation as in the approach presented in Figure 3.2, the performance properties of the turbofans can be directly mapped into the aircraft sizing procedure. As shown in Figure A.1, the thrust and fuel flow maps of the turbofan discussed in Section 3.2.3.1 are directly interfaced in the process. According to the ratio of $T_{des}/MTOW$, the total design thrust requirement T_{des} is calculated for an initial value of MTOW. With the formulation of a degree of hybridization for useful power H_{Puse}, the design thrust of the turbofan $T_{des,TF}$ and of the electrical fan $T_{des,EF}$ is calculated as demonstrated in Section 3.2.6.1. $T_{des,TF}$ enables the computation of the maximum thrust of the turbofan $T_{max,TF}$ and the fuel flow characteristics. $T_{max,TF}$ is used for the computation of the the maximum thrust of the overall propulsion system T_{max} stored in the thrust table. The fuel flow is directly linked to the fuel flow parameter in the energy table.
As a side note, for a commercial transport aircraft equipped with turboprops both procedures can be practically employed. Either the thrust and fuel flow characteristics of the turboprops are computed in maps and interfaced with the aircraft environment as presented in Figure A.1. Or the turboprop is split between a propeller model and a turboshaft model interfaced as in Figure 3.2. The propeller model is integrated as a propulsive device with a performance map. The turboshaft model is implemented as a combustion engine with a power map and an efficiency map as discussed in Section 3.2.3.3.